Characterization of

Plasma-Enhanced Atomic Layer Deposited Ga_2O_3 using $Ga(acac)_3$ On GaN

by

Mei Hao

A Dissertation Presented in Partial Fulfillment
of the Requirements for the Degree
Doctor of Philosophy

Approved April 2018 by the
Graduate Supervisory Committee:

Robert J. Nemanich, Chair
Ralph Chamberlin
Fernando Ponce
Srabanti Chowdhury

ARIZONA STATE UNIVERSITY

May 2018

ABSTRACT

This research has studied remote plasma enhanced atomic layer deposited Ga_2O_3 thin films with gallium acetylacetonate ($Ga(acac)_3$) as Ga precursor and remote inductively coupled oxygen plasma as oxidizer. The Ga_2O_3 thin films were mainly considered as passivation layers on GaN. Growth conditions including $Ga(acac)_3$ precursor pulse time, O_2 plasma pulse time, N_2 purge time and deposition temperature were investigated and optimized on phosphorus doped Si (100) wafer to achieve a saturated self-limiting growth. A temperature growth window was observed between 150 ℃ and 320 ℃. Ga precursor molecules can saturate on the substrate surface in 0.6 s in one cycle and the plasma power saturates at 150 W. A growth rate of $0.31\ \text{Å/cycle}$ was observed for PEALD Ga_2O_3. Since the study is devoted towards Ga_2O_3 working as passivation layer on GaN, the band alignment of Ga_2O_3 on GaN were further determined with X-ray Photoemission Spectroscopy and Ultraviolet Photoemission Spectroscopy. Two models are often used to decide the band alignment of a heterojunction: the electron affinity model assumes the heterojunction aligns at the vacuum level, and the charge neutrality level model (CNL) which considers the presence of an interface dipole. The conduction band offset (CBO), valence band offset (VBO) and band bending (BB) of PEALD Ga_2O_3 thin films on GaN were $0.1\ \pm 0.2\ eV$, 1.0 ± 0.2 eV and 0.3 eV respectively. Type-I band alignments were determined. Further study including using PEALD Ga_2O_3 as passivation layer on GaN MOS gate and applying atomic layer etching to GaN was described.

ACKNOWLEDGMENTS

Firstly, I would like to express how grateful I am of my supervisor. My supervisor kept inspiring me a direction on my research. I could have the accomplishment today mostly because of his vise advices. I always remember the words said by Alexander the Great: “I am not afraid of an army of lions led by a sheep; I am afraid of an army of sheep led by a lion.” The Ph.D. study is somehow like a war we are fighting. I am a sheep led by the lion, but I win the war finally.

During the period of my Ph.D. study, I have get a lot of help from people inside and outside my lab. I would like to thank Brianna Eller and Jialing Yang for the patient instructions for the training of the experiment tools and explanation of the theory. I have also get helpful ideas from Yu Yang and Xingye Wang. We have been talking about basics of equipment, quantum physics and things like that. One year before I leave, our lab has recruited more students who’s much younger than me, Yichen, Jessa and Daniel. They are very curious on everything. They did a lot to help on some labor work. Also, I really enjoyed the time answering their questions. Outside my lab, I would like to should my appreciation of Chufeng Li. He has a very deep understand of physics theory. When I have something that I don’t understand, I usually go to him for help. Most of the cases, he could give an answer.

I appreciate the help from my family. I had some health issues during my Ph.D. study. My husband has been taking good care of me. I also get some financial support from my parents, which helped a lot.

Besides the technical knowledge I got, I have also learned something else from my supervisor. He loves his family a lot. He has great achievements on his career as a

professor, at the meantime, he has a very good relationship with his wife, children, grand-children. His attitude will inspire me for my whole life.

TABLE OF CONTENTS

Page

LIST OF FIGURES vi

LIST OF TABLES x

CHAPTER

1 INTRODUCTION 1

1.1 Ga_2O_3 as a wide band gap semiconductor material 3

1.2 GaN as a semiconductor material and GaN-based transistors....................... 5

1.3 Custom-built Remote plasma enhanced Atomic Layer Deposition............. 16

1.4 Advantages of PEALD.. 17

1.5 ALD *in-situ* reaction mechanism 18

2 EUIPMENT AND EXPERIMENTS 30

2.1 XPS and UPS 30

2.2 Background Noise analysis in the XPS measurement 32

2.3 Film composition, thickness and band gap calculation.............................. 36

2.4 Band alignment and photoemission spectroscopy..................................... 42

2.5 Plasma-enhanced atomic layer deposition (PEALD) 49

2.6 Atomic force microscopy (AFM)... 51

2.7 X-ray reflectivity.. 53

3 PEALD Ga_2O_3 GROWTH CHARATERIZATION....................................... 58

3.1 Introduction 59

3.2 Experiment 62

3.3 Results and Discussion... 63

3.4 Conclusion 66

4 BAND ALIGNMENT OF PEALD GA_2O_3 ON GAN 73

4.1 Introduction 73

4.2 Experiment 75

4.3 Results 78

4.4 Discussion 84

5 FUTURE WORK: IMPROVEMENT OF GAN-BASED MOS GATES 90

5.1 Ga_2O_3 working as interfacial layer 90

5.2 Stacked interlayer with Ga_2O_3 and Al_2O_3 on GaN. 94

5.3 Advantages and disadvantages of dry plasma etching of GaN 95

5.4 Atomic layer etching of GaN 98

RFERENCES 104

LIST OF FIGURES

Figure Page

1. Schematic for β-Ga_2O_3 Crystal Structure in Three Dimensions 2
2. Basics Structures of Ga_2O_3-based Transistors 4
3. Schematic of GaN Crystal 6
4. Ideal Band Diagram for a Free-standing GaN.. 7
5. Band Diagram for GaN with Fermi Level Pinning States 7
6. Examples of GaN-based Transistors with Dielectrics Working as Gate Insulator .. 9
7. Failure mechanisms for Gate Leakage 10
8. Schematic of Oxygen Plasma and Plasma Sheath with a Substrate in Contact 11
9. A Typical Cycle of Plasma-Assisted ALD Process 12
10. Optical Spectra for (a) Oxygen, (b) Hydrogen and (C) Nitrogen Plasma 13
11. Basic Configuration of Plasma Rectors in PEALD 13
12. The Publication of Plasma Assisted ALD in The Recent 30 Years 15
13. Schematic of the PEALD System in NSL at Arizona State University 16
14. Schematic for a PEALD Cycle 17
15. Optimized PEALD Process of a Cycle for The Self-limiting Deposition 17
16. Comparison of PEALD and Thermal ALD Growth Rate 18
17. Ideal Packing of Precursor Ligands 21
18. Possible Growth Per Cycle (GPC) Variation with Deposition Temperature with the Growth Window 22
19. Equipment in the Nano-Science Lab at ASU Connected by an Ultra-high Vacuum T-line 30

20. X-ray Photoemission Process and Energy Band Diagram 31
21. Schematic of Binding Energy Reference of the Sample and The Analyzer 32
22. Schematic and Basic Constitution of the XPS System at the NSL, ASU 32
23. Photoemission-charged Sample Surface with Exaggerated Roughness................ 33
24. Schematic for a Secondary Electron Emission Process 34
25. Schematic for an Auger Electron Process 35
26. A Typical XPS Graph and Different Fitting Method 36
27. Band Gap Calculation from the O 1s Energy Loss Spectra 41
28. Schematic for a photoemission process in UPS measurements 42
29. Charge Transfer Between the Metal Fermi Level and Semiconductor CNL 44
30. Charge neutrality level (CNL) is the weighted average of density of states 46
31. S-factor of Insulators with Different Dielectric Constant ε 46
32. Schematic for the Plasma Enhanced Atomic Layer Deposition System 49
33. An Example of UPS Spectrum.. 51
34. Schematic for an Atomic Force Microscope (AFM) System 52
35. Possible Artifacts from AFM Measurement 52
36. AFM Images of PEALD Ga_2O_3 on Si with 20 μm × 20 μm Scan Size 52
37. Schematic of X-ray Reflectivity... 53
38. Schematic of the Mechanism for X-ray Reflectivity Measurements 53
39. XRR Image of a 30 nm PEALD Al_2O_3 Film on Si 54
40. Schematic for a $Ga(acac)_3$ Molecule 60
41. Schematic for a PEALD Self-limiting Cycle 63
42. Characterization of ALD Pulse Timing... 65

43. ALD Growth Rate vs Temperature 65

44. Schematic for the Band Gap of PEALD Ga_2O_3 Thin Films Determined by ELS . 66

45. XPS Graph of Ga 3d, C 1s and O 1s Electrons for as-received, Chemical Cleaned, and Plasma Cleaned GaN 79

46. XPS Spectra for Cleaned GaN, as Grown PEALD Ga_2O_3, and Annealed Ga_2O_3 . 80

47. XPS and UPS Spectra of PEALD As-grown Ga_2O_3 Thin Films on Si 81

48. Band Alignment of As-grown PEALD Ga_2O_3 on GaN 83

49. Relationship of Dielectric Band Gap and Band offsets on GaN 84

50. XPS for GaN with Different Cleaning Methods 91

51. Characterization of GaN MOSFETs with PEALD Al_2O_3 as Gate Insulator. Prepared in Collaboration with Srabanti Chowdhury, *et, cl* 91

52. Capacitance-Voltage Characterization of GaN MOSFET with PEALD Al_2O_3 as Insulator and 1 Monolayer Ga_2O_3 as Passivation. Prepared in collaboration with Srabanti Chowdhury, *et, cl* 92

53. Simulated $\alpha - Al_2O_3/GaN(0001)$ Stacked Structure with(a) and without (b) a Ga-O-Ga Interlayer 93

54. Simulated DOS for $\alpha - Al_2O_3/GaN$ with and without a Ga-O-Ga Interlayer 94

55. Schematic for GaN MOSHEMT with stacked Ga_2O_3 and Al_2O_3. Prepared in Collaboration with Srabanti Chowdhury, *et, cl* 94

56. Characterization of Current-Voltage for GaN MOSCAP with and without Al-O-Al Interlayer. Prepared in Collaboration with Srabanti Chowdhury, *et, cl* 95

57. XPS for GaN and SiO_2 with Stacked Interlayer with Ga_2O_3 and Al_2O_3 95

58. Unevenly Etched Mesa Sidewall After 3 min Plasma with 600 W ICP Power and 60W RF Power Measure with SEM 96

59. Degraded Photoresist Mask After 3 min Plasma with 600 W ICP Power and 60 W RF Power Measured with SEM 97

60. SEM Images of GaN Bottom Surface after ICP Etching 97

61. Influence of Cl_2 Concentration on the Surface RMS with 500W ICP Power, 60W RF Power and 0.66 Pa Pressure 98

62. Schematic of Proposed Atomic Layer Etching (ALE) Processes for Etch Damage Removal 99

63. GaN ALE Process with Oxygen Plasma or H_2O_2 as Oxidizer and HF, TMA as Reactants to Remove Oxides 100

64. GaN ALE Process with Oxygen Plasma or H_2O_2 as Oxidizer and HF, TMA as Reactants to Remove Oxides 100

LIST OF TABLES

Tables Pages

1. Material Properties of Ga_2O_3 and Other Alternative Semiconductors 4

2. Summary of Parameters for GaN-based Transistors 9

3. XPS Bulk Sensitivity Factor and Surface Sensitivity Factor 40

4. The Material Properties and Parameters for Different Semiconductors................ 45

5. Calculated Valence Band Offset and Conduction Band Offset of Various Materials on Ga_2O_3 Based on the Charge Neutrality Model (CNL) 45

6. Calculated Valence Band Offset and Conduction Band Offset of Various Materials on GaN based on the Charge Neutrality Model (CNL) 45

7. Parameters for Various Dielectrics, Whereas Gap is Band Gap (eV). 45

8. Alternative UV Source 50

9. Safety Date Sheet for $Ga(acac)_3$ and Comparable Ga Precursor Trimethygallium 60

10. Schematic for a PEALD Self-limiting Cycle 63

11. Core Level Energy for Ga 3d, C 1s and O 1s from XPS Spectra 79

12. XPS Ga 3d, Ga-2p and Al 2p core 81

CHAPTER 1

INTRODUCTION

In this study, plasma enhanced atomic layer deposited Ga_2O_3 using gallium acetylacetonate as gallium precursor and oxygen plasma as oxidizer is studied. The growth parameters have been varied to achieve saturation growth conditions. The effect of a monolayer of Ga_2O_3 as a passivation layer on GaN has also been studied. Electrical properties of GaN-based MOSFET were measured, and different plasma treatments on GaN were used to achieve a surface for dielectric deposition. It was found that a N_2/H_2 plasma clean with residual oxygen could introduce about a monolayer of Ga_2O_3 on GaN which could improve the GaN-based MOS gate's electrical properties including higher breakdown and reduced hysteresis. Consequently, PEALD Ga_2O_3 working as a passivation layer on GaN becomes a primary focus for this project

In chapter 2, the equipment and experiments were discussed. The main equipment used in this study were PEALD, XPS, UPS, XRR and AFM. A section is included to outline the mechanism and specific application of each system. The advantages and disadvantages, and examples were discussed for each system.

In chapter 3, the PEALD process for deposition of Ga_2O_3 using $Ga(acac)_3$ is presented. The growth conditions, such as plasma RF power, oxygen plasma pulse time, N_2 purge time and deposition temperature was studied to achieve saturation growth. Also, thin film properties such as growth rate, density, refractive index and band gap at different deposition conditions are discussed. A comparable result was achieved in this research compared with alternative deposition techniques and alternative deposition precursors.

In chapter 4, the band alignment of Ga_2O_3 and GaN on different materials is presented. Band alignment models include the Charge Neutrality model and the electron affinity model. The experiments mainly focused on the band alignment of Ga_2O_3 on GaN which is discussed in detail.

In Chapter 5, atomic layer etching (ALE) of GaN is proposed. An overview of the traditional dry plasma etching method and how the disadvantages might be related to the failure mechanism of GaN based MOS gate was discussed. An atomic layer etching system for GaN was now under construction in the Nanoscience lab at ASU. A surface with reduced damage, impurities and surface states density could be achieved with this system.

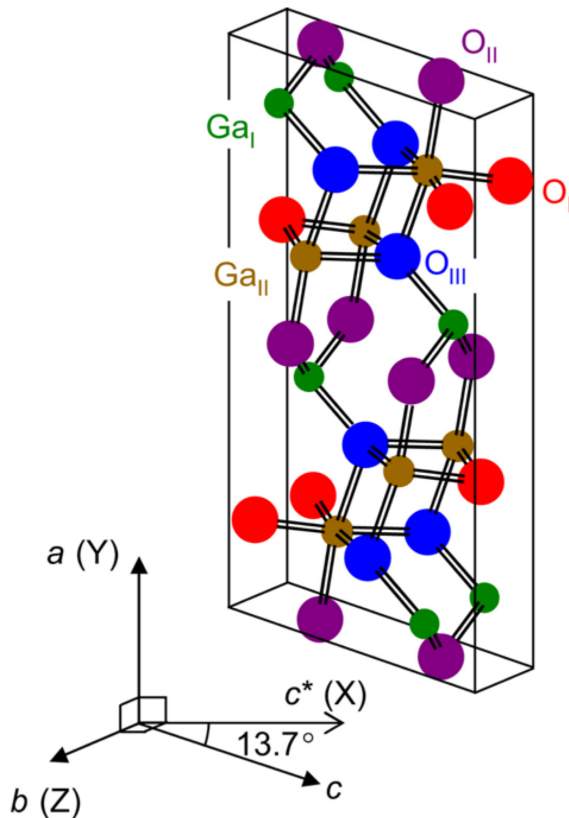

Figure 1.1 Schematic for β-Ga_2O_3 crystal structure in three dimensions.

1.1 Ga_2O_3 as a wide band gap semiconductor material: electronic states and applications

Ga_2O_3 is an ultra-wide band gap (4.7 eV-4.9eV) semiconductor material[1][2]. Ga_2O_3 has five possible crystalline structures, including $\beta - Ga_2O_3$, $\alpha - Ga_2O_3$, $\gamma - Ga_2O_3$, $\delta - Ga_2O_3$ and $\varepsilon - Ga_2O_3$, among which $\beta - Ga_2O_3$ is the most stable form[3][4]. The crystal structure of $\beta - Ga_2O_3$ shown in Fig 1.1. Ga (1) and Ga (2) are gallium in different crystal graphical position, same as O(1), O(2) and O(3) respectively. The relative size of oxygen and gallium atoms are not scaled [17]. Ga_2O_3 has wide application as a transparent conducting oxides (TCOs)[1], deep UV detector[5], gas sensor[6][7], UV detectors[6], MSFETS[8][9], photodetectors[10] and solar cells[11]. Ga_2O_3 thin films have been deposited by various techniques, including Metal-Organic Chemical Vapor Deposition (MOCVD), Atomic Layer Deposition (ALD)[12], metal-organic vapor phase epitaxy [13], pulsed laser deposition[14][1], and sol-gel process [15] . Ga_2O_3 has a large theoretical breakdown field (7.56MV/cm) compared with other semiconductors, such as Si and GaN [16]. Table 1.1 shows the Material properties of Ga_2O_3 and other alternative semiconductors such as Si, GaAs, SiC, GaN and diamond[5], [18]–[20]. [5], [18]–[20].

Whereas: μ, electron mobility at room temperature; ε, dielectric constant; E_g, bang gap between the valence band maximum and conduction band minimum; Baliga figure of merit (BFOM) ratio, defined by the following equation[21]:

$$\mathrm{BFOM} = \epsilon * \mu * E_g^3$$

	$\mu(cm^2/V \cdot s)$	ε	$E_g(eV)$	BFOM Ratio	$V_{breadown}$ (MV/cm)
Si	1300	11.4	1.1	1.0	0.3
GaAs	5000	13.1	1.4	9.6	0.4
SiC	260	9.7	2.9	3.1	2.5
GaN	1500	9.5	3.4	24.6	3.3
Ga_2O_3	900	9	4.2-4.9	33	8
Diamond	1900	5.5	5.5	88.1	10

Table 1.1 Material properties of Ga_2O_3 and other alternative semiconductors.

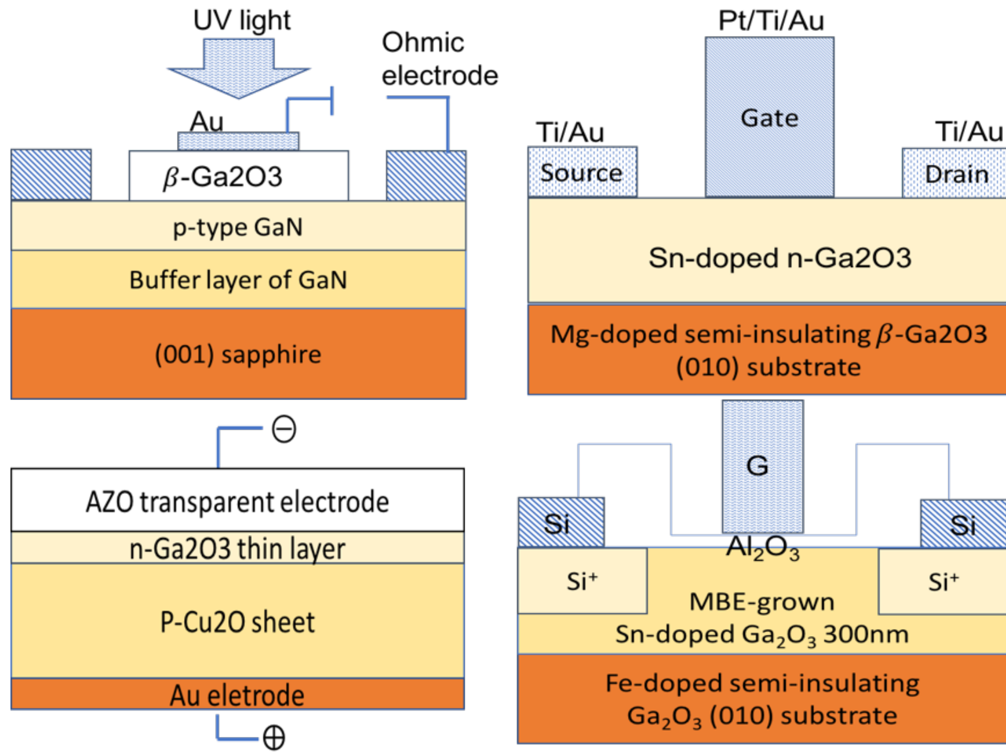

Figure 1.1 Basics structures of Ga_2O_3-based transistors.

The BFOM ratio for Si is set as 1. So BFOM ratio of a semiconductor A is $\frac{BFOM_A}{BFOM_{Si}}$

$V_{breadown}$, breakdown voltage of the semiconductor.

Ga_2O_3 has a wide application such as in Gas sensor, Deep UV sensor, MESFET, solar cell and MOSFET. Fig. 1.2 shows some basics structures of Ga_2O_3-based transistors, Deep UV sensor device based on β-Ga_2O_3/GaN heterojunction[6][7](upper-left); Ga_2O_3 MESFET[22][9](upper-right); AZO/n-Ga_2O_3/p-Cu2O solar cell[11](lower-left) and Schematic of depletion-mode Ga_2O_3 MOSFET[22] (lower-right).

1.2 GaN as a semiconductor material and GaN-based transistors

GaN is one of the next-generation semiconductor materials due to its excellent material properties including wide band gap, high electron mobility and high saturation velocity. Despite the recent progress of GaN-based high power/frequency transistors. The interface states related or surface defects is still a main reason hindering the fabrication of GaN-based field effect transistors. Leakage current through the gate[23], current collapse over the drain[24], and shorter life-time of Schottky contacts[25] were caused by the defect states. In order to improve the transistor functions, GaN surface pretreatments, surface defects, interface states and electronic configurations of GaN and different contacting materials, band alignment of GaN on various materials and Ga_2O_3 working as passivation interfacial layer on GaN will be discussed in this section.

1.2.1 GaN as a semiconductor

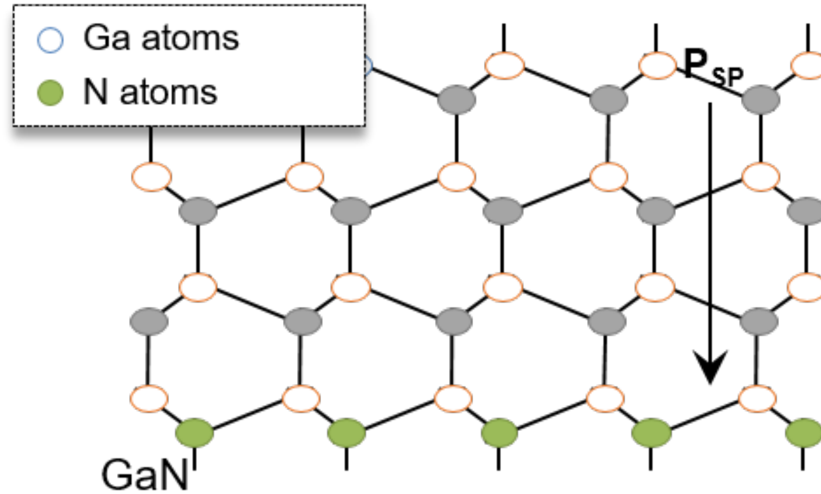

Figure 1.2 Schematic of GaN crystal, the sizes of Ga and O atom are not normalized.

In this study, PEALD Ga_2O_3 is mainly used as passivation layer for GaN. GaN is a III-V semiconductor with a Wurtizite crystal structure. As is shown is Fig. 1.3.GaN has lattice parameters of a=3.189 Å and c=5.185 Å.

GaN is a polarized material with strong surface pinning states. In the ideal case of a free-standing GaN. The surface potential should be calculated as:

$$\phi_s = -\frac{qN_{ss}^2}{2\mathcal{E}\mathcal{E}_0 N_d}$$

whereas, q is the charge of an electron, ϵ is the relative permittivity, ε_0 is the vacuum permittivity, N_d is the doping density of GaN, and N_{ss} is the surface states net charge. The ideal band diagram is shown in Fig. 1.4 [18].

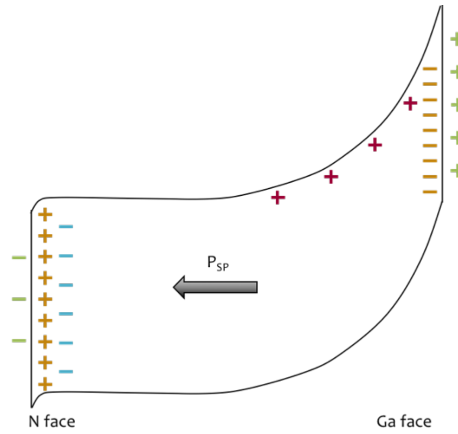

Figure 1.3 Ideal band diagram for a free-standing GaN.

However, experimental band diagram for GaN is as Fig. 1.5. This is probably due to the surface states. GaN is a polarized material, so the polarization charge has been calculated to be $1.37 \times 10^{13}\ Charges/cm^2$. The experimental potential on the Ga-face would be extremely large according to the theory as is shown in Fig 1.4. However, the experimental band bending of GaN on Ga-face is 0.3 eV as is shown in Fig. 1.5, which indicates surface charge compensation. According to the Charge neutrality nature of free standing material, the overall charge of the material is expected to be Zero.

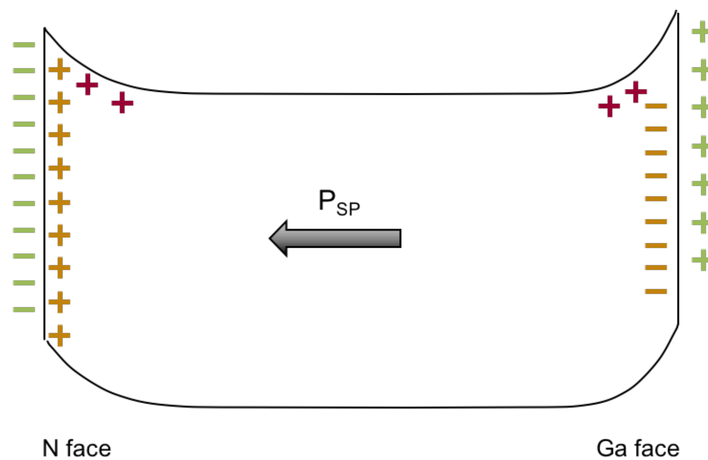

Figure 1.4 Band diagram for GaN with fermi level pinning states.

The polarization of GaN could affects high mobility transistors by possibly introducing interface states, thus increasing gate leakage[27], [28]. The magnitude of the interface states density is usually two orders larger for a GaN-dielectrics surface than Si-SiO_2 interface[29]. However, pretreatment of GaN in ECR or remote N_2 plasma could reduce N-related vacancies and thus interface states, at the same time, a Ga_2O_3 layer could form isovalent bonding between GaN and a dielectric[29][30]. Ga_2O_3 has also been reported to work as a gate insulator on GaN with a low interface states density of $2.53 \times 10^{11} cm^{-2} eV^{-1}$[31]. For these reasons, Ga_2O_3 has been a key factor, if not the most important factor, in the fabrication process of GaN based metal-oxide-semiconductor (MOS) field effect transistors.

1.2.2 GaN-based transistors

GaN is a promising next-generation semiconductor due to the large band gap (3.4 eV), high electron mobility (10^7 cm/s) and high breakdown field (3 MV/cm). Fig. 1.6 shows GaN-based (a) HEMT (b) JFET, (c) CAVET and (d) MOSFET devices and Table 1.1 presents operation situations [32]–[34].

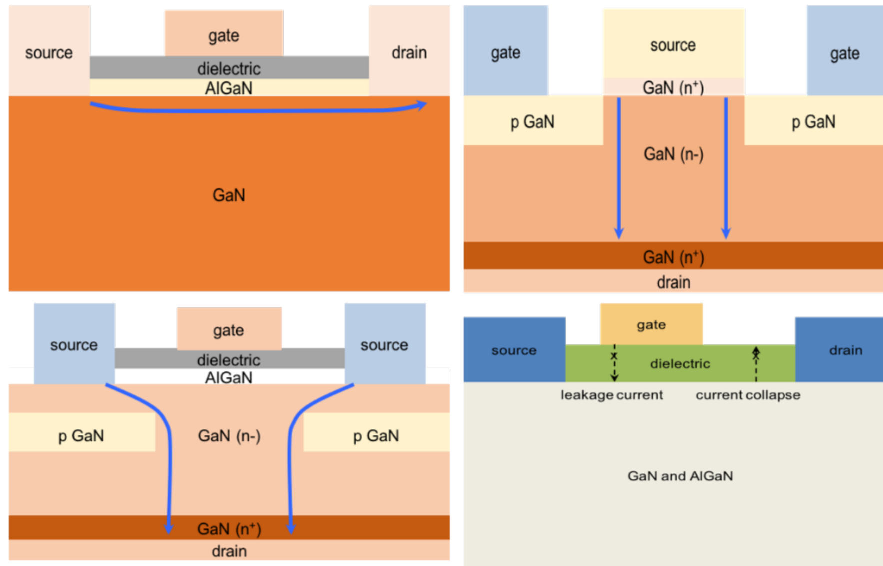

Figure 1.5 Examples of GaN-based transistors with dielectrics working as gate insulator

requirements	**MOSFET**	**HEMT**	**JFET**	**CAVET**
channel electron mobility ($cm^2/(V•s)$)	100~200	1500~2000	900~1100	1500~2000
drift region electron mobility ($cm^2/(V•s)$)	900~1100	NA	900~1100	900~1100
breakdown field (MV/cm)	3	3	3	3
operation mode	E-mode	D-mode	E-mode	D-mode

Table 1.1. Summary of parameters for GaN-based transistors

1.2.3 Failure mechanism of GaN-based transistors

Gate leakage

Leakage current through the gate has been attributed to electron tunneling due to several mechanisms, including thermionic emission, thermionic field emission, multistep or two steps trap-assisted tunneling, Frenkel-Poole emission[35], hopping conduction and Fowler-Norheim tunneling. Some of the failure mechanisms are described in Fig. 1.7. ALD gate dielectrics has been reported to increase the breakdown voltage and channel current while decreasing the gate leakage current[36].

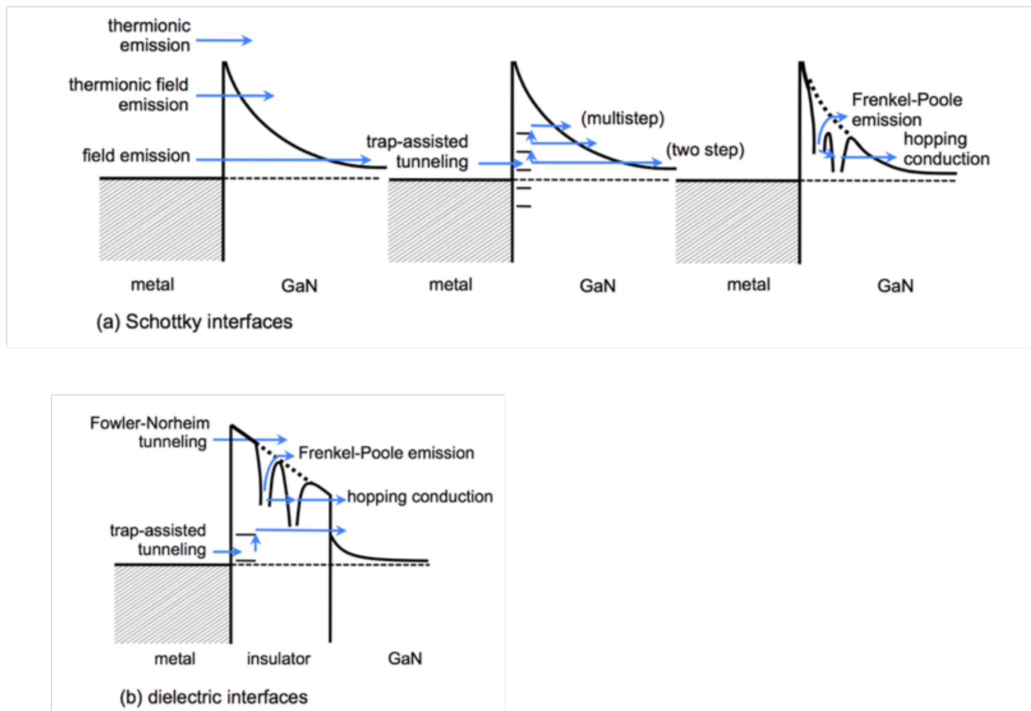

Figure 1.6 Failure mechanisms for gate leakage[36].

Current collapse

Besides the leakage current, another obstacle that has limited GaN-based transistor properties is current collapse. This describes a phenomenon of gate current

reduction when high frequency gate swings were applied. It was first proposed by Vetury *et al.* to explain the current reduction in the 2DEG channel of AlGaN/GaN structure.

Materials are often described in in four different forms-solid, liquid, gas, plasma. Plasma is the most widely existing material in the universe, however, on the earth, plasma only exist in labs and lightning. For the plasma configurations. Inductively coupled plasma (ICP)[37] capacitively coupled plasma (CCP)[38] and electron cyclotron resonance (ERC)[39], [40] plasma are the most commonly plasma reactors. Plasma with fully ionization are called hot plasma[41], [42] and partial ionization as cold plasma [43].

Plasma is charge quasi-neutral at macroscopic length scales; and generally negative ions can be neglected. In the plasma, the temperature of electrons could be 1 eV – 5 eV, typically 3 eV, while ions and gas species are at 300 K-500 K. In the plasma reactor, the positive space charge layer is formed between the plasma and the substrate surfaces in contact, and this phenomenon is named as the Debye Sheath[44], [45].

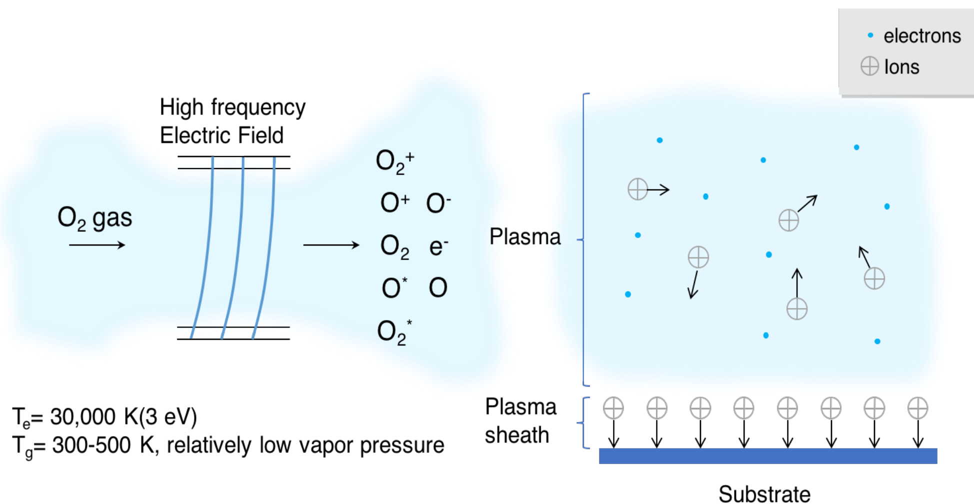

Figure 1.9 Schematic of Oxygen plasma and plasma sheath with a substrate in contact.

The plasma sheath could be collision less in cases when the ion mean free path is longer than sheath thickness, or collisional in cases when the ion mean free path is shorter than

sheath thickness. For example, when the pressure is larger than 100 mTorr. The ion flux could be increased by increasing the plasma power or decreasing the gas pressure so to reduce collisions.

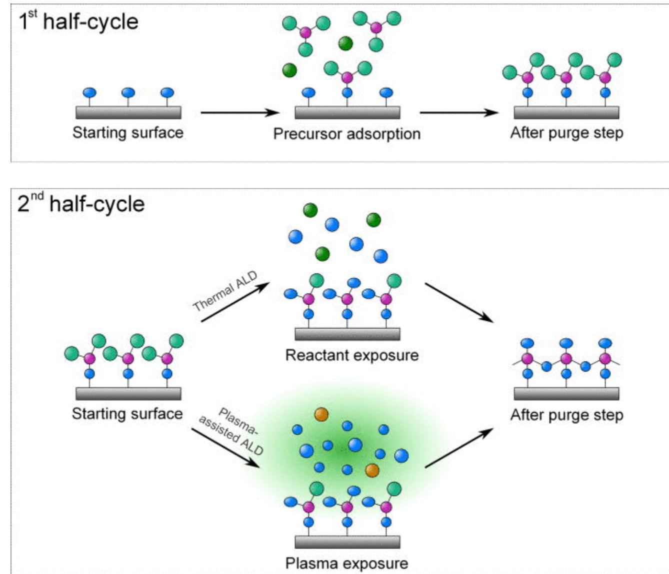

Figure 1.10. a typical cycle of Plasma-Assisted ALD process.

Fig.1.10. shows a typical PEALD cycle. For the first half-cycle, a substrate with –OH groups on the surface react with precursors to chemisorb the precursor molecules, or the precursor molecule may be physically absorbed on the surface without ligand exchange. The second half-cycle is an oxidation process. The radicals, or sometimes ion, will oxides the precursor and leave the reaction product on the surface with –OH group. N_2 gas purge is applied between each step to prevent CVD-like reactions.

Plasma assisted atomic layer deposition typically consists of four steps shown in Fig.1.11. For plasma assisted ALD, O_2, H_2 and N_2 are the most commonly used plasma. The visible spectra of the plasma usually could help to distinguish the plasma species. Fig. 1.11 shows the optical spectra for Oxygen Hydrogen and Nitrogen plasma. The basic configuration of plasma rectors is shown as Fig. 1.12[46].

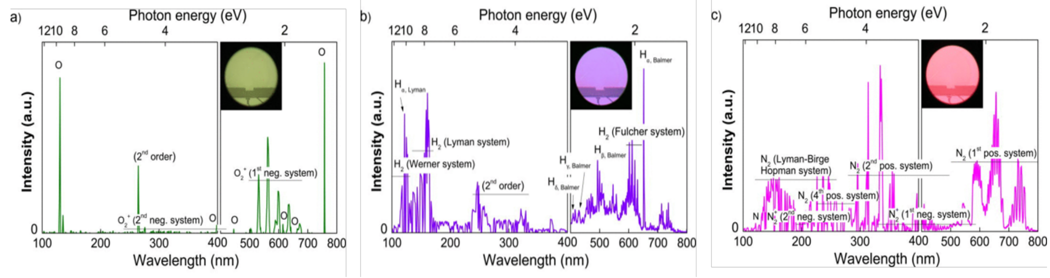

Figure 1.11. Optical spectra for (a) Oxygen, (b) Hydrogen and (C) Nitrogen plasma[46].

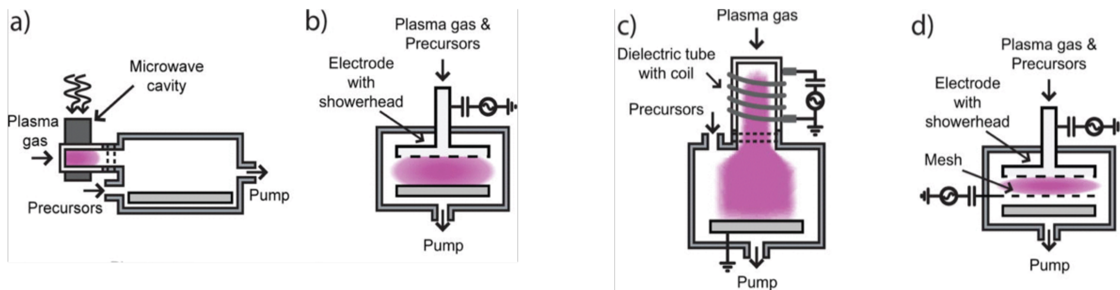

Figure 1.12. Basic configuration of plasma rectors in PEALD.

Fig. 1.12 (a) shows a radical-enhanced plasma process. The ions and electrons can recombine during the process of flowing into the chamber. The radical density is therefore relatively less than the remote plasma reactor. (b) is a capacitively coupled plasma(CCP) reactor. This configuration is a direct plasma rector and widely used in industry for plasma deposition and plasma etching. Usually, CCP reactors for research and develop have a larger gap (~10cm) than industrial configurations. (c) is a remote plasma rector, which has the same configuration as the PEALD system used in this study. (d) is a capacitively coupled plasma with a grounded mash between the electrode with showerhead and the other side of the capacitor.

An inductively coupled plasma has a comparatively higher energy than a conductively coupled plasma. The ion energy in the inductively coupled plasma are usually 10 times higher than that in conductively coupled plasma. In a reactor equipped with an ICP

source for (a) various gas pressures (at power of 200 W) and (b) various plasma powers (at a pressure of 8 mTorr), the ion energy distribution is different as is shown in Fig. 1.13(a) and Fig. 1.13(b). It is easy to imagine that with a higher pressure; the gas molecule density would be higher which could introduce more ion collions. Based on the collision model of ions in the plasma, a higher pressure usually leads to an ion distribution with lower energy. RF power is another parameter that influences the plasma energy distribution. RF power is supplied to excite the plasma. Higher RF power leads to higher excitation of the plasma species. It is obvious that the ion energy distribution will be higher with a higher RF power. The plasma configuration also influences the ion energy distributions (IEDs). Usually ICP plasma has a higher IEDs than CCP[47][38] under similar condition.

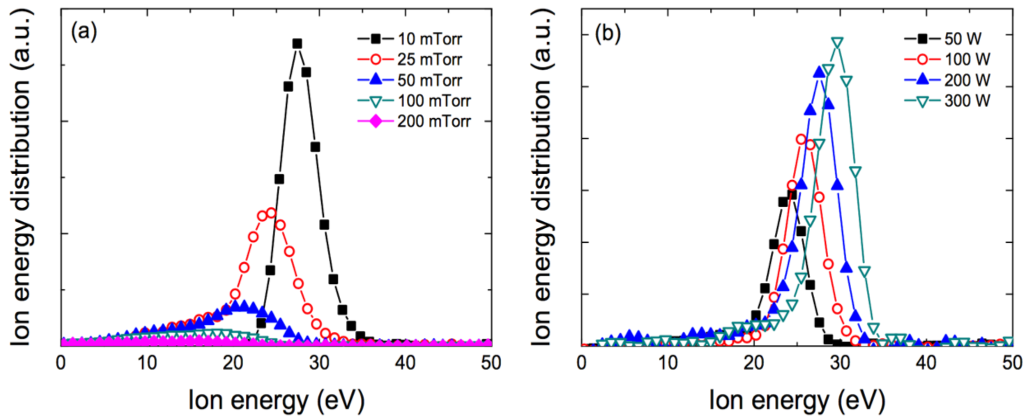

Figure 1.13 Ion energy distributions (IEDs) for ions in an Ar plasma [46].

Atomic layer deposition, belongs to the chemical vapor deposition CVD class. As the need of thin films with nanometer thickness has been increasing, the ALD process has been increasing. Moore's law, describes the size improvement of chips. As the chips become smaller and smaller, ALD is more and more widely used during processing. As is

shown in Fig. 1.14, there is increasing publications focused on plasma assisted ALD. The plasma assisted ALD process could deposited various materials[46], [48]–[50], [34], [51], [52]. The publication on PEALD has been increasing as well as shown in Fig. 1.14.

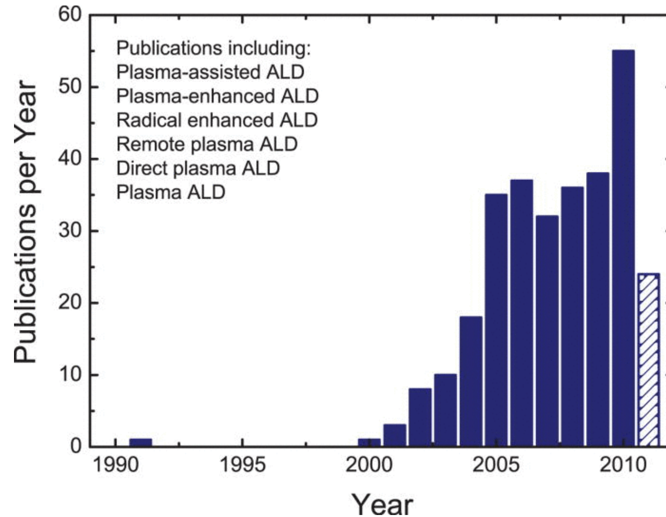

Figure 1.14 The publication of plasma assisted ALD in the recent 30 years.

1.3 Custom-built Remote plasma enhanced Atomic Layer Deposition

In this study, Ga_2O_3 thin films were deposited by a PEALD system in the NanoScience Lab at ASU. The precursor is held in a closed stainless-steel container covered by a heating jacket to achieve the desired temperature. An appropriate temperature of the precursor provides sufficient vapor pressure for deposition. High purity Ar gas carries the precursor molecules through the pipeline to the ALD chamber. Two-way valves are used to control the flow of the precursor. For N_2 and O_2 gas, three-way valves are used to control the gas flow. A butterfly valve in front of the turbo pump is used to maintain the pressure in the chamber, which is typically 100 mTorr for most depositions. A heater beneath the sample stage is applied to control the temperature of the sample substrate and is called the deposition temperature. A remote plasma reactor 25 cm above the sample was generated by inductively coupled coil with rf source. For the

chamber side-walls, a temperature of 80℃ is maintained to keep the chamber clean. A Schematic for the custom-built PEALD is shown as Fig 1.15. Thin films of SiO_2, HfO_2, Ga_2O_3, Al_2O_3 and ZnO were deposited using TDMAS, $[(CH_3)(C_2H_5)\mathrm{N}]_4Hf$, Ga(acac)₃, DMAI, and TMZn as metal precursor respectively.

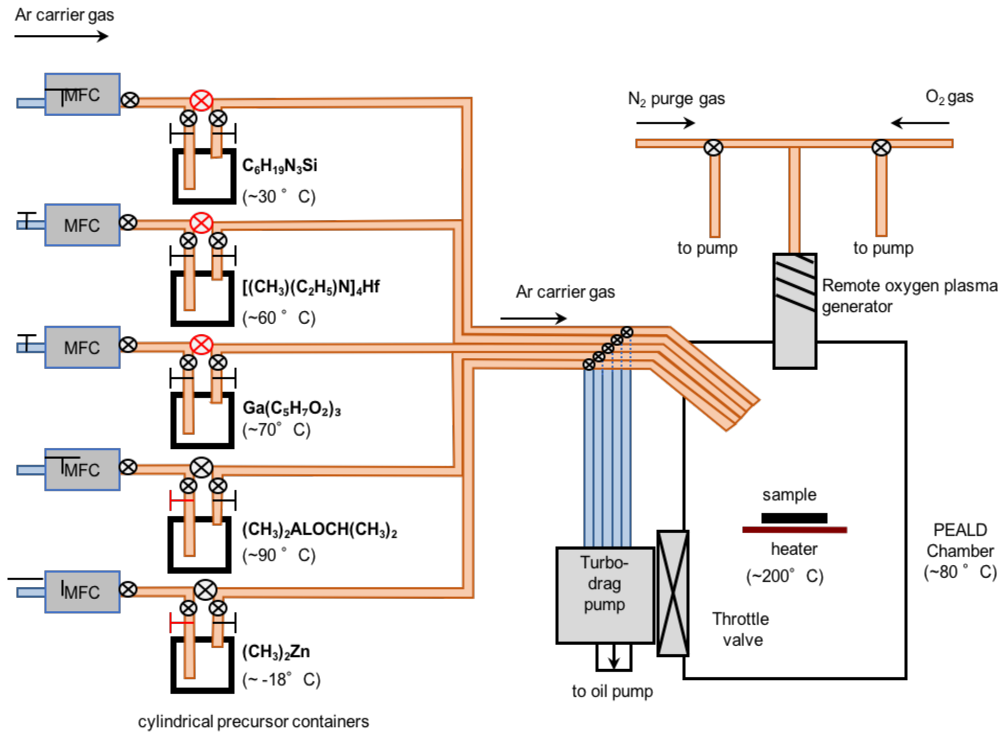

Figure 1.15 Schematic of the PEALD system in NSL at Arizona State University.

A PEALD cycle starts with a surface with $-\mathrm{OH}$ groups. First the precursor will be absorbed on the surface by ligand exchange; a following N_2 purge will remove the unabsorbed precursor molecules and byproduct; thirdly remote plasma radicals will oxidize the absorbed precursor and produce metal oxide and the surface; lastly, another N_2 purge will remove all the byproducts and unreacted precursors, leaving a new $-\mathrm{OH}$ rich surface. This process and the timing is shown as Fig. 1.16 and Fig 1.17.

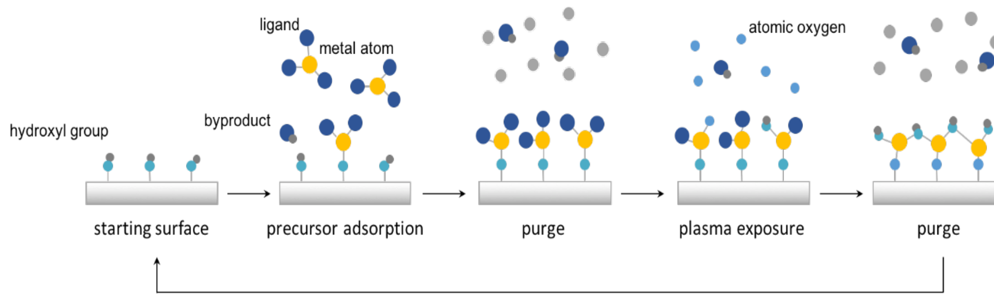

Figure 1.16 Schematic for a PEALD cycle

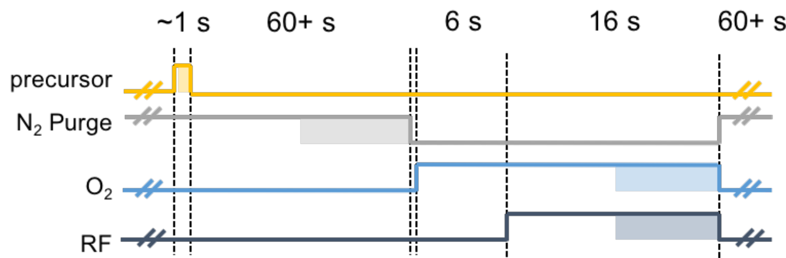

Figure 1.17 Optimized PEALD process of a cycle for the self-limiting deposition.

1.4 Advantages of PEALD

PEALD has relatively higher growth rates than thermal ALD. Plasma species are generated with a higher reactively than H_2O or O_3. High reactively of the oxidizer leads to a higher growth rate. For a plasma enhanced ALD process, the deposition could take place at a lower temperature. High reactively of the plasma species promised chemical reaction with less thermal energy on the surface. Fig. 1.18 to show an example of how much higher the growth rate using PEALD is than that of thermal ALD. For plasma assisted ALD, there could be a wider choice of precursors. Some precursors do not react with H_2O or O_3, but they could react with plasma species due to the higher reactivity. Also, less contamination has been observed within PEALD thin films than thermal ALD films. In the PEALD process, there could be a better control of film properties like stoichiometry, density and crystallinity.

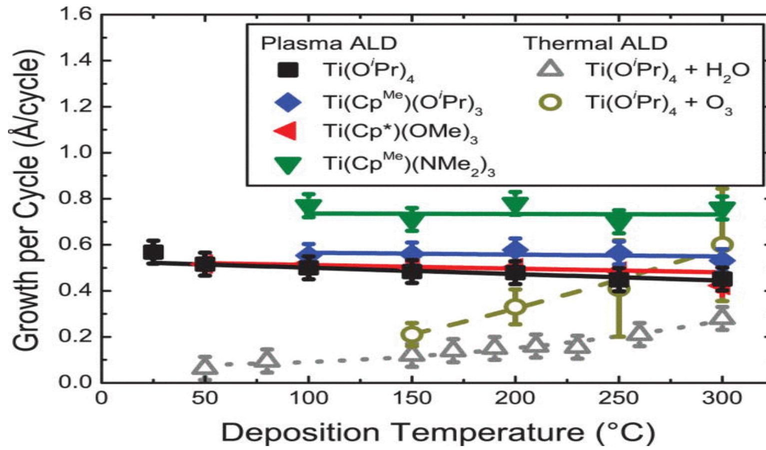

Figure 1.18 Comparison of PEALD and thermal ALD growth rate[46].

1.5 ALD *in-situ* reaction mechanism

Atomic layer deposition(ALD) is a technique to deposit thin films in a monolayer by monolayer fashion. An ALD process is extradinarily controlled and combines a number of cycyles based on gas phase chemical reactions. A nondecomposing precursor is aborsorbed on the surface for each step. Most ALD in-situ reactions follow the reaction rules[53]:

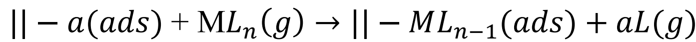

$$|| - a(ads) + \mathrm{M}L_n(g) \rightarrow || - ML_{n-1}(ads) + aL(g)$$

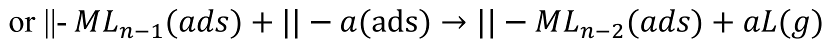

or $||- ML_{n-1}(ads) + || - a(\mathrm{ads}) \rightarrow || - ML_{n-2}(ads) + aL(g)$

where, ads means absorbed species, g meand gas phase, $|| - a$ usually means a clean surface with hydroxal groups. M represents metal molecule and L represents the ligands. In the absorption reaction, it is possible that more than one ligand will exchange with the surface group. The oxygen redicals are of high reactivity, so for most absorbed precursors, full oxidation of the ligands would be expected as[54]:

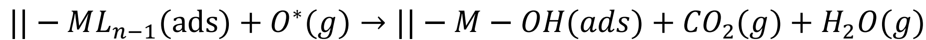

$$|| - ML_{n-1}(\mathrm{ads}) + O^*(g) \rightarrow || - M - OH(ads) + CO_2(g) + H_2O(g)$$

In case of using water as oxidizer, the oxidation reaction would be like[53]:

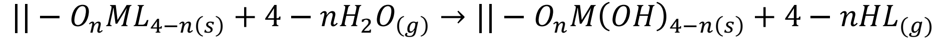

$$|| - O_nML_{4-n(s)} + 4 - nH_2O_{(g)} \rightarrow || - O_nM(OH)_{4-n(s)} + 4 - nHL_{(g)}$$

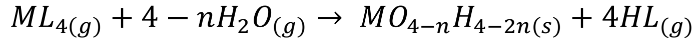

$$ML_{4(g)} + 4 - nH_2O_{(g)} \rightarrow MO_{4-n}H_{4-2n(s)} + 4HL_{(g)}$$

In this study, PEALD Ga_2O_3 uses Ga(acac)$_3$ as the metal precursor, and there is a samilar ALD process to deposition of IrO_2 using Ir(acac)$_3$, the reaction would be like[53][54]:

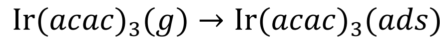

$$\mathrm{Ir}(acac)_3(g) \rightarrow \mathrm{Ir}(acac)_3(ads)$$

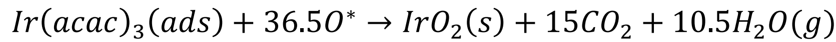

$$Ir(acac)_3(ads) + 36.5O^* \rightarrow IrO_2(s) + 15CO_2 + 10.5H_2O(g)$$

For the plasma enhanced ALD, during the plasma pulse, combustion of the absorbed precursor leaving only oxides and possible hydroxyl groups on the surface. Ga(acac)$_3$ follows the same reaction mechanism:

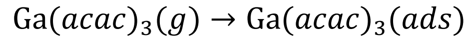

$$\mathrm{Ga}(acac)_3(g) \rightarrow \mathrm{Ga}(acac)_3(ads)$$

$$2Ga(acac)_3(ads) + 84\ O^* \rightarrow Ga_2O_3(s) + 30\ CO_2 + 21\ H_2O(g)$$

For alternative precursor, such as $GaMe_3$ and oxygen plasma process, the chemical reaction is as follows[54]:

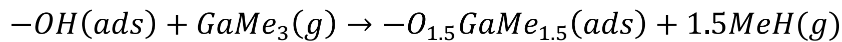

$$-OH(ads) + GaMe_3(g) \rightarrow -O_{1.5}GaMe_{1.5}(ads) + 1.5MeH(g)$$

Besides the chemical reaction mechanism, the spatial distribution of precursor molecules on the substrate, and the influence of steric hindrance of ligands on the growth rates are also studied. A couple of models to explain the theoretical growth rate from the molecule

species have been developed[55]–[57] by Puurunen R. For the ideal case the precursor ligand package is shown in Fig.1.8.1. In this case, the number of ligand is:

$$\Delta C_l = n\Delta C_M - \Delta C_a$$

where ΔC_M is the number of precursor molecules per unit area, which is equal to the number of the metal atoms per unit area, n is the number of ligands for each precursor molecule, ΔC_a is the number of released ligand per unit area after absorption. In many cases, different absorption methods would take place at the same time on the same surface, which makes the calculation of these parameters difficult. An assumption was made to further modify this model. In the ideal case, the precursor would package like Fig.1.8.1. The ligands are very tightly packed in the ideal case. A ligand coverage is further introduced to the model as:

$$\theta = \frac{\Delta C_l}{\Delta C_L^{maxthr}}$$

where, ΔC_L^{maxthr} is the maximum ideal ligand packaging density and ΔC_l is the real ligand packing density. ΔC_L^{maxthr} could be easily get from the ideal packaging structure.

$$\Delta C_L^{maxthr} = \frac{1}{\sqrt[2]{3r_L^2}}$$

θ is unity, however, it is very difficult to determine the ligand coverage experimentally. The θ is usually less than 1 due to the steric hindrance and limited reactive sites on the surface.

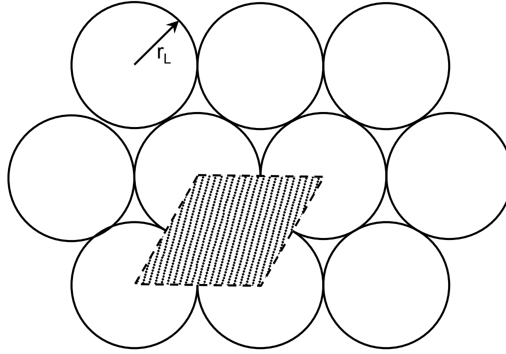

Figure 1.19 Ideal packing of precursor ligands[55]. Copyright 2003, WILEY-VCH Verlag GmbH & Co.

A reactive site reaction ratio is introduced to consider the situation where only a fraction of the reactive sites can serve as adsorption sites.

$$f = \frac{\Delta C_a}{C_a}$$

where, f is the reaction ratio of the active sites, C_a is the active sites per unit area and ΔC_a is the reactive sites that serve as adsorption sites. It is possible to determine the number of metal atoms per unit area by considering the previously discussed relation:

$$\Delta C_M = \frac{1}{n}(\theta \Delta C_L^{maxthr} + f C_a)$$

The growth per cycle would be:

$$\Delta h = \frac{M}{\rho N_A n}(\theta \Delta C_L^{maxthr} + f C_a)$$

where, Δh is the introduced height by the chemical reaction for every cycle, which is the same definition as growth rate per cycle (GPC). M and ρ are the material mass number (molecule mass) and density respectively, N_A is the Avogadro's number, which is 6.02×10^{23}/mole as a constant.

To evaluate the growth rate of a PEALD process, temperature is another factor that influences the growth rate. Fig. 1.20 shows some different GPC variations over substrate temperature.

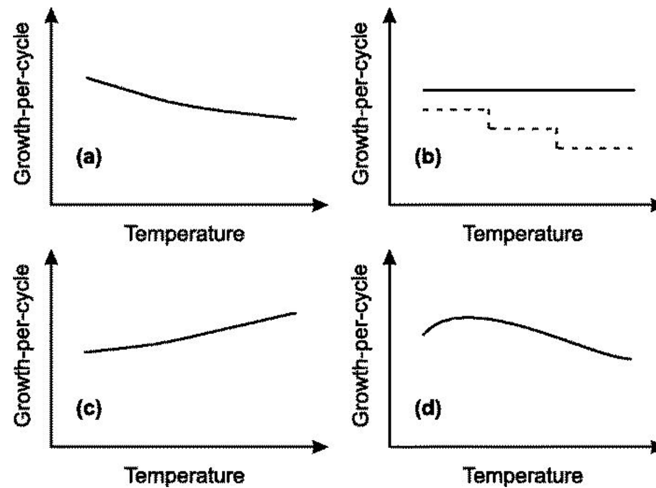

Figure 1.20 Possible growth per cycle (GPC) variation with deposition temperature with the growth window.

REFERENCE

[1] L. M. Garten, A. Zakutayev, J. D. Perkins, B. P. Gorman, P. F. Ndione, and D. S. Ginley, "Structure property relationships in gallium oxide thin films grown by pulsed laser deposition."

[2] "Polarized Raman spectra in β-Ga2O3 single crystals," *J. Cryst. Growth*, vol. 401, pp. 330–333, Sep. 2014.

[3] L. Li, W. Wei, and M. Behrens, "Synthesis and Characterization of α-, β-, and γ-Ga 2 O 3 prepared from Aqueous Solutions by Controlled Precipitation."

[4] "β-Ga2O3 versus ε-Ga2O3: Control of the crystal phase composition of gallium oxide thin film prepared by metal-organic chemical vapor deposition," *Appl. Surf. Sci.*, vol. 420, pp. 802–807, Oct. 2017.

[5] T. C. Lovejoy *et al.*, "Band bending and surface defects in β -Ga_2O_3," *Appl. Phys. Lett.*, vol. 100, no. 18, p. 181602, Apr. 2012.

[6] H. Feng *et al.*, "Fabrication and UV-sensing properties of one-dimensional β-Ga_2O_3 nanomaterials," *Phys. status solidi*, vol. 210, no. 9, p. n/a-n/a, Jun. 2013.

[7] Y. M. Juan *et al.*, "Effects of humidity and ultraviolet characteristics on β-Ga_2O_3 nanowire sensor," *RSC Adv.*, vol. 5, no. 103, pp. 84776–84781, Oct. 2015.

[8] M. Higashiwaki, K. Sasaki, A. Kuramata, T. Masui, and S. Yamakoshi, "Gallium oxide (Ga_2O_3) metal-semiconductor field-effect transistors on single-crystal β-Ga_2O_3 (010) substrates," *Appl. Phys. Lett.*, vol. 100, no. 1, p. 13504, Jan. 2012.

[9] "MBE grown Ga2O3 and its power device applications," *J. Cryst. Growth*, vol. 378, pp. 591–595, Sep. 2013.

[10] T. Oshima, T. Okuno, N. Arai, X. Zi-Li, Z. Rong, and X. Chang-Tai, *Appl. Phys. Express*, vol. 1, 2008.

[11] T. Minami *et al.*, *Appl. Phys. Express*, vol. 6, 2013.

[12] M. Nieminen, L. Niinisto, and E. Rauhalab, "Growth of gallium oxide thin films from gallium acetylacetonate by atomic layer epitaxy."

[13] G. Wagner *et al.*, "Homoepitaxial growth of β-Ga_2O_3 layers by metal-organic vapor phase epitaxy," *Phys. Status Solidi*, vol. 211, no. 1, pp. 27–33, 2014.

[14] F.-P. Yu, S.-L. Ou, and D.-S. Wuu, "Pulsed laser deposition of gallium oxide films for high performance solar-blind photodetectors," *Opt. Mater. Express*, vol. 5, no.

5, p. 1240, May 2015.

[15] T. Minami *et al.*, *Japanese J. Appl. Phys. Tadatsugu Minami al Jpn. J. Appl. Phys. Jpn. J. Appl. Phys*, vol. 39, no. 6A, pp. 524–526, 2000.

[16] "Low temperature Ga2O3 atomic layer deposition using gallium tri-isopropoxide and water," *Thin Solid Films*, vol. 546, pp. 31–34, Nov. 2013.

[17] "Polarized Raman spectra in β-Ga2O3 single crystals," *J. Cryst. Growth*, vol. 401, pp. 330–333, Sep. 2014.

[18] J. Yang, B. S. Eller, and R. J. Nemanich, *J. Appl. Phys.*, vol. 116, no. 12, p. 123702, Sep. 2014.

[19] Q. Wang *et al.*, "Direct Band Gap Silicon Allotropes," *J. Am. Chem. Soc.*, vol. 136, no. 28, pp. 9826–9829, Jul. 2014.

[20] W. Dai, H. Wang, S. Chen, D. Li, and D. Zhou, "Effect of point defects on band-gap properties in diamond structure photonic crystals," *J. Appl. Phys.*, vol. 111, 2012.

[21] "IEEE Xplore Full-Text PDF:" [Online]. Available: http://ieeexplore.ieee.org/stamp/stamp.jsp?arnumber=43098. [Accessed: 26-Oct-2017].

[22] M. Higashiwaki *et al.*, *Cit. Appl. Phys. Lett. Appl. Phys. Lett. Appl. Phys. Lett. J. Appl. Phys.*, vol. 1031, no. 10, 2013.

[23] M. A. Khan *et al.*, *Cit. Appl. Phys. Lett. J. Appl. Phys. J. Appl. Phys. J. Appl. Phys. Appl. Phys. Lett.*, vol. 77, no. 10, 2000.

[24] R. Vetury, N. Q. Zhang, S. Keller, and U. K. Misha, “The impact of surface states on the DC and RF characteristics of AlGaN/GaN HFETs,” *IEEE Trans. Electron Devices*, vol. 48, no. 3, pp. 560–566, 2001.

[25] E. D. Readinger, B. P. Luther, S. E. Mohney, and E. L. Piner, *J. Appl. Phys. Appl. Phys. Lett. J. Vac. Sci. Technol. A Vacuum, Surfaces, Film. Microstruct. Ti/Al ohmic contacts Appl. Phys. Lett. GaN Appl. Phys. Lett.*, vol. 89, no. 75, pp. 1004–2582, 2001.

[26] J. Yang, “Interface Electronic State Characterization of Plasma Enhanced Atomic Layer Deposited Dielectrics on GaN,” 2014.

[27] S. Ganguly, A. Konar, Z. Hu, H. Xing, and D. Jena, *Cit. Appl. Phys. Lett*, vol. 101, 2012.

[28] U. Karrer, O. Ambacher, and M. Stutzmann, *Cit. Appl. Phys. Lett. Appl. Phys. Lett. J. Appl. Phys. J. Appl. Phys. J. Appl. Phys. Appl. Phys. Lett. Appl. Phys. Lett.*, vol. 771, no. 63, pp. 1267–1685, 2012.

[29] R. Therrien, G. Lucovsky, and R. Davis, *Appl. Surf. Sci.*, vol. 166, no. 1–4, pp. 513–519, Oct. 2000.

[30] F. Ren *et al.*, “Effect of temperature on metal–oxide–semiconductor field-effect transistors Effect of temperature on Ga 2 O 3 " Gd 2 O 3 …/GaN metal–oxide–semiconductor field-effect transistors,” *Cit. Appl. Phys. Lett. Appl. Phys. Lett. GaN Appl. Phys. Lett. J. Chem. Phys.*, vol. 73, no. 10, 1998.

[31] C.-T. Lee, H.-W. Chen, and H.-Y. Lee, *Cit. Appl. Phys. Lett. Appl. Phys. Lett. J. Chem. Phys. Appl. Phys. Lett. J. Appl. Phys.*, vol. 821, no. 10, 2003.

[32] U. K. Mishra, P. Parikh, and Yi-Feng Wu, *Proc. IEEE*, vol. 90, no. 6, pp. 1022–1031, Jun. 2002.

[33] “Characterization of interface and border traps in ALD Al2O3/GaN MOS capacitors with two-step surface pretreatments on Ga-polar GaN,” *Appl. Surf. Sci.*, vol. 317, pp. 1022–1027, Oct. 2014.

[34] H.-Y. Shih, F.-C. Chu, A. Das, C.-Y. Lee, M.-J. Chen, and R.-M. Lin, “Atomic Layer Deposition of Gallium Oxide Films as Gate Dielectrics in AlGaN/GaN Metal–Oxide–Semiconductor High-Electron- Mobility Transistors.”

[35] P. K. Rao, *J. Appl. Phys. J. Appl. PhysicsAu Schottky contacts Heterostruct. Appl. Phys. Lett.*, vol. 110, no. 94, pp. 13716–23703, 2011.

[36] P. D. Ye *et al.*, *Appl. Phys. Lett.*, vol. 86, no. 6, p. 63501, Feb. 2005.

[37] D. S. Rawal *et al.*, *Thin Solid Films*, vol. 520, no. 24, pp. 7212–7218, Oct. 2012.

[38] M. Long, *IEEE Trans. Plasma Sci.*, vol. 34, no. 2, pp. 443–454, Apr. 2006.

[39] R. J. Shul *et al.*, “ECR, ICP, AND RIE PLASMA ETCHING OF GaN.”

[40] S. Kasthurirangan, A. N. Agnihotri, C. A. Desai, and L. C. Tribedi, *Rev. Sci. Instrum.*, vol. 83, no. 7, p. 73111, Jul. 2012.

[41] A. A. Sahai, T. C. Katsouleas, S. Gessner, M. Hogan, C. Joshi, and W. B. Mori, 2013, pp. 618–622.

[42] M. Sharif and A. Rafique, “Hot plasma waves in Schwarzschild magnetosphere,”

Astrophys. Space Sci., vol. 325, no. 2, pp. 227–240, Feb. 2010.

[43] "Cold plasma: A new technology to modify wheat flour functionality," *Food Chem.*, vol. 202, pp. 247–253, Jul. 2016.

[44] G. Foroutan and A. Akhoundi, *J. Appl. Phys.*, vol. 112, no. 7, p. 73301, Oct. 2012.

[45] "Correlation of the Debye sheath thickness and (Cr,Al)N coating properties for HPPMS, dcMS, CAE and PCAE processes," *Surf. Coatings Technol.*, Sep. 2017.

[46] H. B. Profijt, S. E. Potts, M. C. M. van de Sanden, and W. M. M. Kessels, *J. Vac. Sci. Technol. A Vacuum, Surfaces, Film.*, vol. 29, no. 5, p. 50801, Sep. 2011.

[47] H. B. Profijt, P. Kudlacek, M. C. M. van de Sanden, and W. M. M. Kessels, *J. Electrochem. Soc.*, vol. 158, no. 4, p. G88, Apr. 2011.

[48] R. K. Ramachandran *et al.*, "Plasma enhanced atomic layer deposition of Ga_2O_3 thin films," *J. Mater. Chem. A*, vol. 2, no. 45, pp. 19232–19238, Oct. 2014.

[49] V. R. Rai, V. Vandalon, and S. Agarwal, *Langmuir*, vol. 26, no. 17, pp. 13732–13735, Sep. 2010.

[50] H.-Y. Shih, F.-C. Chu, A. Das, C.-Y. Lee, M.-J. Chen, and R.-M. Lin, "Atomic Layer Deposition of Gallium Oxide Films as Gate Dielectrics in AlGaN/GaN Metal–Oxide–Semiconductor High-Electron- Mobility Transistors."

[51] I. Donmez, C. Ozgit-Akgun, and N. Biyikli, *J. Vac. Sci. Technol. A Vacuum, Surfaces, Film.*, vol. 31, no. 1, p. 01A110, Jan. 2013.

[52] V. R. Rai, V. Vandalon, and S. Agarwal, *Langmuir*, vol. 26, no. 17, pp. 13732–

13735, Sep. 2010.

[53] K. Knapas and M. Ritala, *Crit. Rev. Solid State Mater. Sci.*, vol. 38, no. 3, pp. 167–202, 2013.

[54] K. Knapas and M. Ritala, *Chem. Mater.*, vol. 23, no. 11, pp. 2766–2771, Jun. 2011.

[55] R. L. Puurunen, *Chem. Vap. Depos.*, vol. 9, no. 6, pp. 327–332, Dec. 2003.

[56] "Chromium(III) supported on aluminum-nitride-surfaced alumina: characteristics and dehydrogenation activity," *J. Catal.*, vol. 213, no. 2, pp. 281–290, Jan. 2003.

[57] R. L. Puurunen *et al.*, in *2011 16th International Solid-State Sensors, Actuators and Microsystems Conference*, 2011, pp. 978–981.

[58] V. Miikkulainen, M. Leskelä, M. Ritala, and R. L. Puurunen, *J. Appl. Phys.*, vol. 113, no. 2, p. 21301, Jan. 2013.

[59] T. Kamimura *et al.*, *Appl. Phys. Lett.*, vol. 104, no. 19, p. 192104, May 2014.

CHAPTER 2

EQUIPMENT AND EXPERIMENTS

Most of the experiments described herein were carried out at the nanoscience lab at ASU. Fig 2.1 shows the overall arrangement of the equipment connected with an ultra-high vacuum (UHV) T-line. The equipment connected through the T-line includes 2 load locks, UPS, AES, XPS, a newer XPS/UPS, e-beam, UV spectrometer, 2 MBE systems, oxide PEALD, H_2 plasma, ALE, fluoride PEALD, iPlasma, ECR system. *Ex-situ* AFM and wet bench for chemical cleaning will also be mentioned in this chapter.

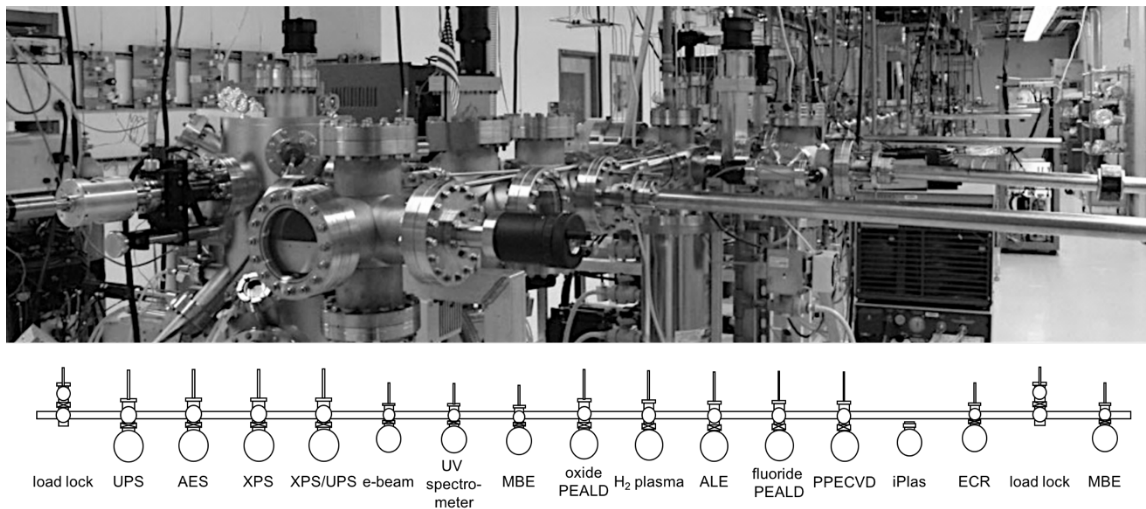

Figure 2.1 Equipment in the nano-science lab at ASU connected by an ultra-high vacuum T-line.

2.1 X-ray Photoelectron Spectroscopy (XPS) and Ultraviolet Photoelectron Spectroscopy (UPS)

Photoemission techniques are built based on the famous photon electron effect, described by Albert Einstein. X-ray photoemission spectroscopy (XPS) has been widely

used in band alignment for heterojunction measurements [1], identification of dopants' oxidation states, chemical bond shifts [2] and atomic constitution [3]. The photoemission system basically contains a monochromatic photon source and an analyzer. X-ray Photoelectron Spectroscopy (XPS) and Ultraviolet Photoelectron Spectroscopy (UPS) are the most commonly used photoemission techniques [4]– [14]. Photoemission spectroscopy, also called photoelectron spectroscopy (PES) is a widely used technique to determine the electron binding energy of a given material. X-ray Photoelectron Spectroscopy (XPS), also known as Electron Spectroscopy for chemical Analysis (ESCA), first developed by Kai Siegbahn in 1957 is the most widely used technique in material analysis.

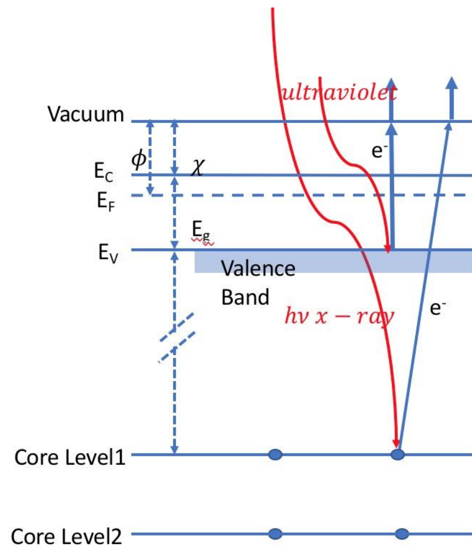

Figure 2.2 X-ray photoemission process and energy band diagram.

As is shown in Fig 2.2, the technique is an application of the photoelectric effect. X-ray photons are from the Al $K\alpha$ transition with an energy of 1486.6 eV. The electrons from the material were excited by the photon and leave the material surface with a certain

kinetic energy. The relation of the kinetic energy KE, photon energy $h\nu$, binding energy E_B and work function ϕ is as follows:

$$KE = h\upsilon - (E_B + \phi)$$

usually, the XPS spectrum is plotted by intensity (a.u.) verses Binding Energy (eV). The Fermi Level is aligned between the sample and analyzer as is shown in Fig. 2.1.2. Thus, the energy scale of XPS spectra usually start from the fermi level energy at eV.

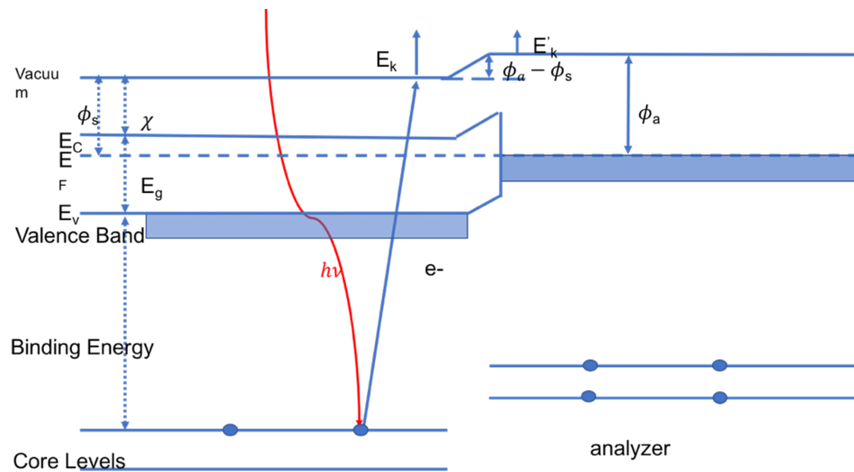

Figure 2.3. Schematic of binding energy reference of the sample and the analyzer

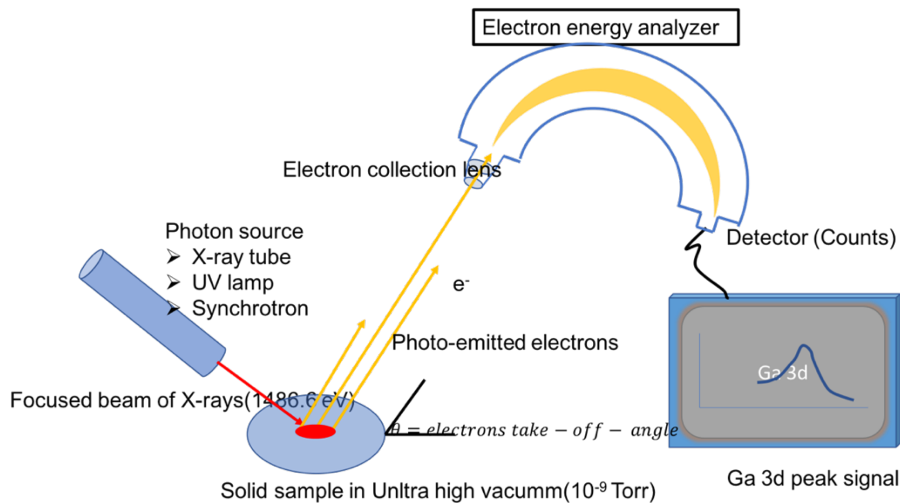

Fig. 2.4. Schematic and Basic constitution of the XPS system at the NSL, ASU.

2.2 Background Noise analysis in the XPS measurement

2.2.1 Surface charging during the XPS measurements

During the photoemission process, electrons are excited and leave the material surface. In case of low conductivity, the surface can become charged, causing a peak shift to a higher binding energy [15]. As is shown in Fig.2.5 the positive charge accumulated on the sample surface hence forms a local potential. The potential varies slightly over the sample surface, so the XPS peaks FWHM are larger, and the peak positions shift to a higher binding energy [16].

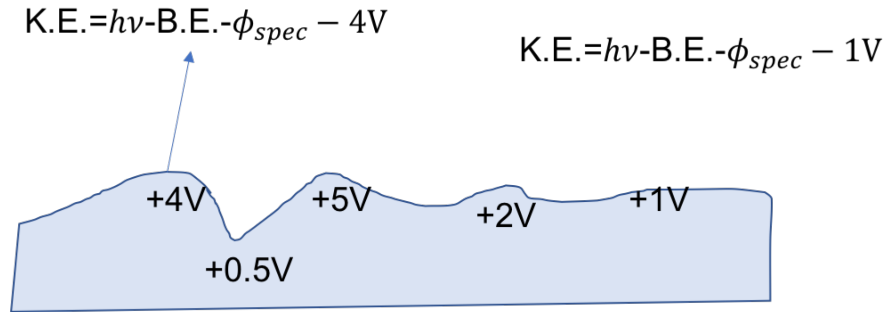

Fig.2.5. Schematic of a photoemission-charged sample surface with exaggerated roughness.

The kinetic energy of the photo emitted electron is

$$K.E. = h\upsilon - B.E - \phi_{spec} - V_{Charging}$$

where K.E is the kinetic energy (K.E.), $h\upsilon$ is the photon energy. $\phi_{spec}$is the work function, and $V_{Charging}$ is the voltage caused by the surface charging varies along the sample surface. The surface charging could cause the peak to be broader and the core level position to shift to a higher binding energy.

Secondary electrons

During the process of photoemission, some electrons will leave the sample and reach vacuum with a kinetic energy of of $K.E. = h\upsilon - B.E - \phi_{spec}$, however, some electrons

will undergo inelastic collision with electrons in the sample [17]. Those electrons excited by the photon emitted electrons are called secondary electrons. This process will cause a background peak at a higher binding. As is Shown in Fig. 2.6, the inelastic tail peak is called Plasmon peak. The secondary electron might also cause a shake-up peak, which would also contribute to the background signal [17].

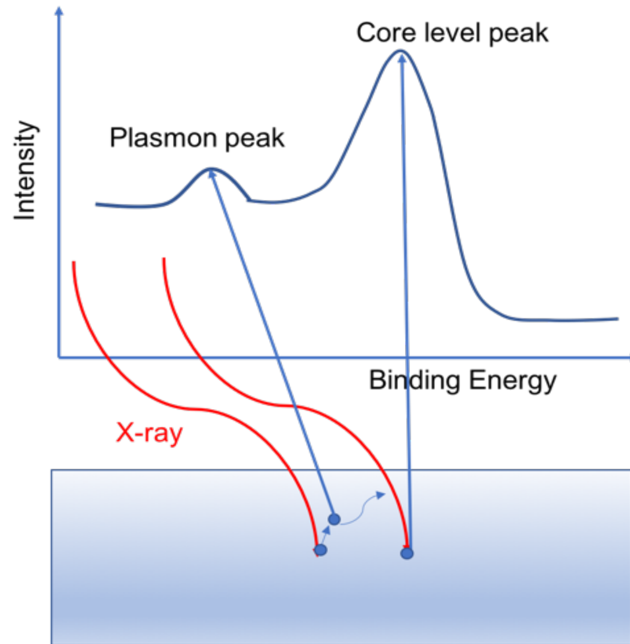

Fig.2.6. Schematic for a secondary electron emission process.

Auger peaks

During the process of photoemission, auger electron transition can occur simultaneously. The photoemission process would leave a hole in the core level. Some electrons at higher orbital energies might fall into the hole and transmit the energy to a third electron. The third electron could be emitted from the thin film to vacuum with a specified energy. This specified energy for Auger electrons is not related to the energy of the X-ray and it is a fingerprint of the atom energy levels. This phenomenon is widely used as Auger Electron Spectroscopy (AES) to characterize materials [18][19].

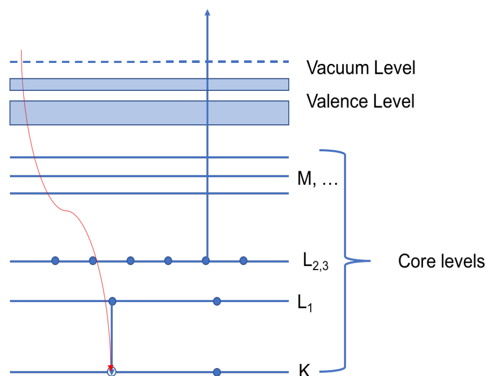

Fig. 2.7. Schematic for an Auger electron process.

Ghost peaks

The x-ray source is placed at high vacuum to prevent contamination. However, there are some cases when the x-ray source is contaminated, causing background noise in the XPS signal. Background noise caused by this reason are called ghost peaks.

Satellite peaks

In this study, x-ray photons are from Kα transition of Al source, which should be at a monochromatic energy level. However, other transitions are inevitable while the $K\alpha$ transition remains dominant. The photon energy could be at different levels other than 1486.6 eV, causing a different peak energy shift, which is called a satellite peak.

2.2.2 Fitting method for XPS graphs.

To analyze the XPS data, different fitting methods were applied to get better results. Based on the previous discussion. Fig. 2.1.4 shows various fitting methods considering backgrounds caused by the possible background process. upper-left graph is a typical original XPS graph; upper-right is the worst XPS-peak fitting; lower-left is fitting method considering secondary electrons and lower-right is fitting methods considering x-ray

satellites, chemically shift-species, shake-up peaks, Plasmon or other losses. The last one is considered as the best fitting method.

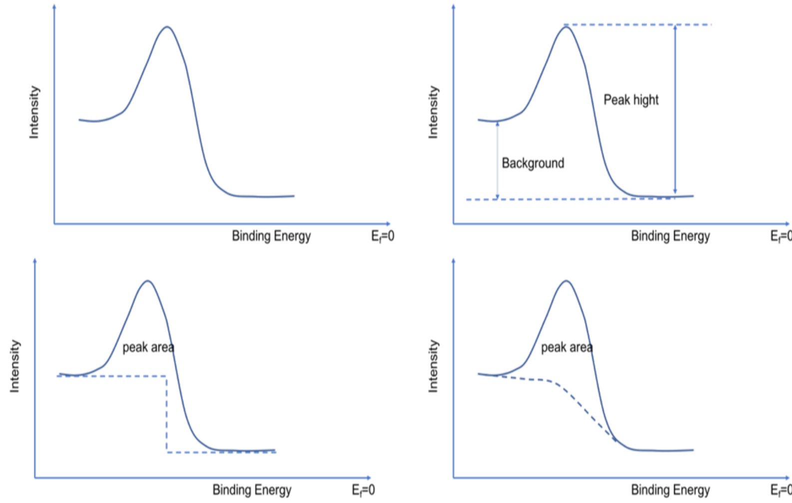

Fig. 2.8. A typical XPS graph and different fitting method.

2.3 Film composition, thickness and band gap calculation from XPS measurements

The composition of a thin film could be determined by analyzing the core level XPS intensities. For example, for Ga_2O_3 thin film, the concentration of an element X is calculated as [20][21]:

$$\%concentration = \frac{I_n}{s_n} / \Sigma_n^M \frac{I_n}{S_n}$$

Where, I_n is the integrated area of XPS peak for the nth elements, and s_n is the XPS sensitivity factor. M presents the total number of the elements in the thin film.

Atomic sensitivity factors for XPS are derived by setting the atomic sensitivity factor for F 1s as 1.00. Empirically derived data set from Physical Electronics and Varian IEE. The Data sheet is given in Table.1. The factor S is used as quantitative analysis of XPS data and using it the XPS peak area can be turned into atomic numbers in arbitrary unit [22].

Concentration and stoichiometry of a material could be derived by applying the sensitivity factors to the XPS data. The relative atomic number is given by:

$$n = \frac{I}{S}$$

The peak area is the integrated density of photoelectrons detected over the core level binding energy range. Theoretically, the peak area is derived as:

$$I = nf\sigma yAT\lambda$$

where n is the atomic density in cm^{-3}, f is the flux density of the X-ray, σ is the cross-section for the photoemission process, A is the area of the XPS analyzer that could detect the photoelectrons, T is the analyzer detection efficiency, and λ is the mean free path of the photoelectrons, which will be discussed later. Usually, the XPS detection depth limit could be a couple of photonelectron mean free path.

Atom ratio of elements 1 and 2 can be calculated as:

$$n_1 : n_2 = \frac{I_1}{s_1} : \frac{I_2}{S_2}$$

For thin films with thickness below the mean free path or thin absorbed species. The bulk sensitivity factor S doesn't work properly any more. A surface sensitivity factor S can be derived from the bulk sensitivity factor. Considering the XPS peak area of surface absorbed species, the theoretical intensity should be derived as:

$$I = n'f\sigma yAT\lambda$$

whereas n' is the atomic surface density in unit of cm^{-2}, while the rest parameters remain the same.

Hence the surface sensitivity factor $S' = \frac{S}{\lambda}$

Line	Element	Bulk S	Surface S	line	Bulk S	Surface S
1s	Li	0.0202	0.013			
	Be	0.059	0.039			
	B	0.13	0.09			
	C	0.25	0.18			
	N	0.42	0.33			
	O	0.66	0.57			
	F	1.00	1.00			
	Ne	1.5	1.8			
$2P^a$	Na	2.3	4.0	**2s**	0.13	0.08
	Mg	0.12	0.077		0.20	0.13
	Al	0.18	0.12		0.23	0.15
	Si	0.29	0.18		0.26	0.18
	P	0.39	0.26		0.29	0.20
	S	0.54	0.37		0.33	0.23
	Cl	0.73	0.51		0.37	0.27
	Ar	0.96	0.69		0.40	0.30
	K	1.24	0.92		0.43	0.34
	Ca	1.58	1.20		0.47	0.38
$2p_{3/2}$	Sc	1.65	1.31	**$3P^a$**	0.50	0.42
	Ti	1.20	0.99		0.54	0.48
	V	1.3	1.1		0.21	0.14
	Cr	1.5	1.35		0.21	0.14
	Mn	1.7	1.6		0.22	0.14
	Fe	2.0	2.0		0.26	0.17
	Co	2.5	2.8		0.35	0.23
	Ni	3.0	3.65		0.50	0.32
	Cu	4.2	5.6		0.65	0.42
	Zn	4.8	7.4		0.75	0.49

Line	Element	Bulk S	Surface S	line	Bulk S	Surface S
3d[a]	Ga	5.4	10.2		0.84	0.55
	Ge	0.38	0.24		0.92	0.62
	As	0.53	0.34		0.98	0.66
	Se	0.67	0.44		1.05	0.72
	Br	0.83	0.54		1.14	0.79
	Kr	1.02	0.69		1.23	0.86
	Rb	1.23	0.82		1.30	0.92
	Sr	1.48	1.00		1.38	1.00
	Y	1.76	1.20		1.47	1.09
	Zr	2.1	1.45		1.04	0.78
$3d^{5/2}$	Nb	2.4	1.7		1.10	0.85
	Mo	2.75	1.95		1.17	0.92
	Tc	1.9	1.37		1.24	1.00
	Ru	2.15	1.6		1.30	1.07
	Rh	2.4	1.83		1.38	1.17
	Pd	2.7	2.05		1.43	1.24
	Ag	3.1	2.4		1.52	1.37
	Cd	3.5	2.8		1.60	1.50
	In	3.9	3.2		1.68	1.64
	Sn	4.3	3.6		1.77	1.82
	Sb	4.8	4.2		1.00	0.64
	Te	5.4	4.9		1.23	0.79
	I	6.0	5.6		1.44	0.93
	Xe	6.6	6.5		1.72	1.12
	Cs	7.2	7.4		2.0	1.31
	Ba	7.9	8.7		2.35	1.55
4f[a]	Hf	2.05	1.30	**$4d^{5/2}$**	1.42	1.00
	Ta	2.4	1.53		1.50	1.07
	W	2.75	1.76		1.57	1.13
	Re	3.1	2.0		1.66	1.20
	Os	3.5	2.34		1.75	1.28

Line	Element	Bulk S	Surface S	line	Bulk S	Surface S
$4f^{7/2}$	Ir	3.95	2.55		1.84	1.36
	Pt	2.55	1.64		1.92	1.44
	Au	2.8	1.83		2.05	1.55
	Hg	3.15	2.1		2.15	1.64
	Ti	3.5	2.34		2.25	1.75
	Pb	3.85	3.5		2.35	1.87
	Bi	2.25	2.9		2.5	2.04
	Th	7.8	5.9		3.5	2.95
	U	9.0	7.0		3.85	3.35

Table. 2.1 XPS bulk sensitivity factor (Bulk S) and surface sensitivity factor (Surface S) chart [23]

Thin film thickness can also be derived from the XPS data and electron mean free path. And the band gap can be derived from the Plasmon peak. For example, the band gap of PEALD Ga_2O_3 can be derived from Energy Loss Spectrum (ELS) as is Shown in Fig. 2.4. Band gap measurement from Energy Loss Spectra (ELS).

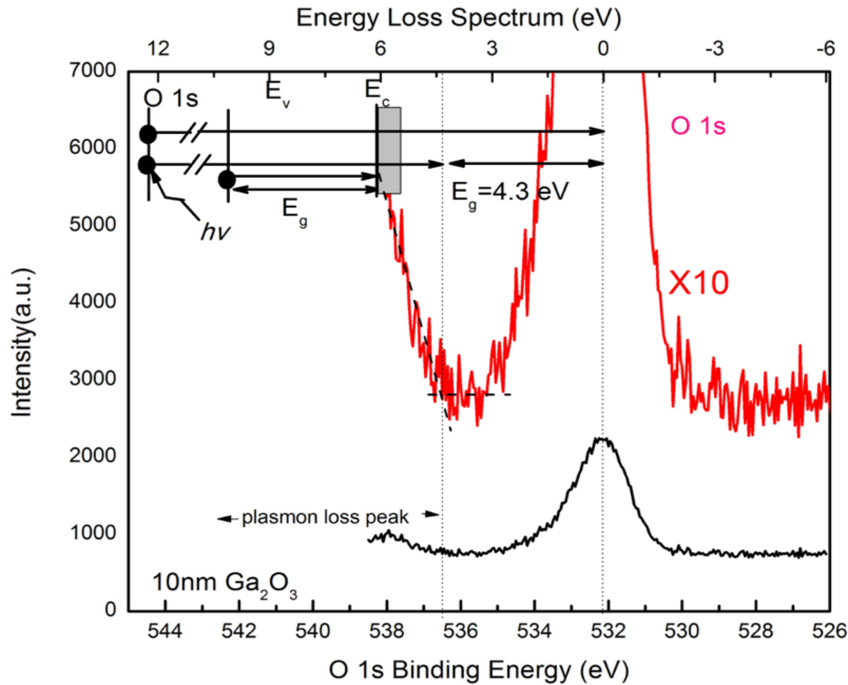

Figure 2.9 Band gap calculation from the O 1s energy loss spectra from 10 nm Ga2O3 on Si.

Energy loss spectra (ELS) have been used to determine the band gap of PEALD thin films usually by analyzing the O 1s peak XPS spectra [24]. During the photoemission process, most electrons will leave the surface with a certain kinetic energy. Some electrons could react with bond electrons in the higher core level or valence band, providing energy to excite the electron to the conduction band or vacuum level. The kinetic energy of the photoemission electron will decrease, and additional peaks will show at higher binding energy, called energy loss spectra. By analyzing the minimum binding energy of the ELS and the core level energy, the energy difference of valence band maximum (VBM) and conduction band minimum (CBM), namely band gap can be easily derived.

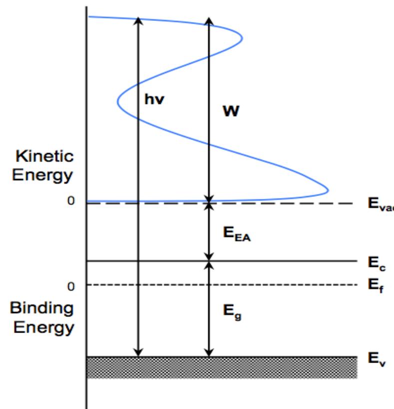

Figure 2.11 Schematic for a photoemission process in UPS measurements.

2.4 Band alignment and photoemission spectroscopy

Interface states and electronic configurations between two materials are very important information of a heterojunction. Ga_2O_3, as a wide band gap semiconductor material, has been combined with various materials such as GaAs, GaN, Al_2O_3 et. cl. A CBO of 1.5 ± 0.2 eV and CBO of 0.7 ± 0.2 eV has been reported for the interface of Al_2O_3/n-Ga_2O_3 heterojunction. Similar results have been observed using the Fowler-Nordheim model by analyzing the tunneling current of Al_2O_3/n-$Ga_2O_3(-201)$ interface[1]. The electron affinity and charge neutrality level models are the most commonly used model to decide the band alignment. X-ray/ultraviolet photoemission are the mostly commonly used equipment to measure the electronic states of a heterojunction.

Electron affinity Model

Band alignment of a heterojunction has attracted much interest since 1938, when Schottky and Mott developed a theory to explain the relation of the bands. So far, two different models have been commonly used to decide the band alignment. One is the

electron affinity model which assumes that the vacuum of two different material should align at the interface. In this model, the conduction band offset should be the difference of their electron affinities. Based on this assumption, the conduction band offset should be

$$\Delta E_C = \chi_1 - \chi_2$$

where ΔE_C is the conduction band offset, χ_1 is the electron affinity for the first material and χ_2 is the electron affinity for the other. This model is usually used in the case of semiconductor-semiconductor heterojunction or high-k dielectric-semiconductor interface[2].

Take Ga_2O_3 on GaN heterojunction for example, the conduction band offset should be:

$$\Delta E_C = \chi_{Ga2O3} - \chi_{GaN}$$

where χ_{Ga2O3} is the electron affinity for Ga_2O_3 and χ_{GaN} is the electron affinity for GaN. It would be easy to derive the valence band offset by considering of the band gap:

$$\Delta E_C = (\chi_1 + E_{g1}) - (\chi_2 + E_{g2}) = (I_1 - I_2)$$

Where I_1, I_2 are the photo threshold voltage for material 1 and material 2 in contacts. E_{g1} and E_{g2} are the band gap for material 1 and material 2 respectively. The photo threshold voltage for amorphous Ga_2O_3, oxygen covered GaN[3], Al_2O_3 and SiO_2 are 6.7eV,6.8eV, 8.5eV and 9.9 eV respectively. Based on the electron affinity model, the conduction band offset of Ga_2O_3, Al_2O_3 and SiO_2 on GaN are -0.1eV, 1.7eV, and 3.1eV respectively.

Charge Neutrality Level (CNL) Model

Charge neutrality level (CNL) model is one of the most commonly used models to deduce the band alignment of materials in contact with each other[4]. It was proposed theoretically by Tekedor and Flores and later refined by Tersoff. The CNL is one of the

most important parameters for semiconducting materials. The CNL of a material is the weighted average of density states as is shown in Fig 2.22. In this model, the vacuum level does not align any more, instead, there is some interface states of the heterojunction. For example, if the metal if in contact with a dielectric, the electron wave function will decay exponentially across the interface [5]. The electron waves across the interface will form available sates on the other side of the heterojunction. The states will function like donor states near the conduction band and acceptor states near the valence band [6]. Because of the charge transfer at the interface, a surface dipole and a local voltage would be formed. In such case, the vacuum levels do not align any more, instead, it is the CNL that aligns.

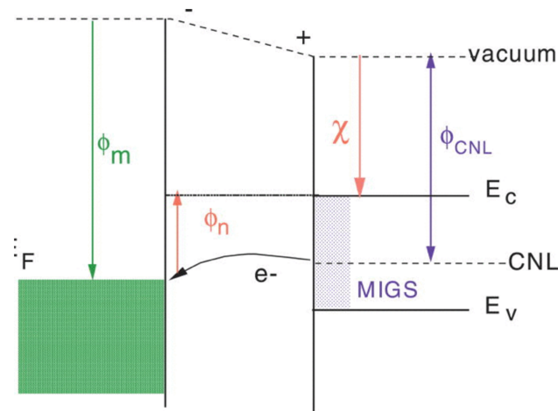

Figure 2.22 Charge transfer between the metal Fermi level and semiconductor CNL.

	Band gap (eV)	EA (eV)	ε_∞	CNL(eV)						
				Calc. here	Tersoff	Van de walle	Zunger	TB	Expt.	Used
Si	1.12	4.05	12	0.3	0.36	0.3		0.03	0.35	0.2
Ge	0.67	4.13	16		0.18	-0.25		-0.3	0.11	0.1
SiC 3C	2.35	4.55	6.7	1.61		1.26		1.44		1.3
SiC 6H	3.05	3.85	6.7	1.9						1.55
SiC 4H	3.25	3.65	6.7							1.55
AlP	2.56	2.8	8.0		1.27	1.69	1.5	1.13		1.3
GaP	2.25	3.2	9.1	0.83	0.81	1.0	0.97	0.83	1.0	0.8
InP	1.34	4.4	9.6		0.76	0.58	0.86	0.86		0.6
AlAs	2.16	3.54	9.1	0.92	1.05	1.02	1.0	0.92	1.02	0.92
GaAs	1.45	4.15	10.9	0.5	0.50	0.42	0.5	0.52	0.54	0.55
InAs	0.36	4.9	12.3	0.69	0.45	0.16	0.44	0.50		0.50
AlSb	1.7	3.6	10.2		0.55	0.05	0.35	0.53	0.56	0.4
GaSb	0.75	4.06	14.4		0.07	-0.28	-0.07	0.16	0.07	0.06
InSb	0.17	4.59	15.7	0.22	0.01	-0.34	-0.06	0.22	0.00	0.15
InN	0.76	5	7.9	1.87		1.88	1.88	1.50		1.87
GaN	3.2	3.3	6.0	2.88		2.17	2.14	2.37	2.45	2.3
AlN	6.2	0.6	4.8	3.97		2.87	2.94	2.97		2.8
ZnO	3.4	4.6	4	3.27						3.27

Table 2.2 The material properties and parameters for different semiconductors.

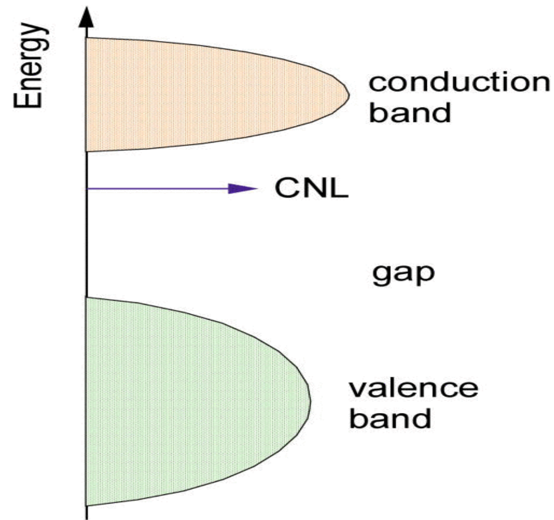

Figure 2.23 Charge neutrality level (CNL) is the weighted average of density of states.

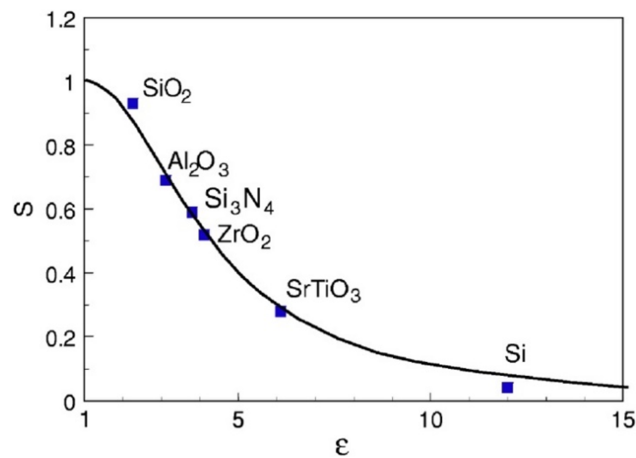

Figure 1.23 S-factor of insulators with different dielectric constant ε.

To combine the of electron affinity Model and charge neutrality level model, an empirical factor S is developed which is based on the dielectric constant of the material. S factor for different materials with different dielectric constant ε are shown in Fig. 1.23[10] and the relation is as:

$$s = \frac{1}{1 + 0.1(\epsilon_{\infty} - 1)^2}$$

when S=1, which represent the Schottky Mott limit, the heterojunction aligns at the vacuum level for highly unscreened cases, and when S=0, which represents the Bardeen limit, the heterojunction aligns at the Charge neutrality level for highly screened cases.

$$\Delta E_V = E_{CNL1} - E_{CNL2} - S[(E_{g2} + \chi_2) - ((E_{g1} + \chi_1) - (E_{CNL2}))]$$

where, E_{CNL1} and E_{CNL2} are the calculated charge neutrality level for material 1 and material 2 in contact respectively.

$$\Delta \mathrm{V} = E_{CNL1} - E_{CNL2} - S[(E_{g2} + \chi_2) - ((E_{g1} + \chi_1) - (E_{CNL2}))]$$

whereas, when S=1, in the case of Schottky limit, the heterojunction aligns at the vacuum level, for the other limit case of S=0, Bardeen limit, the heterojunction aligns at the Charge neutrality level. In this theory, the CNL is not always the Fermi level. Instead, there could be an energy off from the CNL to the Fermi level. The relationship of CNL and gap ration is shown Fig. 2.24.

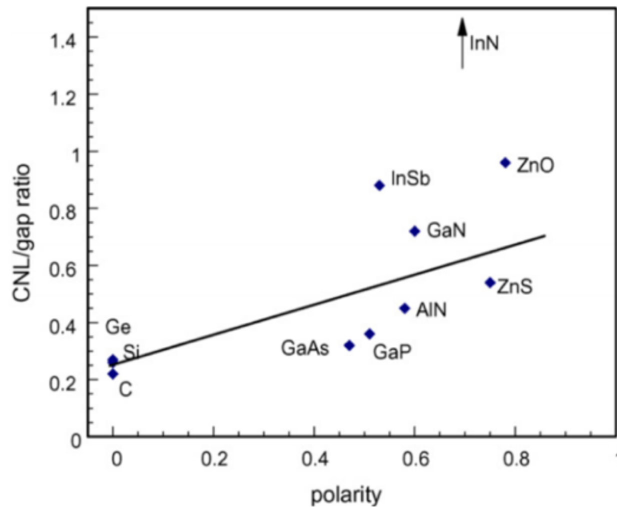

Fig. 2.24. Variation of CNL/gap ratio

Material	Band offset	
	VBO	CBO
$GaAs$	2.4	0.8
$InAs$	2.6	1.8
Al_2O_3	1.5	0.7
GaN	1.1	0.5

Table 2.3 Calculated valence band offset and conduction band offset of various materials on Ga_2O_3 based on the Charge Neutrality Model (CNL) [1].

Material	Band offset	
	VBO	CBO
AlN	0.4	2.4
Al_2O_3	3.0	2.4
Ga_2O_3	0.7	0.5
Gd_2O_3	0.7	1.9
HfO_2	1.6	1.1
Hf_2SiO_4	1.7	1.6
$LaAlO_3$	1.3	1.1
La_2O_3	0.7	2.0
$PbTiO_3$	-0.2	0.4
Sc_2O_3	0.7	2.0
Si_3N_4	0.8	1.3
SiO_2	3.1	2.6
$SrTiO_3$	0.2	-0.1
Ta_2O_5	1.1	0.1
Y_2O_3	0.8	1.9
ZnO	0.9	-0.7
ZrO_3	1.6	1.1

Table 2.4 Calculated valence band offset and conduction band offset of various materials on GaN based on the Charge Neutrality Model (CNL)[4].

	Gap(eV)	EA(eV)	CNL(eV)	ε_∞	S	S(Expt.)
HfO_2	6.0	2.4	3.7	4	053	0.52
ZrO_2	5.8	2.5	3.6	4.8	0.41	0.52
$HfSiO_4$	6.5	2	3.6	3.8	0.56	
La_2O_3	6.0	2	2.4	4	0.53	
LaALO_2	5.6	2.5	3.8	4	0.53	
$SrTiO_3$	3.3	3.9	2.3	6.1	0.28	0.28
PbO_3	3.4	3.5	1.9	6.25	0.27	
Ta_2O_5	4.4	3.3	3.3	4.84	0.4	
Ga_2O_3	4.8	3.5	2.8	4.2	0.49	
Gd_2O_3	5.8	2.4	2.3	4.8	0.41	
Al_2O_3	8.8	1	6	3.12	0.69	0.69
SiO_2	9	0.9	4.5	2.25	0.86	0.95
Si_2N_4	5.3	2.1	2.6	3.8	0.56	0.59

Table 2.5 Parameters for various dielectrics, whereas Gap is band gap (eV).

2.5 Plasma-enhanced atomic layer deposition (PEALD)

The PEALD system is the key equipment in this study. All the metal precursors are stock in containers maintained at a certain temperature. The flow of metal precursors into the ALD chamber are controlled by mass flow controller (MFC) and N_2 valves. Inductively coupled plasma reactor source with RF at 13.56 MHZ.

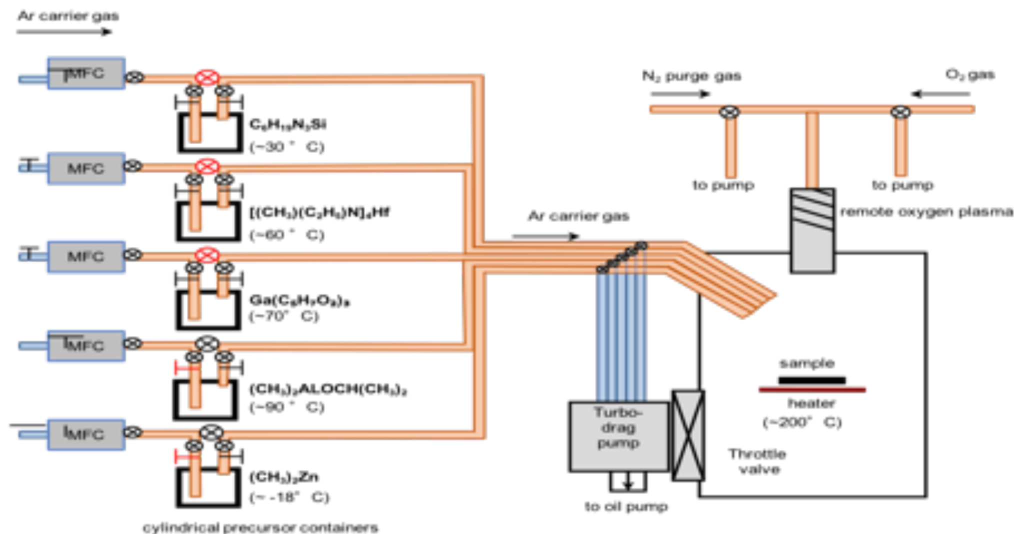

Figure 2.25 Schematic for the plasma enhanced atomic layer deposition system.

Ultraviolet photoelectron spectroscopy (UPS)

Ultraviolet photoelectron spectroscopy (UPS) was developed in 1962 by David W. Turner at Imperial College and Oxford University. UPS utilizes low energy ultraviolet photons and various UV photon sources as developed afterwards a listed in Table 2.6. For the UPS system at NSL lab, the UV source was from a helium lamp with an energy of 21.2eV.

Gas	Photon energy (eV)	Wavelength (Å)
Ar I	11.7	1060
Ne I	16.8	738
He I	21.2	585
Ne II	26.9	461
Ar II	30.3	409
He II	40.8	304

Table 2.6 Alternative UV source

Photoemission electrons leave the sample surface with much lower kinetic energy compared with those in the XPS photoemission process. Fig. 2.26 shows an example of a UPS spectra.

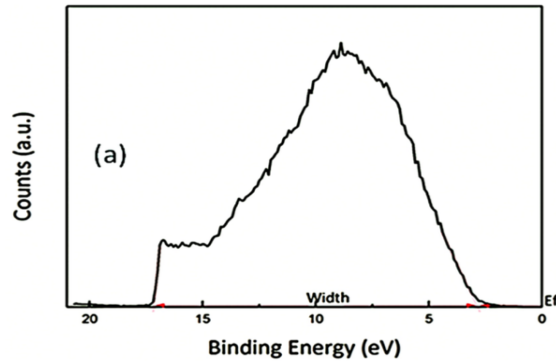

Figure 2.26 An example of UPS spectrum [25].

2.6 Atomic force microscopy (AFM)

Atomic force microscopy(AFM), also called scanning force microscopy (SFM) has a resolution of several angstrom [26]. AFM has a microscopic resolution 1000 times better than that of a microscope. The tip is in "contact" with the sample surface and the laser gets reflected by the backside of the tip. A photodiode detects the reflected laser and the height of the surface is so derived. The basic idea of AFM is shown in Fig. 2.27. Possible AFM artifact due to steep cave sample topography (left) AFM artifact due to steep curvature sample topography (right) is as shown in Fig. 2.28.

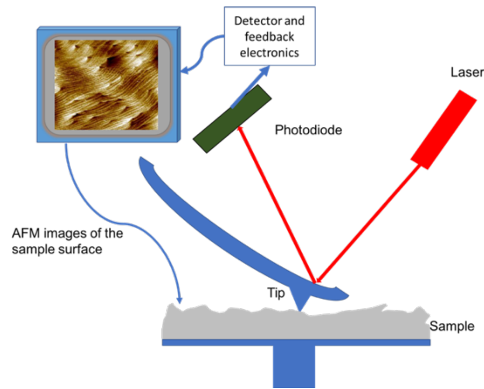

Figure 2.27 Schematic for an Atomic Force Microscope (AFM) system.

Figure 2.28 Possible artifacts from AFM measurement.

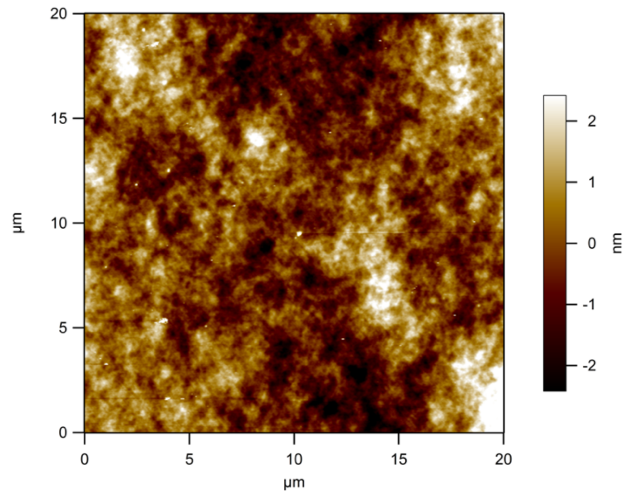

Fig. 2.29. AFM images of PEALD Ga_2O_3 on Si with 20 µm × 20 µm scan size.

The AFM image, despite a high resolution, is not necessarily a good reflection of the surface situation. In many cases, there can be artifacts, for example, the tip might not get anywhere in the steep cave, so the sample topography will be measured as the right part of Fig. 2.28(a). Also, in the opposite case, when there is a steep curvature on the surface,

the tip couldn't go to any corner of the curvature, so the sample topography is measured as the right part of Fig. 2.28(b) Fig 2.29 is an example of an AFM image of a polished Si wafer (100) face.

2.7 X-ray reflectivity

X-ray reflectivity (XRR) is a technique used to measure thin film density and thickness and surface roughness of one thin layer or multiple layers nondestructively. The mechanism is as shown in Fig. 2.30 and Fig. 2.31. X-ray has a refractive index smaller than 1. The incident x-ray gets refracted on the sample surface and reflected on the interface between different layers. Interference of x-rays forms a pattern. Film thickness, density, and roughness can be derived from the XRR graph [27].

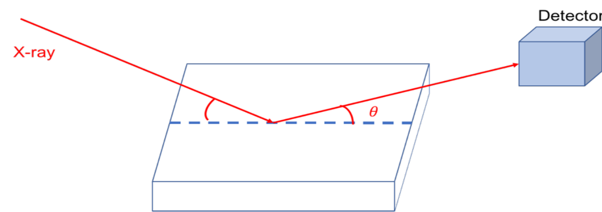

Figure 2.30 Schematic of x-ray reflectivity.

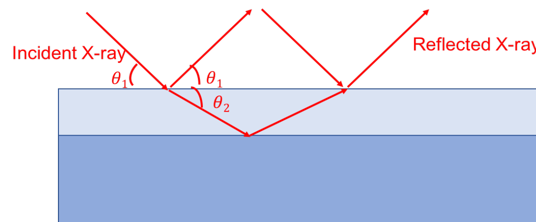

Figure 2.31 Schematic of the mechanism for X-ray reflectivity measurements.

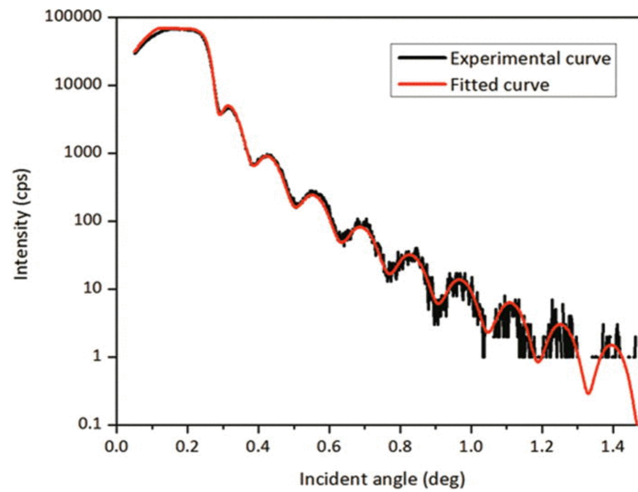

Figure 2.32 XRR image of a 30 nm PEALD Al_2O_3 film on Si.

2.8 REFERENCE

[1] N. A. Khan, M. Mumtaz, M. M. Ahadian, and A. Iraji-zad, “X-ray photo-emission studies of Cu1−xTlxBa2Ca3Cu4O12−y superconductor thin films,” Phys. C Supercond., vol. 449, no. 1, pp. 47–52, Nov. 2006.

[2] A. Talbi *et al.*, “Nitridation of InP(1 0 0) substrates studied by XPS spectroscopy and electrical analysis,” *Mater. Sci. Eng. A*, vol. 437, pp. 254–258, 2006.

[3] A. Majid, N. Ahmad, M. Rizwan, S. Ud-din Khan, F. Abdulraqeb Ahmed Ali, and J. Zhu, “Effects of Mn Ion Implantation on XPS Spectroscopy of GaN Thin Films,” *J. Electron. Mater.*, vol. 47.

[4] P. Pal, P. Kumar, A. V., A. Dogra, and A. G. Joshi, *J. Appl. Phys.*, vol. 116, no. 5, p. 53704, Aug. 2014.

[5] J. Portman, H. Zhang, K. Makino, C. Y. Ruan, M. Berz, and P. M. Duxbury, *J. Appl. Phys.*, vol. 116, no. 17, p. 174302, Nov. 2014.

[6] M. Kaur, "Photoinduced Charge Transfer at Metal Oxide/Oxide Interfaces Prepared with Plasma Enhanced Atomic Layer Deposition," 2016.

[7] J. C. Dhar, A. Mondal, N. K. Singh, and K. K. Chattopadhyay, *J. Appl. Phys.*, vol. 113, no. 17, p. 174304, May 2013.

[8] Y. He *et al.*, "Invited Article: High resolution angle resolved photoemission with tabletop 11 eV laser," *Rev. Sci. Instrum.*, vol. 87, no. 1, p. 11301, Jan. 2016.

[9] A. J. Leenheer, P. Narang, N. S. Lewis, and H. A. Atwater, *J. Appl. Phys.*, vol. 115, no. 13, p. 134301, Apr. 2014.

[10] S. Kumar, R. Prakash, R. J. Choudhary, and D. M. Phase, *J. Appl. Phys.*, vol. 120, no. 12, p. 125309, Sep. 2016.

[11] M. Schaefer and R. Schlaf, *J. Appl. Phys.*, vol. 118, no. 6, p. 65306, Aug. 2015.

[12] J. Osterwalder, *J. Phys. Condens. Matter*, vol. 24, no. 17, p. 171001, May 2012.

[13] J. Yang, B. S. Eller, and R. J. Nemanich, "Surface band bending and band

alignment of plasma enhanced atomic layer deposited dielectrics on Ga- and N-face gallium nitride," *J. Appl. Phys.*, vol. 116, no. 12, p. 123702, Sep. 2014.

[14] H. Optical Society of America. and Y. American Institute of Physics., *Review of scientific instruments.*, vol. 87, no. 1. Optical Society of America, 1930.

[15] "Surface morphological influence on charging at metal–insulator interface in XPS depth profiling," *Appl. Surf. Sci.*, vol. 228, no. 1–4, pp. 292–296, Apr. 2004.

[16] I. J. Villar-Garcia *et al.*, *Phys. Chem. Chem. Phys.*, vol. 13, no. 7, pp. 2797–2808, Feb. 2011.

[17] M. Cao, N. Zhang, T.-C. Hu, F. Wang, and W.-Z. Cui, *J. Phys. D. Appl. Phys.*, vol. 48, no. 5, p. 55501, Feb. 2015.

[18] "Time-dependent investigation of sub-monolayers of Ni on Pd using Positron-annihilation induced Auger Electron Spectroscopy and XPS," *Surf. Sci.*, vol. 643, pp. 178–182, Jan. 2016.

[19] C.-Y. Tang, R. T. Haasch, and S. J. Dillon, *Chem. Commun.*, vol. 52, no. 90, pp. 13257–13260, Nov. 2016.

[20] *Appl. Surf. Sci.*, vol. 135, no. 1–4, pp. 318–330, Sep. 1998.

[21] J.-N. Kim, K.-S. Shin, B.-O. Park, J.-H. Lee, N.-K. Kim, and S.-H. Cho, *Smart Mater. Struct*, vol. 12, no. 3, pp. 565–570, 2003.

[22] "Studies of iron and iron oxide layers by electron spectroscopes," *Appl. Surf. Sci.*, vol. 252, no. 2, pp. 330–338, Oct. 2005.

[23] C. D. Wagner, *J. Electron Spectrosc. Relat. Phenom. Elsevier Sci. Publ. B.V*, vol. 32, pp. 99–102, 1983.

[24] J. Yang, B. S. Eller, M. Kaur, and R. J. Nemanich, *J. Vac. Sci. Technol. A Vacuum, Surfaces, Film.*, vol. 32, no. 2, p. 21514, Mar. 2014.

[25] J. Yang, B. S. Eller, and R. J. Nemanich, *J. Appl. Phys. GaN AlGaN J. Vac. Sci. Technol. A Vacuum, Surfaces, Film. J. Appl. Phys. J. Appl. Phys.*, vol. 1161, no. 10, pp. 123702–14111, 2014.

[26] "Insight into Hybrid Nanoscopy Techniques: STED AFM & STORM AFM," *Biophys. J.*, vol. 106, no. 2, p. 396a, Jan. 2014.

[27] W. H. Briscoe *et al.*, "Synchrotron XRR study of soft nanofilms at the mica–water interface," *Soft Matter*, vol. 8, no. 18, p. 5055, Apr. 2012.

CHAPTER 3

CHARACTERIZATION OF PLASMA ENHANCED ATOMIC LAYER DEPOSITED GA_2O_3 USING $GA(ACAC)_3$

In this research, gallium oxide (Ga_2O_3) thin films were deposited with remote plasma-enhanced atomic layer deposition using gallium (III) acetylacetonate ($Ga(acac)_3$). Growth conditions including $Ga(acac)_3$ precursor pulse time, O_2 plasma pulse time, N_2 purge time and deposition temperature were investigated and optimized on phosphorus doped Si (100) substrates.

Growth rate of 0.31 Å/cycle within a growth window between 150 ℃ and 320℃ has been observed. The growth in incomplete at temperature lower at 150 ℃ , while decomposition of precursor was observed at temperature above 320℃. PEALD Ga_2O_3 thin films are amorphous, with a band gap of 4.3$\pm$ 0.1 eV determined by energy loss spectroscopy (ELS) from the O 1s spectra, smaller compared than the 4.8 ~ 4.9 eV band-gap of beta-crystal Ga_2O_3[1]. PEALD Ga_2O_3 thin films, though not intentionally doped, are slightly n-type due to oxygen vacancies or other related defects. The density of Ga_2O_3 is 4.3 g/cm^3 measured with x-ray reflectivity. The atomic concentration of Ga_2O_3 thin films is as Ga: O=1:1.5 with a 10% error measured with XPS signal density.

3.1 Introduction

Ga_2O_3 is a wide band gap material with a band gap of 4.7-4.9 eV [1] for the different crystal morphology. It has five crystal structures, which are $\beta - Ga_2O_3$, $\alpha - Ga_2O_3$, $\gamma - Ga_2O_3$, $\delta - Ga_2O_3$, $\varepsilon - Ga_2O_3$[2]. $\beta - Ga_2O_3$ is the most stable form[3], and it has a band gap of 4.9 eV[4], theoretical breakdown voltage of 8 MV/cm, electron mobility of 300 $cm^2V^{-1}s^{-1}$ [5]. Ga_2O_3 has good thermal and chemical stability, with

melting point 1725℃ for $\beta - Ga_2O_3$ [6]. Ga_2O_3 thin film has been applied in gas sensor[7][8], UV detectors[7], FETs[6,7] and solar cells[11].

Crystalline Ga_2O_3, especially the most stable beta-phase, has been widely used in the past few years. However, the deposition temperature is usually high to deposit crystal Ga_2O_3 thin films. Amorphous Ga_2O_3 thin films have attracted research interest recently as room temperature growth is possible [12]–[14].

Ga_2O_3 thin film has been deposited by various techniques, such as Metal-Organic Chemical Vapor Deposition (MOCVD)[15], Atomic Layer Deposition (ALD)[16], metal-organic vapor phase epitaxy [17],pulsed laser deposition[18][19], and sol-gel process [20] .

For atomic layer deposition, a variety of precursors have been reported, such as trimethylgullium [21]–[23] , Gallium acetylactonate [16], $Ga_2(NMe_2)_6$ [24][25], dimethyl gallium isopropoxide (DMGIP) [15], gallium tris(alkoxide) complex ($\{GaH(L_2)\}_2$) and dimeric complex $(GaMe(L_2))_2$[26]. All the precursors have to be volatile and thermally stable. Precursor molecules must be able to react with surface groups, chemisorbed and reach saturation in a short time[27]. Different precursors have different *in-situ* chemical reaction mechanisms which can influence the growth parameters and thin film qualities [27][28]. Plasma assisted atomic layer deposition has a advantages than themal ALD [29], including reduced deposition temperature, increased choice of precursors, good control of stoichiometry, increased growth rate and enhanced processing versatility. For plasma enhanced atomic layer deposited Ga_2O_3 thin films, reported precursors include trimethyl-gallium[23][24], tris (2,2,6,6-tetramethyl-3,5-heptanedionate) gallium(III) $Ga(TMHD)_3$[32], $[(CH_3)_2GaNH_2]_3$[33]and trimethylgallium $Ga(CH_3)_3$ [31][34].

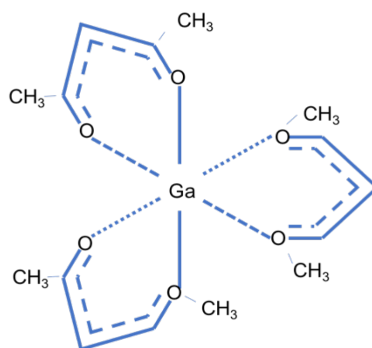

Figure 3.1 Schematic for a $Ga(acac)_3$ molecule.

$Ga(CH_3)_3$ is the most popular Ga precursor for ALD Ga_2O_3. However, $Ga(CH_3)_3$ is pyrophoric. $Ga(acac)_3$, is an alternative precursor for Ga_2O_3 by atomic layer deposition. $Ga(acac)_3$ reacts with H_2O, O_3 but not O_2 gas[16], however, with oxygen plasma enhanced ALD. Low temperature growth of Ga_2O_3 has been observed. In this research, plasma enhanced Atomic Layer Deposited Ga_2O_3 has been studied. Theoretically, PEALD Ga_2O_3 with $Ga(acac)_3$ should have a growth rate a little lower than that of TMG (0.53 Å/cycle) [31] due to the steric hindrance of $Ga(acac)_3$ molecules. A schematic for the $Ga(acac)_3$ molecule is shown in Fig 3.1 and a safety comparison was made between $Ga(acac)_3$ and TMG as shown in table 3.1.

	TMG	**$Ga(acac)_3$**
Chemical Formula	$Ga(CH_3)_3$	$Ga(C_5H_7O_2)_3$
Melting Point	-19 ℃	197 ℃
Safety Hazard	pyrophoric	non-pyrophoric

Table 3.1 Safety date sheet for $Ga(acac)_3$[35] and comparable Ga precursor trimethygallium[36].

In this research, the precursor molecules were carried through the pipelines bypassing the precursor container. $Ga(acac)_3$ has a vapor pressure of a 1 mTorr at ~90 ℃ , which provide sufficient molecules for deposition. $Ga(acac)_3$ molecules could be absorbed on the substrate surface chemically or physically [37]:

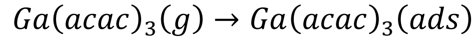

$$Ga(acac)_3(g) \rightarrow Ga(acac)_3(ads)$$

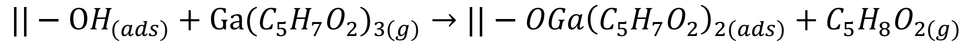

$$|| - OH_{(ads)} + \mathrm{Ga}(C_5H_7O_2)_{3(g)} \rightarrow || - OGa(C_5H_7O_2)_{2(ads)} + C_5H_8O_{2(g)}$$

Where $||$ represents the substrate surface and $-\mathrm{OH}$ represents the surface hydroxyl groups. The "ads" represents absorbed species and "g" represents the gas phase. The precursor gets absorbed in the sample surface, either by physically absorption due to van de waals force without ligand exchange or chemically absorption with acetyl acetone exchange with the hydroxyl group on the surface.

During the oxygen plasma pulse, combustion of the absorbed precursor leads to a Ga_2O_3 surface possibly with hydroxyl groups. The reaction during the oxygen plasma pulse would be like:

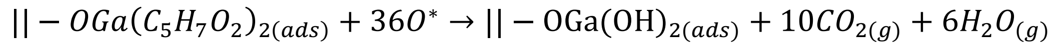

$$|| - OGa(C_5H_7O_2)_{2(ads)} + 36O^* \rightarrow || - \mathrm{OGa(OH)}_{2(ads)} + 10CO_{2(g)} + 6H_2O_{(g)}$$

The byproduct H_2O can also react with the precursor. However, the purge step could remove all the byproduct to prevent chemical reaction like[28]:

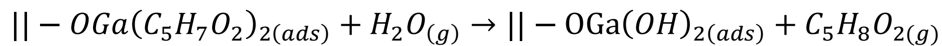

$$|| - OGa(C_5H_7O_2)_{2(ads)} + H_2O_{(g)} \rightarrow || - \mathrm{OGa}(OH)_{2(ads)} + C_5H_8O_{2(g)}$$

Besides the precursor, oxidizer has also been investigated[38]. For exsample, ALD Ga_2O_3 with $Ga(acac)_3$ and H_2O, ozone, and O_2 gas was reported. A growth rate of 0.23 Å/cycle with water and 0.21 Å/cycle with ozone has been reported, Also, no growth was observed so far by using O_2 gas as oxidizer[16]. In this study, oxidation process is radical-driven, which has a relatively long mean free path than ions and it is more reactive than oxygen gas. PEALD thin film tends to exhibit a better purity than ALD with water and Ozone [29].

3.2 Experiment

Ga_2O_3 thin films were deposited using a custom-built PEALD system, with $Ga(acac)_3$ and oxygen plasma. A base pressure of 5×10^{-7} Torr was maintained in the chamber, and during deposition, a pressure of 100 mTorr was maintained with a throttle valve in front of the turbo pump as is shown in Fig. 2. The $Ga(acac)_3$ precursor is heated to a temperature of 70 ℃ to maintain sufficient flux; thirdly, a 6s O_2 gas purge preceded the plasma step, afterwards a 200 W RF power with and 13.56 MHZ frequency to generate the O_2 plasma above the sample stage. The distance between the sample and O_2 plasma generator is about 25 cm, which helps to enable the flux of enough radicals and reduce the ion concentration that might cause damages on the surface.

A PEALD cycle consists four main steps. Before each cycle, the sample surface is rich of hydroxyl groups. Firstly, ultra-high purity Ar gas (99.999%) carries the $Ga(acac)_3$ molecules into the chamber, some molecules are chemisorbed on the surface, some are chemisorbed on the surface and the rest are wandering in the chamber; secondly, N_2 gas was carried into the chamber, this helps to remove residual $Ga(acac)_3$ molecules and byproducts from the chamber; Thirdly, oxygen plasma, mainly the radicals, oxidized the

absorbed ligand, and in some cases the byproducts; Lastly, another N_2 purge step will remove the by products in the chamber and leave a –OH group on the surface.

The growth rates were calibrated by x-ray reflectivity (XRR) and x-ray photoemission spectroscopy (XPS). The stoichiometry and electron bonding states are calibrated by XPS. For the XPS, it contains a K-alpha Al x-ray source, which is monochromatic at1484.6 eV energy. XPS. The filament for x-ray source is operated at 15 kV and 30mA. An analyzer is used to analyze the energy of the photo-emitted electrons. The deposition temperature is monitored both via a thermocouple and a pyrometer.

3.3 Results and Discussion

Self-limiting growth

A PEALD cycle consists four main steps as is shown in Fig. 3.3. All the steps are self-limiting after saturation. The first step is the precursor absorption, the second step is a N_2 purge, the third step is oxygen plasma exposure and last step is another N_2 purge. In this study, the saturation of each step, the plasma power and the temperature was studied to optimize the timing for each step.

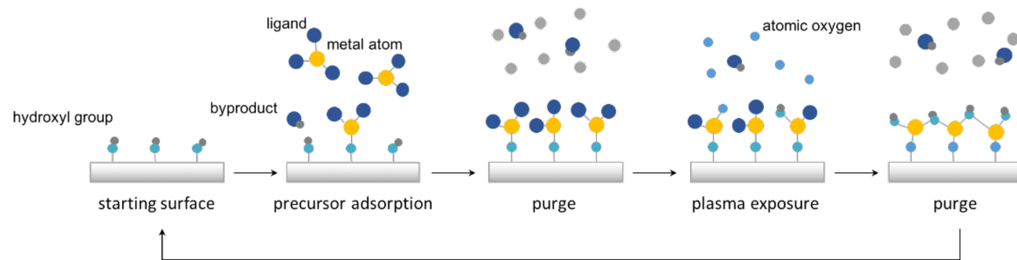

Figure 3.3 Schematic for a PEALD self-limiting cycle.

PEALD growth window

Low temperature deposition is one of the advantages of PEALD. For the PEALD process, temperature influences the growth rate greatly. In this study, the deposition

could happen at room temperature (30℃). At temperature lower than 150 ℃, a growth rate lower than 0.3 Å /cycle has been observed, suggesting an incomplete reaction, also for temperature higher than 320 ℃ thermal desorption occurs. A growth window is observed at temperature between 150℃ and 320℃, which is a large growth window shown in fig. 5. (b). As is shown in Fig. 5. (a), a saturation of Ga(acac)$_3$ does was observed at 0.6s. In this study, increased nitrogen purge time increased the GPC, maybe suggesting a prolonged nitrogen purge time can facilitate the deposition process by removing physisorbed layers and thereby augmenting the reaction between the chemisorbed layers and oxygen plasma. An oxygen plasma RF power of 100 W provided enough reactivity of oxygen radicals; Oxygen plasma pulse time of 16 s to achieve full oxidation. Nitrogen purge time of 160s to help increase the reactive sites for precursor adsorption, which is very interesting as nitrogen gas rarely influence the reaction other than remove extra molecules. This is relatively a long purge time compared with commercial ALD process and the reason is probably due to the big chamber of the PEALD system. Fig. 3.4. shows a growth rate of PEALD Ga_2O_3 using Ga(acac)$_3$ variation with Ga(acac)$_3$ pulse time, oxygen plasma RF power, O_2 plasma pulse time and N_2 purge time. Fig. 3.5 shows growth rate of PEALD Ga_2O_3 using Ga(acac)$_3$ variation with temperature. Incomplete reaction and desorption with lower growth rate on temperature lower than 150 ℃ and higher than 320 ℃ has been observed. A saturation of constant growth rate has been observed at temperature in between.

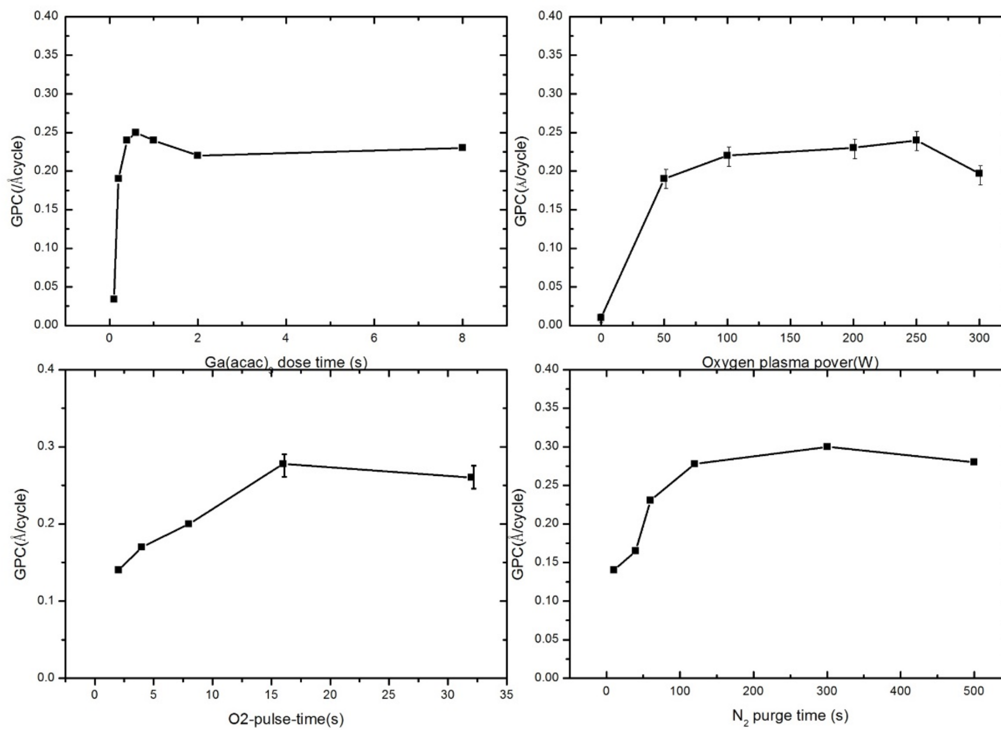

Figure 3.4 Characterization of ALD pulse timing.

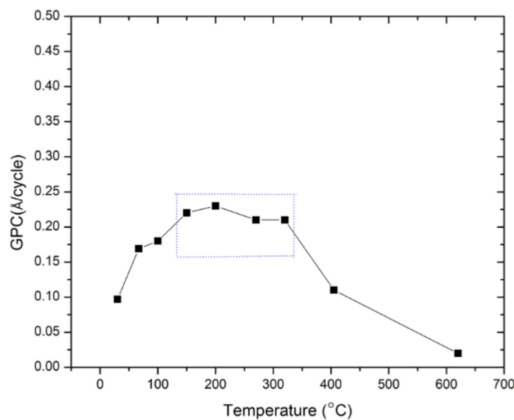

Figure 3.5 ALD growth rate vs temperature.

The band gap of PEALD Ga_2O_3 was determined to be 4.3 eV by energy loss spectra (ELS) of O 1s core level position in this study, smaller than that of crystal Ga_2O_3 with

reported band gap (4.2eV- 4.9eV), which indicate the films to be amorphous. The XPS and ELS graph is shown in Fig. 3.6.

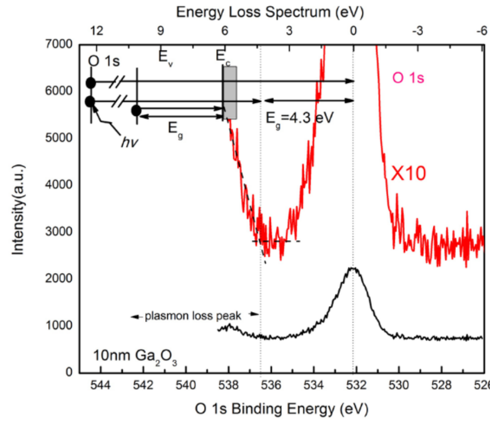

Figure 3.6 Schematic for the band gap of PEALD Ga_2O_3 thin films determined by ELS.

3.4 Conclusion

In this study, remote plasma enhanced atomic layer deposited Ga_2O_3 was deposited on Si wafers using $Ga(acac)_3$ as an alternative to pyrophoric Ga precursor TMG and oxygen plasma as oxidizer. In this study, influence of different parameters, including $Ga(acac)_3$ dose time, O_2 plasma pulse time, plasma power, N_2 purge time and deposition temperature were studied. With different parameters, growth rate, density, bonding states of the Ga_2O_3 thin films were studied. A self-saturated growth was obtained with a growth rate of 0.3 Å/cycle using longer than 0.6 s $Ga(acac)_3$ dose time, longer than 8s oxygen plasma pulse time, more than 100 W plasma power, longer than 120 s N_2 purge time, and a window temperature between 150 ℃ and 320 ℃, Thin films with mass density of 4.3 g/cm^3 and bang gap of 4.3± 0.1 eVwas observed for a self-saturated growth. Compared with a growth rate of 0.53 Å /cycle of PEALD Ga_2O_3 with TMG, the growth rate of 0.30 Å/cycle is relatively comparable, also the safety of using non-pyrophoric precursor has

obvious advantage over pyrophoric precursor TMG. The Ga:O ratio is determined to be 2:3 by XPS. The PEALD process with $Ga(acac)_3$, which has an obvious advantage than the pyrophoric precursor, has comparable considerable growth rate and film qualities.

3.5 REFERENCE

[1] T. Onuma *et al.*, *Cit. Appl. Phys. Lett. Appl. Phys. Lett. Appl. Phys. Lett. J. Appl. Phys. Appl. Phys. Lett. J. Chem. Phys.*, vol. 103, no. 10, pp. 41910–13504, 2013.

[2] R. Roy, V. G. Hill, and E. F. Osborn, "Polymorphism of Ga 2 O 3 and the System Ga 2 O 3 —H 2 O," *J. Am. Chem. Soc.*, vol. 74, no. 3, pp. 719–722, Feb. 1952.

[3] X. Feng, Z. Li, W. Mi, Y. Luo, and J. Ma, "Mg-doped β-Ga 2 O 3 films with tunable optical band gap prepared on MgO (110) substrates by metal-organic chemical vapor deposition," 2015.

[4] F. Zhu, Z. Yang, W. Zhou, and Y. Zhang, *Appl. Surf. Sci.*, vol. 252, no. 22, pp. 7930–7933, Sep. 2006.

[5] M. Higashiwaki, K. Sasaki, A. Kuramata, T. Masui, and S. Yamakoshi, *Phys. Status Solidi Appl. Mater. Sci.*, vol. 211, no. 1, pp. 21–26, 2014.

[6] F. Litimein, D. Rached, R. Khenata, and H. Baltache, *J. Alloys Compd.*, vol. 488, pp. 148–156, 2009.

[7] H. Feng *et al.*, "Fabrication and UV-sensing properties of one-dimensional β-Ga $_2$ O $_3$ nanomaterials," *Phys. status solidi*, vol. 210, no. 9, p. n/a-n/a, Jun. 2013.

[8] Y. M. Juan *et al.*, "Effects of humidity and ultraviolet characteristics on β-Ga $_2$ O $_3$ nanowire sensor," *RSC Adv.*, vol. 5, no. 103, pp. 84776–84781, Oct. 2015.

[9] "MBE grown Ga2O3 and its power device applications," *J. Cryst. Growth*, vol. 378, pp. 591–595, Sep. 2013.

[10] K. D. Chabak *et al.*, *Cit. Appl. Phys. Lett. Appl. Phys. Lett. Appl. Phys. Lett. Appl. Phys. Lett.*, vol. 1091, no. 10, pp. 213501–133503, 2016.

[11] T. Minami *et al.*, *Appl. Phys. Express*, vol. 6, 2013.

[12] M. D. Heinemann, J. Berry, G. Teeter, T. Unold, and D. Ginley, *Cit. Appl. Phys. Lett. Appl. Phys. Lett. Appl. Phys. Lett. Appl. Phys. Lett. Appl. Phys. Lett. J. Chem. Phys.*, vol. 108, no. 10, pp. 22107–13504, 2016.

[13] A. A. Dakhel, "W doping effect on the dielectric properties of amorphous Ga 2 O 3 films grown on Si substrate for low-k applications," 2012.

[14] S. Cui, Z. Mei, Y. Zhang, H. Liang, and X. Du, "Room-Temperature Fabricated

Amorphous Ga_2O_3 High-Response-Speed Solar-Blind Photodetector on Rigid and Flexible Substrates,” *Adv. Opt. Mater.*, vol. 5, no. 19, p. 1700454, Oct. 2017.

[15] H. Lee *et al.*, “ALD and MOCVD of Ga2O3 Thin Films Using the New Ga Precursor Dimethylgallium Isopropoxide, Me2GaOiPr,” *Chem. Vap. Depos.*, vol. 17, no. 7–9, pp. 191–197, Sep. 2011.

[16] M. Nieminen, L. Niinisto, and E. Rauhalab, “Growth of gallium oxide thin films from gallium acetylacetonate by atomic layer epitaxy.”

[17] G. Wagner *et al.*, “Homoepitaxial growth of β-Ga_2O_3 layers by metal-organic vapor phase epitaxy,” *Phys. Status Solidi*, vol. 211, no. 1, pp. 27–33, 2014.

[18] F.-P. Yu, S.-L. Ou, and D.-S. Wuu, “Pulsed laser deposition of gallium oxide films for high performance solar-blind photodetectors,” *Opt. Mater. Express*, vol. 5, no. 5, p. 1240, May 2015.

[19] L. M. Garten, A. Zakutayev, J. D. Perkins, B. P. Gorman, P. F. Ndione, and D. S. Ginley, “Structure property relationships in gallium oxide thin films grown by pulsed laser deposition.”

[20] T. Minami *et al.*, *Japanese J. Appl. Phys. Tadatsugu Minami al Jpn. J. Appl. Phys. Jpn. J. Appl. Phys*, vol. 39, no. 6A, pp. 524–526, 2000.

[21] D. J. Comstock and J. W. Elam, “Atomic Layer Deposition of Ga 2 O 3 Films Using Trimethylgallium and Ozone.”

[22] T. G. Allen and A. Cuevas, *Phys. status solidi - Rapid Res. Lett.*, vol. 9, no. 4, pp. 220–224, Apr. 2015.

[23] M. R. Laskar *et al.*, *ACS Appl. Mater. Interfaces*, vol. 8, no. 16, pp. 10572–10580, Apr. 2016.

[24] C. L. Dezelah, J. Niinistö, K. Arstila, L. Niinistö, and C. H. Winter, “Atomic Layer Deposition of Ga 2 O 3 Films from a Dialkylamido-Based Precursor.”

[25] C. L. Dezelah Iv, P. Myllymäki, J. Päiväsaari, K. Arstila, L. Niinistö, and C. H. Winter, “The growth of Er x Ga 22x O 3 films by atomic layer deposition from two different precursor systems,” 2007.

[26] D. Pugh, L. G. Bloor, I. P. Parkin, and C. J. Carmalt, “Gallium Hydride Complexes Stabilised by Multidentate Alkoxide Ligands: Precursors to Thin Films of Ga2O3 at Low Temperatures,” *Chem. - A Eur. J.*, vol. 18, no. 19, pp. 6079–6087, May 2012.

[27] M. Leskela and M. Ritalä, “Atomic layer deposition (ALD): from precursors to

thin film structures," *Thin Solid Films*, vol. 409, pp. 138–146, 2002.

[28] K. Knapas and M. Ritala, "In situ studies on reaction mechanisms in atomic layer deposition," *Crit. Rev. Solid State Mater. Sci.*, vol. 38, no. 3, pp. 167–202, 2013.

[29] H. B. Profijt, S. E. Potts, M. C. M. van de Sanden, and W. M. M. Kessels, "Plasma-Assisted Atomic Layer Deposition: Basics, Opportunities, and Challenges," *J. Vac. Sci. Technol. A Vacuum, Surfaces, Film.*, vol. 29, no. 5, p. 50801, Sep. 2011.

[30] H.-Y. Shih, F.-C. Chu, A. Das, C.-Y. Lee, M.-J. Chen, and R.-M. Lin, "Atomic Layer Deposition of Gallium Oxide Films as Gate Dielectrics in AlGaN/GaN Metal–Oxide–Semiconductor High-Electron- Mobility Transistors."

[31] I. Donmez, C. Ozgit-Akgun, and N. Biyikli, "Low temperature deposition of Ga_2O_3 thin films using trimethylgallium and oxygen plasma," *J. Vac. Sci. Technol. A Vacuum, Surfaces, Film.*, vol. 31, no. 1, p. 01A110, Jan. 2013.

[32] R. K. Ramachandran *et al.*, "Plasma enhanced atomic layer deposition of Ga_2O_3 thin films," *J. Mater. Chem. A*, vol. 2, no. 45, pp. 19232–19238, Oct. 2014.

[33] F. K. Shan, G. X. Liu, W. J. Lee, G. H. Lee, I. S. Kim, and B. C. Shin, "Structural, electrical, and optical properties of transparent gallium oxide thin films grown by

plasma-enhanced atomic layer deposition," *J. Appl. Phys.*, vol. 98, no. 2, p. 23504, Jul. 2005.

[34] I. Donmez, C. Ozgit-Akgun, and N. Biyikli, "Low temperature deposition of Ga2O3 thin films using trimethylgallium and oxygen plasma," *J. Vac. Sci. Technol. A Vacuum, Surfaces, Film.*, vol. 31, no. 1, p. 01A110, 2013.

[35] K.-W. Chang and J.-J. Wu, "Temperature-controlled catalytic growth of one-dimensional gallium nitride nanostructures using a gallium organometallic precursor," *Appl. Phys. A Mater. Sci. Process.*, vol. 77, no. 6, pp. 769–774, Nov. 2003.

[36] C. A. Kraus and F. E. Toonder ', "TRIMETHYL GALLIUM, TRIMETHYL GALLIUM ETHERATE AND TRIMETHYL GALLIUM AMMINE."

[37] K. Knapas and M. Ritala, "In situ Reaction Mechanism Studies on Atomic Layer Deposition of Ir and IrO_2 from $Ir(acac)_3$," *Chem. Mater.*, vol. 23, no. 11, pp. 2766–2771, Jun. 2011.

[38] M. Nieminen, L. Niinisto, and E. Rauhalab, "Growth of gallium oxide thin films from gallium acetylacetonate by atomic layer epitaxy."

CHAPTER 4

BAND ALIGNMENT OF PEASL AMORPHOUS GA_2O_3 THIN FILMS ON GAN

In this study, the band alignment of plasma enhanced ALD amorphous Ga_2O_3 thin films on GaN was studies by *in-situ* x-ray photoemission spectroscopy. PEALD Ga_2O_3 thin film deposited at 200 ℃ on GaN grown on sapphire substrates. The GaN was first cleaned *in-situ* at 680 ℃ and a monolayer of Ga_2O_3 was deposited. The conduction band offset (CBO), valence band offset (VBO) and band bending (BB) of PEALD Ga_2O_3 thin films on GaN were $0.1 \pm 0.2\ eV$, 1 ± 0.2 eV and 0.3 eV respectively. Type-I band alignment was determined. Annealing in N_2 ambient at 400 ℃ does not influence the band offset of PEALD Ga_2O_3 thin films on GaN, which might indicate a lower interface states in between.

4.1 Introduction

Ga_2O_3 is one of the ultra-wide band gap materials with a band gap ranging from 4.7 eV to 4.9 eV[1]. PEALD Ga_2O_3 is amorphous, which theoretically should have a relatively smaller compared with crystal phase. Ga_2O_3 has a high theoretical breakdown field (8 MV/cm)[2]. Ga_2O_3 has been applicated as passivation layer on GaAs[3] and recently on GaN[4]. GaN-based transistors remain one of the most promising next generation power devices due to the large band gap (3.4 eV), high saturation velocity (~$10^7\ cm/s$) and high breakdown field[4]–[7]. Characterization of electronic states and surface chemistry of both Ga_2O_3 and GaN was done *in-situ* with x-ray photoemission spectroscopy[5]. Despite various substrate surface preparation techniques employed[8], [9], GaN as a polarized material, has a bound sheet charge of $2.1 \times 10^{13}\ charge/cm^2$ and surface states compensate the bound sheet charge thus reducing internal the electric field in the

GaN bulk [10]. The surface charge composition mechanism may also be related to the failure mechanism of GaN-based transistors [11].

To improve the performance of GaN-based transistors, oxygen terminated GaN surfaces have often been used as a starting surface for dielectric layer growth, these dielectric layer structures suffer from a range of defects and impurities[11]. However, studies have suggested that an ordered O-Ga-O layer could provide an excellent low defect starting surface for dielectric layer growth[12]. A smooth interface between MBE Ga_2O_3 on GaN has also been reported[13]. In this study, we have employed plasma enhanced ALD (PEALD) to prepare Ga_2O_3 layers on GaN and determined the band alignment using photoemission spectroscopy. The PEALD growth of Ga_2O_3 is achieved in our laboratory using gallium acetylacetonate ($Ga(acac)_3$) precursor and an O_2 plasma as oxidizer. An X-ray and UV photoemission systems (XPS and UPS) are used to determine electronic states including band alignment and chemical composition. Within the PEALD Ga_2O_3 growth window a growth rate of 0.3 Å/cycle per cycle was determined using X-ray reflectivity (XRR) and photoemission indicated a uniform growth per cycle. The band gap of PEALD Ga_2O_3 derived from the XPS energy loss spectra was 4.3 eV.

In this study, electronic states and chemical bond states were mostly measured by X-ray photoemission spectroscopy (XPS). Surface band bending, and band offsets could be derived from the XPS data. According to the method developed by Waldrop, Grant and Kraut, the band bending of GaN could be derived as[14]:

$$\mathrm{BB} = (E_{Cl} - E_v)_{GaN} + E_g - E_c - \Delta E_{Cl,XPS}$$

where, BB is the band bending of GaN, and $(E_{Cl} - E_v)_{GaN}$ is the Ga 3d peak position from the vacuum level, which is assumed to be a constant 17.8 eV. E_g is the band gap of GaN, based on the crystal structure of GaN, E_c is 0.1eV above the Fermi Level, which is derived from the doping density of the C-place GaN. $E_{Cl,XPS}$ is the Ga-3d core level position measured by the XPS, which is 20.8 eV.

Valence band offset could be calculated to be [15], [16]:

$$\Delta E_v = (E_{Ga\ 3d}^{GaN} - E_v^{GaN}) - \left(E_{Ga\ 3d}^{Ga_2O_3} - E_v^{Ga_2O_3}\right) - \Delta E_{Cl}$$

Where ΔE_v represents valence band offset (VBO) between GaN and PEALD Ga_2O_3, $E_{Ga\ 3d}^{GaN}$ and E_v^{GaN} are the Ga 3d core level position valence band maximum of GaN substrate respectively, $E_{Ga\ 3d}^{Ga_2O_3}$ and $E_v^{Ga_2O_3}$ are the Ga 3d core level position and valence band maximum of Ga_2O_3 respectively, ΔE_{Cl} is the core level difference for Ga 3d electron of GaN and Ga_2O_3. In this method, $E_{Ga\ 3d}^{GaN} - E_v^{GaN}$ and $E_{Ga\ 3d}^{Ga_2O_3} - E_v^{Ga_2O_3}$ are both constant independent of band bending. Once the difference of the core level E_{Cl} is measured, the valence band offset ΔE_v could be easily derived.

Conduction band offset could be easily derived from the valence band offset:

$$\Delta E_C = E_{g,Ga_2O_3} - E_{g,GaN} - \Delta E_v$$

Where ΔE_C is the conduction band offset (CBO); E_{g,Ga_2O_3} and $E_{g,GaN}$ are the band gap of Ga_2O_3 and GaN respectively; and ΔE_v is the valence band offset calculated above. In this study, Ga_2O_3 and GaN has a band gap of 4.2 eV and 3.4 eV repectively.

4.2 Experiment

4.2.1 GaN substrate preparation

In this study, PEALD Ga_2O_3 thin films were grown on GaN. The GaN wafers were grown on a 2-inch diameter sapphire substrate by MOCVD. The doping density was $3 \times 10^{18} cm^{-3}$ for the first $1 \mu m$ layer and ~$1 \times 10^{17} cm^{-3}$ for the following $1 \mu m$ layer, which indicated the Fermi level is 0.1 eV below the conduction band minimum (CBM) on the surface. The GaN substrate were diced to be 1 cm^2 sections and first treated with *ex-situ* chemical cleaning with sonication in Acetone, Methanol, NH_4OH solvent for 10 min and followed by a 1min sonication in DI water.

Afterwards, blow dry proceeded with ultra-high purity nitrogen gas (99.999%) to further dry and clean the GaN substrate. After the ex-situ cleaning, the GaN substrate was cleaned with *in-situ* N_2/H_2 plasma at 680 ℃ for 15 min and the flow rates of N_2 and H_2 are 72 sccm and 18 sccm respectively with a pressure of 60mTorr. The flow rates were controlled by mass flow controller and the temperature was measure by a thermocouple connected with the sample heater and a infrared pyrometer outside the chamber. The plasma chamber was maintained at an ultra-high vacuum level with a base pressure of $4 \times 10^{-10} Torr$. The plasma rector was an inductively couple plasma reactor supplied by a radio frequency power (100W, 13.56MHZ). The plasma was generated inside a quartz tube with diameter of 32 mm wrapped around a helicopter copper coil. Metal sheath was set up to prevent plasma contamination outside the coil. The quartz tube was 25 cm above the sample stage. This configuration prevents ion bombardment on the surface and supply enough radicals. The plasma is cold plasma with less than 1% gas ionized. After cleaning, a 2nm PEALD Ga_2O_3 thin film layer was deposited on the polished c-plane GaN.

4.2.2 Plasma enhanced atomic layer deposited Ga_2O_3 thin films on GaN

Band diagram of various PEALD dielectrics on GaN has been investigated, precious study has reported band alignment of PEALD dielectric thin films (HfO_2, Al_2O_3, SiO_2) on GaN[11]. In this study, Ga_2O_3 is deposited using $Ga(C_5H_7O_2)_3$ (gallium acetylacetonate, $Ga(acac)_3$) as Ga precursor maintained at with a heating jacket maintained at 70 ~ 90 ℃ to provide enough molecules for the deposition process. The Ga_2O_3 thin films was deposited at 200 ℃ using $Ga(acac)_3$ and oxygen plasma. The precursor was carried by ultra-high pure Ar gas bypassing the $Ga(acac)_3$ contiener. Timing of the gas pulse is controlled through N_2 value. The flow rates was controlled by Mass flow controllers. The substate temperature was measure with thermocouple connected with the sample heater and double checked with a infrared pyrometer from outside the ALD chamber. The inductively coupled plasma reactor was 25cm above the sample stage. The plasma reactor was 25 cm above the sample generated by a radio frequency (rf) source with 200W power and 13.56 MHZ frequency.

4.2.3 Surface Characterization of band diagrams with photoemission spectroscopy

The PEALD Ga_2O_3 thin films were deposited on the polished c-plane GaN. In-situ XPS measurements was done to the sample after each step. The X-ray is monochromatic with energy 1486.6 eV from Al KLL process. X-ray excited the electrons up to binding energy of 1486.6 eV. The process could detect electron states up to ~10 nm deep into the surface. Excited electrons got focus by electron collection lens and the energy level is analyzed by the electron energy analyzer. The sample is place in an ultra-high vacuum

chamber with a base pressure to be order of 10^{-10} Torr. In this study, electronic states and chemical bond states were mostly measured by X-ray photoemission spectroscopy. Using the method mentioned above, the band diagram of cleaned GaN and band bending of PEALD Ga_2O_3 on GaN were determined from the XPS core levels.

In this study, to investigate the difference of VBM and Ga-3d core level for PEALD Ga2O3, 10 nm of Ga_2O_3 was deposited on phosphorous-doped Si wafer. Both UPS and XPS measurements were done to the sample. XPS has done to GaN substrate after being received, chemical cleaned, and plasma cleaned. Surface band bending, native oxide composition, carbon contamination removal situations were shown in the XPS data. XPS measurements was all done to clean GaN, GaN with 3nm deposited PEALD Ga_2O_3 and after annealing. Band offsets information, stoichiometry, and chemical bonding states could be derived.

4.3 Results

In this study, surface band bending of cleaned GaN with 1 ML of native Ga2O3 was investigated. Also, band offset of Ga2O3/GaN heterojunction was investigated using the electron affinity level model. Comparison of various PEALD dielectrics and beta-Ga2O3 band offsets on GaN were discussed.

4.3.1 Native oxide induced by high temperature plasma cleaning and band bending of GaN

XPS measurements were done to as-received GaN, chemical cleaned GaN and plasma cleaned GaN as is shown in Fig.4.1. There is obvious carben reduction after chemical cleaning but there are still detectable carben peak. However, the in-situ plasma cleaning with N_2/H_2 at 680℃ could remove the carbon contamination below the XPS detection

limit. Due to the ineligible amount of O_2 gas in the chamber and the reactively of plasma and high temperature during cleaning, a monolayer of Ga_2O_3 was observed on the GaN surface.

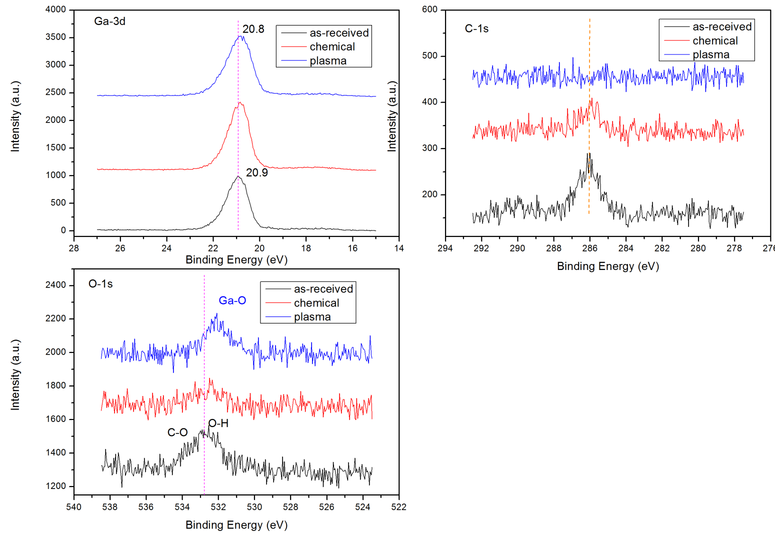

Figure 4.1 XPS graph of Ga 3d, C 1s and O 1s electrons for as-received, chemical cleaned, and plasma cleaned GaN.

Procedure	Ga-3d	Ga-2p	O-1s	C-1s	VBM
As-received	20.9 eV	eV	532.0 eV	286.0 eV	3.3 eV
Chemical cleaned	20.8 eV	eV	531.4 eV	285.8 eV	3.3 eV
Plasma cleaned	20.8 eV	eV	531.4 eV	---	3.3 eV

Table 4.1 Core level energy for Ga 3d, C 1s and O 1s from XPS spectra.

4.3.2 Band offsets of PEALD amorphous Ga2O3 on GaN

XPS measurement were done on GaN before and after cleaning, with PEALD Ga_2O_3 on, and after annealing as is shown in Fig.4.2. X-ray photoemission spectra of GaN and PEALD Ga_2O_3 on GaN could provide the band offsets information. The Valence band of PEALD Ga_2O_3 is 2.5 eV and the Ga-3d peak is 21.4 eV, so the difference between the

Valence band maximum and 3d core level $\left(E_{Ga\ 3d}^{Ga_2O_3} - E_v^{Ga_2O_3}\right)$ should be 18.9 eV. The same value for GaN $(E_{Ga\ 3d}^{GaN} - E_v^{GaN})$ is 17.7 eV, which is consistent with reported values.

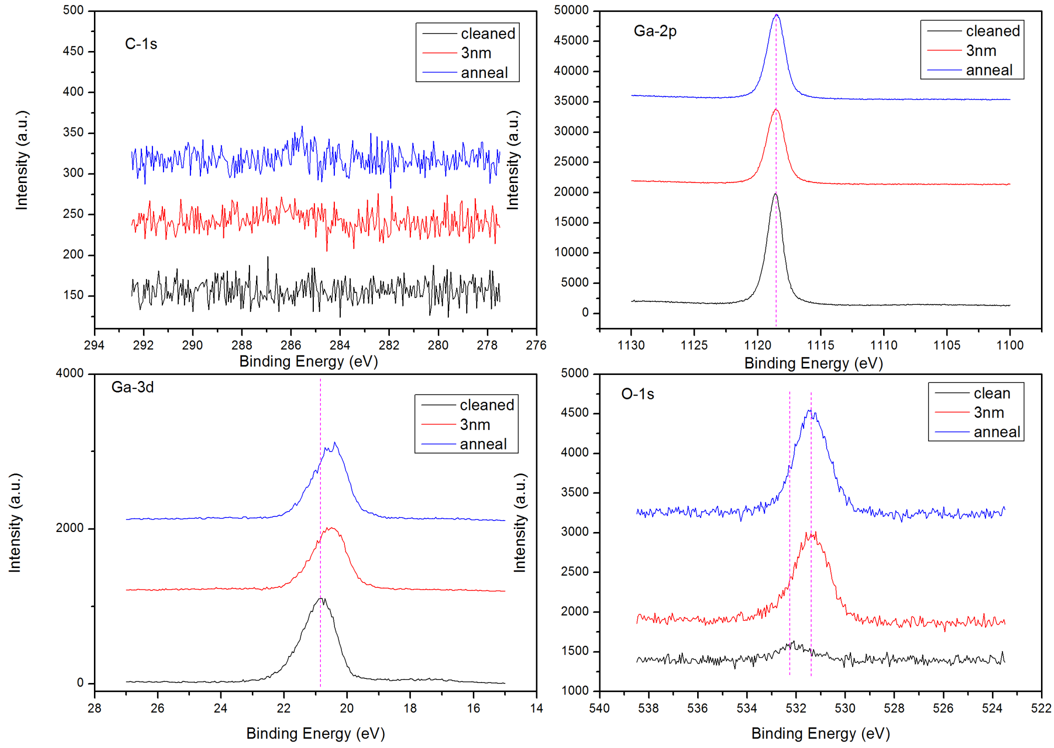

Figure 4.2 XPS spectra for cleaned GaN, as grown PEALD Ga_2O_3, and annealed Ga_2O_3.

Procedure	Ga-3d	Ga-2p	O-1s	VBM
Cleaned	20.9 eV	1118.6 eV	532.0 eV	3.3 eV
3nm Ga_2O_3	20.6 eV	1118.6 eV	531.4 eV	---
annealed	20.5 eV	1186.5 eV	531.4 eV	---

Table 4.2 XPS Ga 3d, Ga-2p and Al 2p core.

Thicker Ga_2O_3 film was grown on Si to get binding energy information. As is shown in Fig. 4。3 (a)The XPS spectra showed that Ga 3d in Ga2O3 as grown thin films has a binding energy of 21.4 eV on Si while Fig. 4.3 (b) showed the valence band maximum if 2.5 eV and the cutoff energy in the detection of ultraviolet light is 16.5 eV, the width of the UPS spectra is 14.0 eV.

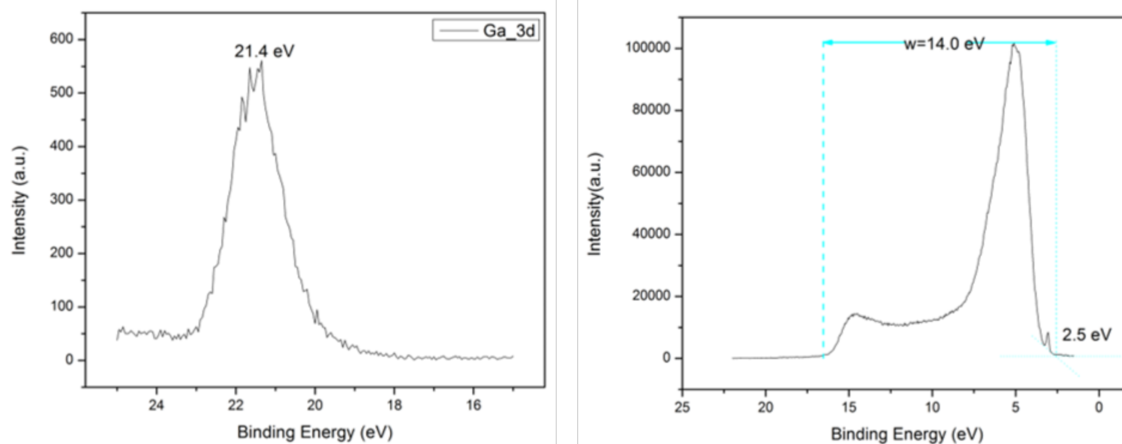

Figure 4.3 XPS and UPS spectra of PEALD as-grown Ga_2O_3 thin films on Si.

Fig. 4.3. (a)XPS and (b)UPS spectra of PEALD as-grown Ga_2O_3 thin films on Si. The XPS spectra shows an Ga 3d core level energy of 21.4 eV. UPS spectra shows a valence

band maximum energy of 2.5 eV and cutoff energy of 16.5 eV. As is discussed previously, the band bending of GaN could be derived as:

$$\mathrm{BB} = (E_{Cl} - E_v)_{GaN} + E_g - E_c - \Delta E_{Cl,XPS}$$

where, BB is the band bending of GaN, and $(\mathrm{E_{Cl}} - \mathrm{E_v})_{\mathrm{GaN}}$ is the Ga 3d peak position from the vacuum level, which is assumed to be a constant 17.8 eV. $\mathrm{E_g}$ is the band gap of GaN, based on the crystal structure of GaN, $\mathrm{E_c}$ is 0.1eV above the Fermi Level, which is derived from the doping density of the C-place GaN. $\mathrm{E_{Cl,XPS}}$ is the Ga-3d core level position measured by the XPS, which is 20.8 eV. It is easy to get that the band bending of GaN is:

BB=17.7 eV +3.4 eV +0.1eV-20.5 eV=-0.3 eV

The band diagram for GaN with cleaned surface would be shown in Fig.4.4.

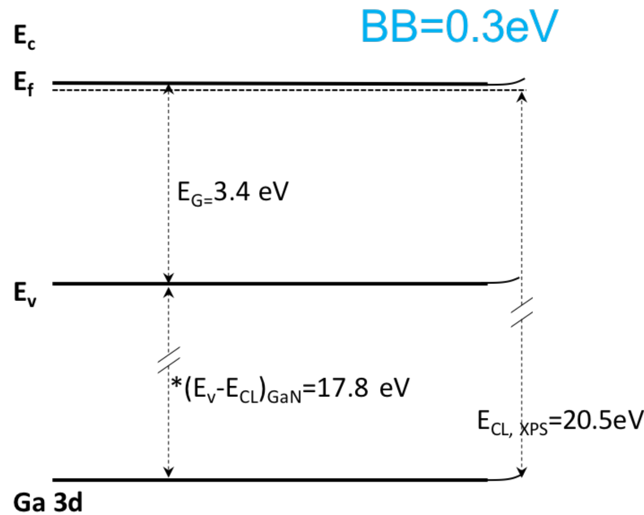

Fig. 4.4 Band diagram of GaN with Ga-surface.

The band offsets could also be derived from the XPS date.

$$\Delta E_v = (E_{Cl} - E_v)_{GaN} - (E_{Cl} - E_V)_{Ga_2O_3} + \Delta E_{Cl}$$

Where the $(E_{Cl} - E_v)_{GaN}$ is assumed to be a constant 17.8eV and $(E_{Cl} - E_v)_{Ga2O3}$ is a constant 18.5eV for as-grown PEALD Ga_2O_3. ΔE_{Cl} is the shift of the Ga-3d peak position before and after deposition of Ga_2O_3 on GaN, 20.8 eV and 20.4 eV respectively. It is easy to get that

$$\Delta E_{CL} = -0.4\ eV$$

and the valence band offset of GaN and Ga_2O_3 is

$$\Delta E_v = 17.8\ \mathrm{eV} - 18.5\ \mathrm{eV} + (-0.4\ \mathrm{eV}) = -0.1\ \mathrm{eV}$$

The Band alignment of PEALD Ga_2O_3 on GaN would be like in Fig. 4.5.

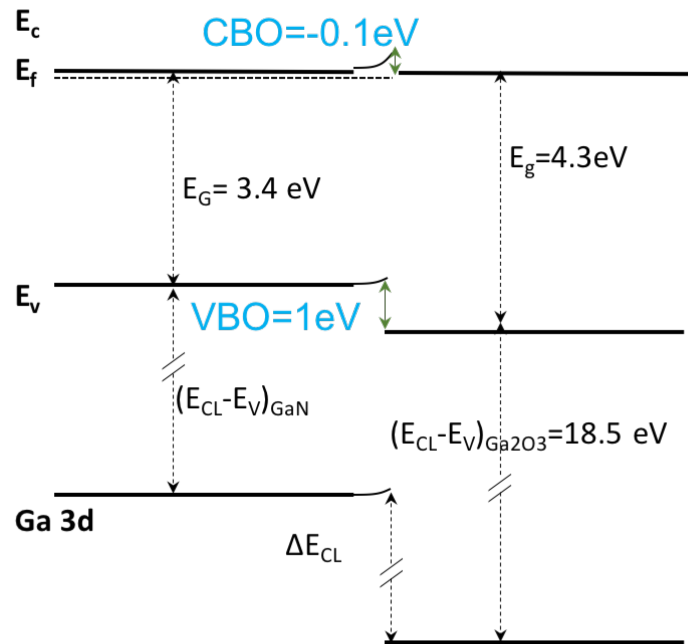

Figure 4.5 Band alignment of as-grown PEALD Ga_2O_3 on GaN.

As is shown in Fig 4.5, the conduction band offset is a $0.10 \pm$ downward band bending, and Valence band offset is a 1eV downward band bending. The band alignment is type-II (staggered gap) heterojunction.

4.4 Discussion

4.4.1 Native Oxide Composition and Surface Band Bending

Ga_2O_3 is a spontaneous polarized material with sheet charge on C-plane Ga face. The polarization induced internal field and surface states could influence the electronic and photo-electronic properties of GaN-based devices [17]. The surface potential caused by the surface polarization charge screen should be[5]:

$$\Phi_s = -\frac{qN_D}{2\mathcal{E}\mathcal{E}_0}W^2$$

Where q is the electron charge ($1.602 \times 10^{-19}C$);N_D is the doping density of GaN ($3 \times 10^{18}cm^{-3}$); $\mathcal{E}$ is the dielectric constant of GaN (9.5); $\mathcal{E}_0$ is the vacuum permeability ($8.86 \times 10^{-12}F/m$); W is the depletion layer width.

The 1 ML of native Ga_2O_3 was introduced to GaN surface after N_2/H_2 plasma cleaning at 680C. The atomic composition of the native oxides could be calculated as[18]:

$$\eta_x = \frac{I_x/S_x}{\Sigma_{i=o}^{n} I_i/S_i}$$

Where η_x is the atomic composition ratio of element x in the thin film; I_x is the integrated intensity from the element x XPS spectra, S_x is the sensitive factor the element x, which depend on the cross section of the photoemission process and irrelevant with experiment conditions; $\Sigma_{i=o}^{n} I_i/S_i$ is the weighted integrated intensity for all the elements in the thin film. Based on this calculation, it is easy to get that around one monolayer of Ga_2O_3 is formed on GaN surface after plasma cleaning. Stoichiometry of Ga_2O_3 thin film could also be derived the same way.

4.4.2 Charge Neutrality Level (CNL) Model and Band Offsets GaN

The band offsets of dielectrics on GaN is relevant with dielectric band gap, dielectric constant and electronic part of dielectric constant. Fig. 4.6 shows the relationship of dielectric band gap and band offset. It is obvious that VBO and CBO both increase with the dielectric band gap.

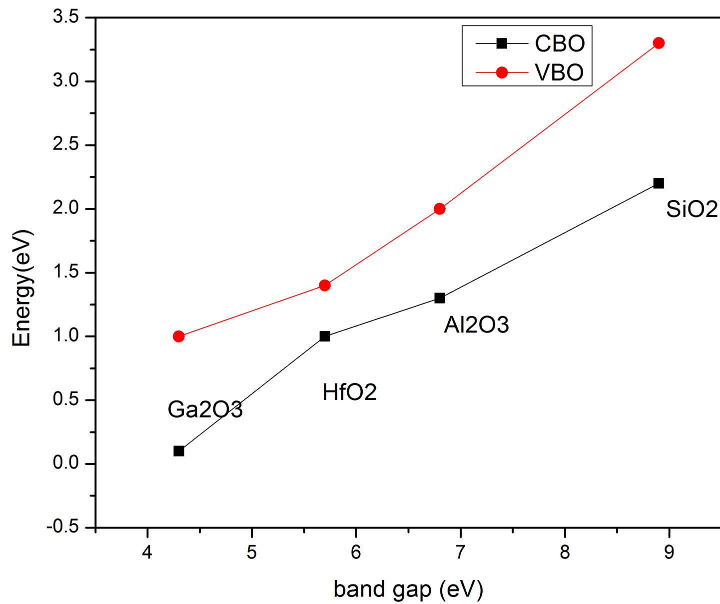

Figure 4.6 Relationship of dielectric band gap and band offsets on GaN**.**

4.5 Conclusion

In this study, the GaN substrates were first cleaned to remove contaminations ex-situ. An in-situ high temperature clean was done to further clean the carbon contamination and to passivate N vacancy defects, while a monolayer of native oxides was introduced. Chemical cleaned GaN has a upward surface band bending of 0.3 eV on C-plane. The Band PEALD Ga_2O_3, with a band gap af 4.3 eV, could passivate some surface defects of GaN. The CBO and VBO is 0.1 eV and 1 eV respectively, smaller than crystal Ga_2O_3.

Dielectrics generally has a conduction band offsets larger than 1 eV to inhibit leakage current over GaN. Typically gate insulator such as HfO_2, Al_2O_3, Gd_2O_3 and SiO_2 has CBO larger than 1 eV[21].

Further study of Ga_2O_3 passivated GaN based transistors will be fabricated to exam the influence on gate insulator such as Al_2O_3 and SiO_2 on GaN MOS gates.

4.6 REFERENCE

[1] T. Onuma *et al.*, *Cit. Appl. Phys. Lett. Appl. Phys. Lett. Appl. Phys. Lett. J. Appl. Phys. Appl. Phys. Lett. J. Chem. Phys.*, vol. 103, no. 10, pp. 41910–13504, 2013.

[2] M. Higashiwaki, K. Sasaki, A. Kuramata, T. Masui, and S. Yamakoshi, "Development of gallium oxide power devices," *Phys. Status Solidi Appl. Mater. Sci.*, vol. 211, no. 1, pp. 21–26, 2014.

[3] M. Passlack, M. Hong, J. P. Mannaerts, R. L. Opila, and F. Ren, "Thermodynamic and photochemical stability of low interface state density Ga2O3–GaAs structures fabricated by in situ molecular beam epitaxy," *Appl. Phys. Lett.*, vol. 69, no. 3, p. 302, Jun. 1998.

[4] A. J. Kerr *et al.*, "Preparation of gallium nitride surfaces for atomic layer deposition of aluminum oxide," *J. Chem. Phys. GaN AlGaN J. Vac. Sci. Technol. A Vacuum, Surfaces, Film. J. Appl. Phys.*, vol. 141, no. 1, 2014.

[5] B. S. Eller, J. Yang, and R. J. Nemanich, *J. Vac. Sci. Technol. A Vacuum, Surfaces, Film. J. Appl. Phys. J. Appl. Phys. J. Vac. Sci. Technol. B Microelectron. Nanom. Struct. Process. Meas. Phenom.*, vol. 31, no. 21, pp. 244503–1828, 2013.

[6] R. D. Long and P. C. McIntyre, "Surface Preparation and Deposited Gate Oxides for Gallium Nitride Based Metal Oxide Semiconductor Devices," *Materials (Basel).*, vol. 5, no. 12, pp. 1297–1335, Jul. 2012.

[7] U. K. Mishra, P. Parikh, and Yi-Feng Wu, "AlGaN/GaN HEMTs-an overview of device operation and applications," *Proc. IEEE*, vol. 90, no. 6, pp. 1022–1031, Jun. 2002.

[8] M. Tutor, E. Preble, M. Williams, X. Xu, D. Tsvetkov, and L. Liu, "Surface preparation of substrates from bulk GaN crystals," *J. Cryst. Growth*, vol. 305, no. 2, pp. 372–376, Jul. 2007.

[9] D. F. Storm *et al.*, "Surface preparation of freestanding GaN substrates for homoepitaxial GaN growth by rf-plasma MBE," *J. Vac. Sci. Technol. B, Nanotechnol. Microelectron. Mater. Process. Meas. Phenom.*, vol. 35, no. 2, p. 02B109, Mar. 2017.

[10] U. Karrer, O. Ambacher, and M. Stutzmann, *Cit. Appl. Phys. Lett. Appl. Phys. Lett. J. Appl. Phys. J. Appl. Phys. J. Appl. Phys. Appl. Phys. Lett. Appl. Phys. Lett.*, vol.

771, no. 63, pp. 1267–1685, 2012.

[11] J. Yang, B. S. Eller, and R. J. Nemanich, "Surface band bending and band alignment of plasma enhanced atomic layer deposited dielectrics on Ga- and N-face gallium nitride," *J. Appl. Phys.*, vol. 116, no. 12, p. 123702, Sep. 2014.

[12] J. Yang, B. S. Eller, and R. J. Nemanich, "Surface band bending and band alignment of plasma enhanced atomic layer deposited dielectrics on Ga- and N-face gallium nitride," *J. Appl. Phys.*, vol. 116, no. 12, p. 123702, Sep. 2014.

[13] Y. C. Chang *et al.*, "MBE grown high k dielectrics Ga 2 O 3 (Gd 2 O 3) on GaN," *J. Cryst. Growth*, vol. 301302, pp. 390–393, 2007.

[14] J. R. Waldrop and R. W. Grant, "Measurement of AlN/GaN (0001) heterojunction band offsets by x-ray photoemission spectroscopy," *Appl. Phys. Lett.*, vol. 68, no. 20, p. 2879, Jun. 1998.

[15] J. R. Waldrop, E. A. Kraut, S. P. Kowalczyk, and R. W. Grant, "Valence-band discontinuities for abrupt (110), (100), and (111) oriented Ge-GaAs heterojunctions," *Surf. Sci.*, 1983.

[16] R. W. Grant, J. R. Waldrop, and E. A. Kraut, "Observation of the Orientation Dependence of Interface Dipole Energies in Ge-GaAs," *Phys. Rev. Lett.*, vol. 40, no. 10, pp. 656–659, Mar. 1978.

[17] O. Ambacher *et al.*, *J. Appl. Phys.*, vol. 85, no. 3222, 1999.

[18] P. Oelhafen, *J. Electron Spectros. Relat. Phenomena*, vol. 34, no. 2, p. 203, Jan. 1984.

[19] V. Nagarajan and R. Chandiramouli, *Appl. Surf. Sci.*, vol. 344, pp. 65–78, 2015.

[20] G. Meloni, S. M. Sheehan, and D. M. Neumark, *J. Chem. Phys.*, vol. 122, no. 101, 2005.

[21] J. Robertson and B. Falabretti, “Band offsets of high K gate oxides on III-V semiconductors,” *J. Appl. Phys.*, vol. 100, no. 1, 2006.

CHAPTER 5

FUTURE WORK: IMPROVEMENT OF GAN-BASED MOS GATES

GaN is one of, if not the most important next-generation semiconductors. metal oxide semiconductor (MOS) gates are fundamental structures of field effect transitors. GaN has a band gap of 3.4 eV and GaN-based transistors could work at high temperature, high power and high frequency. However, there are limitation including leakage current and current collapse that limit the performance of GaN transistors. It has been proposed to apply PEALD Ga_2O_3 as passivation layer between GaN and PEALD Al_2O_3 and this approach represents an opportunity for future research. Fabrication of GaN MOS structures have been fabricated with thermally introduced Ga_2O_3 monolayer before PEALD Al_2O_3 deposition. The breakdown field has been increased and the hysteresis decreased. Passivation using 2nm PEALD Al_2O_3 was also tried between GaN and SiO_2 and considerable results were reported on this structure. To further improve the performance of GaN transistors, atomic layer etching (ALE) was proposed to improve the interface. This section presents preliminary research that established directions for future study.

5.1 Ga_2O_3 working as interfacial layer on GaN surface

In this research, GaN-based MOSFETs and MOSHEMTs with PEALD Al_2O_3 and SiO_2 have been considered. Different processes have been studied, for example, cleaning the GaN surface before dielectric deposition. The N_2/H_2 plasma cleaning process at 680℃, with residual oxygen, introduces about 1ML of Ga_2O_3 on the GaN surface. The ultra-thin layer of Ga_2O_3 may help to improve the electrical properties and provide a larger breakdown voltage and smaller hysteresis.

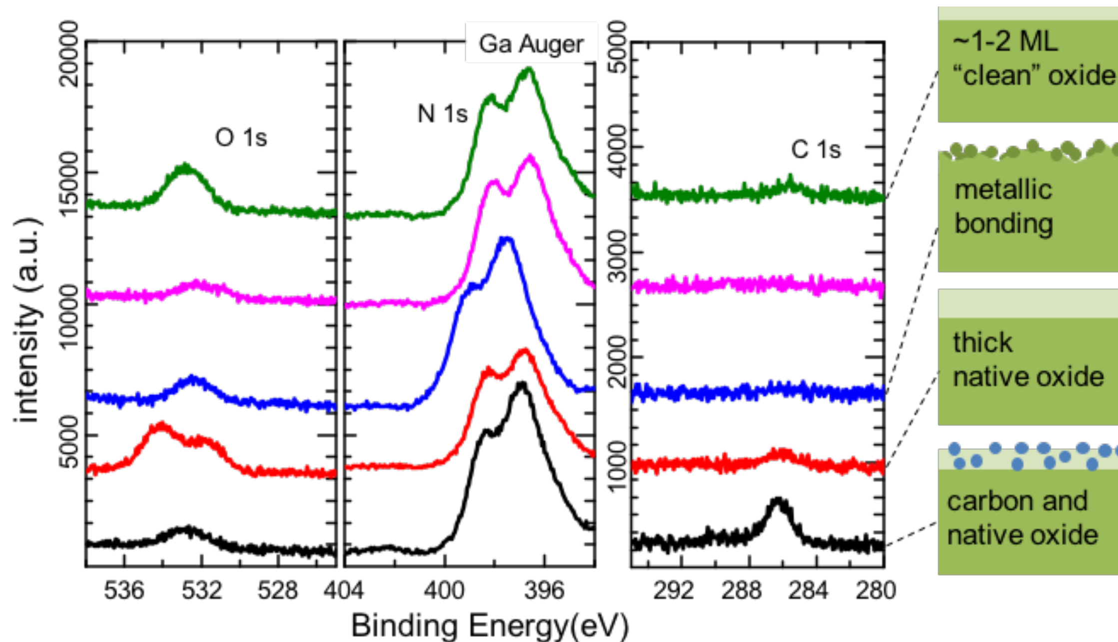

Figure 5.1 XPS for GaN with different cleaning methods.

Fig. 5.1 shows XPS for GaN after different cleaning methods. The black scan is for a wet chemical clean GaN surface, the red represents an O_2 plasma at 100 °C, the blue represents an immersive N_2/H_2 plasma at 680 °C, the purple represents an remote N_2/H_2 plasma cleaning at 680 °C, and the green is the N_2/H_2 plasma with residual oxygen, which introduces 1-2 ML Ga_2O_3.

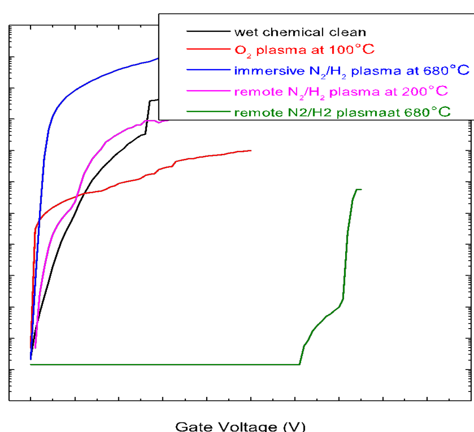

Figure 5.2 I-V characterization of GaN MOSFETs with PEALD Al_2O_3 as gate insulator. Prepared in collaboration with Srabanti Chowdhury, *et, cl.*

From Fig. 5.2. it is evident that the remote N_2/H_2 plasma cleaning at 680 ℃ can introduce a monolayer of O-Ga-O bonds on GaN and increase the breakdown dramatically.

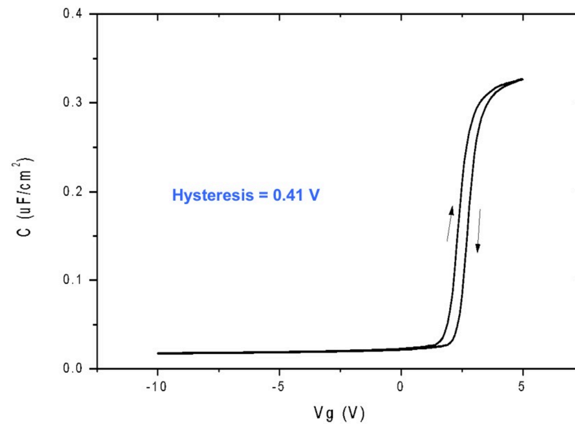

Figure 5.3 Capacitance-voltage characterization of GaN MOSFET with PEALD Al_2O_3 as insulator and 1 monolayer Ga_2O_3 as passivation. Prepared in collaboration with Srabanti Chowdhury, *et, cl*.

Electronic surface states are electrically active and can degrade reliability for GaN-based devices such as MOSFETs, HEMTs, JFETs, and CAVETs. Likely, these surface states pin the Fermi level at ~0.4 eV [1] below the conduction band minimum, where defects may be related to nitrogen vacancies or oxygen donor states. Our studies of surface preparation with a high-temperature remote N_2/H_2 plasma have given the most reliable electrical performance on GaN. High temperatures in remote plasma effectively reduced native contamination without introducing significant additional defects, resulting in a cleaned and passivated GaN surface. Post-deposition treatments vary with the dielectric. Lower temperatures (~400 °C) in N_2 ambient were better suited for Al_2O_3, which reduced defects without inducing poly-crystallization. Higher temperatures (>680 °C) in forming

gas (N_2/H_2) were better suited for SiO_2, where atomic hydrogen may satisfy dangling bonds at the interface.

5.1.1 Characterization of interface states and border traps in ALD Al_2O_3/GaN with Ga_2O_3 as passivation layer.

Both experimental and theoretical results [2] have shown that Ga_2O_3 can decrease the interfacial states between GaN and insulators, such as Al_2O_3 and SiO_2. A model proposed by A.J. Kerr, A. C. Kummel, *et, al*. is that a Al_2O_3/O-Ga-O/GaN interface has ideally low density of interface states which eliminated dangling bonds and bonding defects.

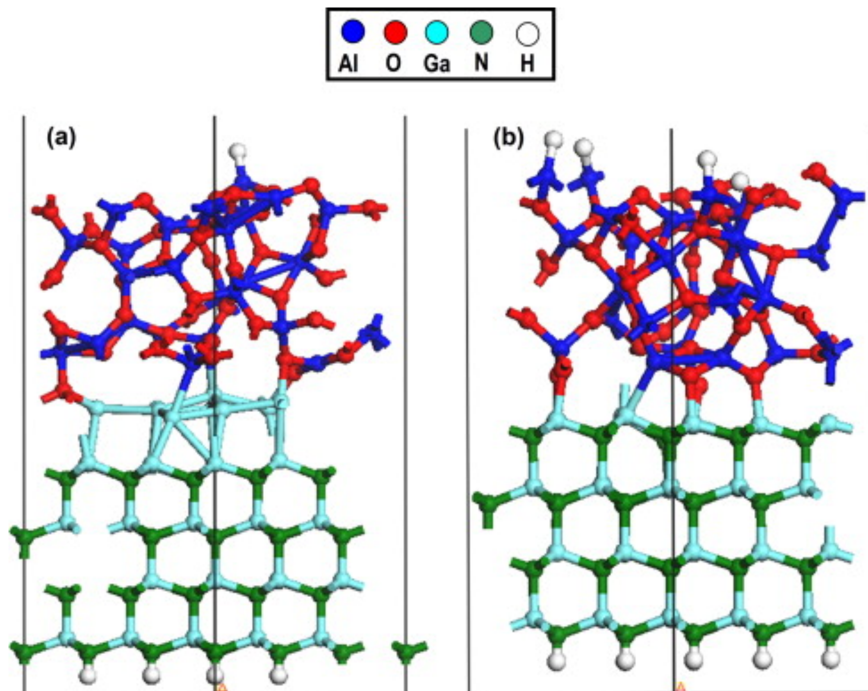

Figure 5.4 simulated $\alpha - Al_2O_3/GaN(0001)$ stacked structure with(a) and without (b) a Ga-O-Ga interlayer [3], [2].

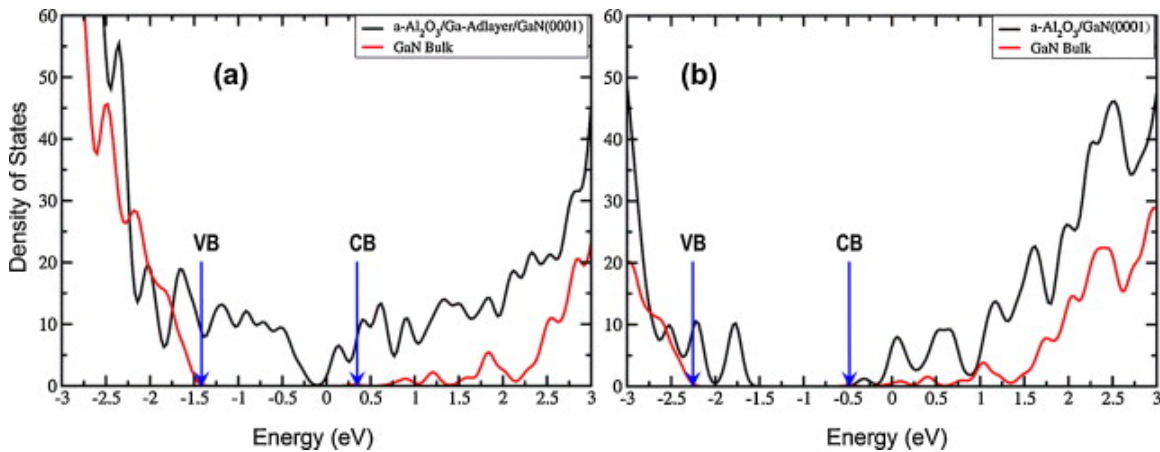

Figure 5.5 Simulated DOS for $\alpha - Al_2O_3/GaN$ with (a) and without (b) a Ga-O-Ga interlayer [3].

5.2 Stacked interlayer with Ga_2O_3 and Al_2O_3 on GaN.

In this study, besides Ga_2O_3 working as passivation layer, PEALD Al_2O_3 working as a passivation layer between GaN and SiO_2 has also been studied. Fig.3.3.3.1 shows the structure of the devices.

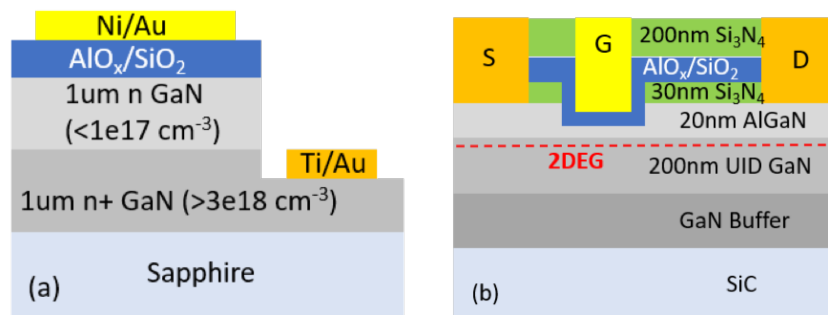

Figure 5.6 Schematic for GaN MOSHEMT with stacked Ga_2O_3 and Al_2O_3. Prepared in collaboration with Srabanti Chowdhury, *et, cl.*

To continue investigating the effects of Ga_2O_3, it would be prudent to evaluate the electrical and interface characteristics of this interface layer as grown by oxygen plasma treatment, thermal oxidation, subcutaneous growth, and PEALD. One would examine

stacked structures using PEALD Al_2O_3 and SiO_2 on GaN to determine the effects on the interface and oxide characteristics.

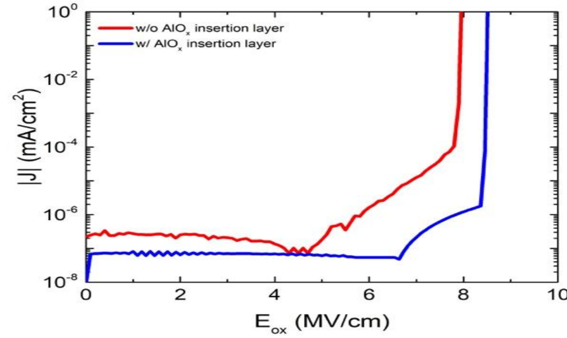

Figure 5.7 Characterization of current-voltage for GaN MOSCAP with and without Al-O-Al interlayer. Prepared in collaboration with Srabanti Chowdhury, *et, cl.*

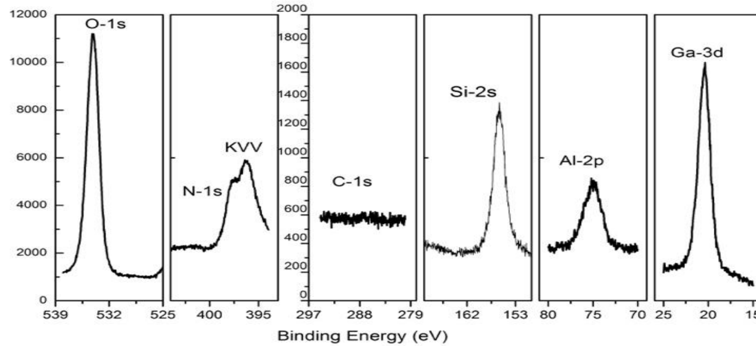

Figure 5.8 XPS for GaN and SiO_2 with stacked interlayer with Ga_2O_3 and Al_2O_3

5.3 Advantages and disadvantages of dry plasma etching of GaN

Etching of GaN is a key process in fabricating GaN-based structures [4]. Due to the high bond energy and chemical inertness of III-Nitride, it is relatively more difficult to develop a wet chemical cleaning method. Traditionally, ICP, RIE [5] [6]and ECR plasma etching on GaN are widely used in fabrication [4]. Plasma assisted etching is mostly based on chemical reactions, physical sputtering, or both processes together

(called ion-assisted plasma etching). An ideal etching process should cause little damage on the surface and leave smooth surface morphology. Inductively coupled plasma dry etching is one of the most widely used plasma reactors [7][8]. The most commonly used chemicals for ICP etching of GaN are Cl_2/Ar_2 plasma [8][9], $Cl_2/BCl_3/Ar$ plasma, Cl_2/BCl_3 plasma, $CH_4/H_2/SF_6$ and $Cl_2/N_2/O_2$ plasma.

Ga_2O_3 has been deposited as a passivation layer on GaN to decrease the interface states density. Besides the possible interface state density that could be caused by the dielectric deposition on GaN, etching induced damage of GaN also influences the interface states between GaN and insulators.

RIE has the comparatively lowest etch rate. Typically, an etch rate ranging from 370nm/min to 900 nm/min was observed using an inductively coupled plasma. During the process of ICP etching, parameters including the plasma power, gas pressure, and RF power were varied to achieve different etching rates.

For an ICP plasma with Cl_2/Ar, the RMS of GaN before etching was 0.58 nm and afterwards 1.38 nm with 100 W RF power and 13.62 nm with 1000 W ICP/300W RF power.

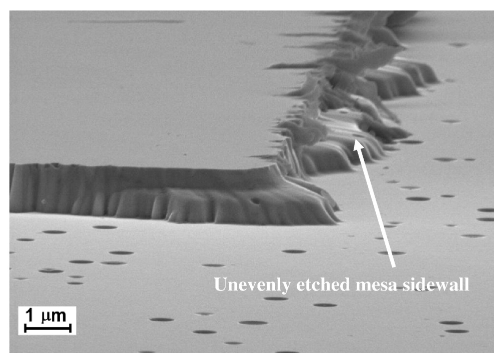

Figure 5.9 Unevenly etched mesa sidewall after 3 min plasma with 600 W ICP power and 60W RF power measure with SEM [10].

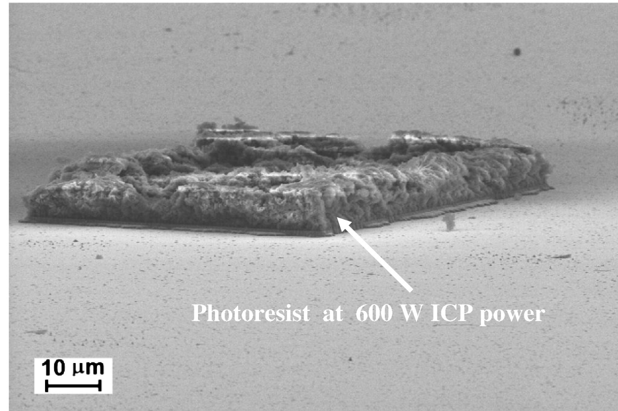

Figure 5.10 Degraded photoresist mask after 3 min plasma with 600 W ICP power and 60 W RF power measured with SEM.

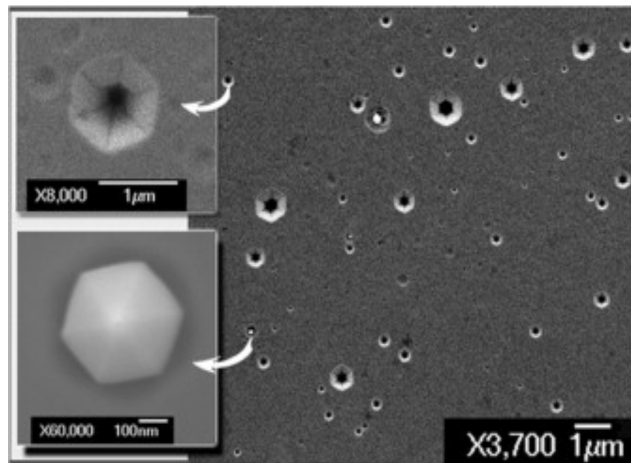

Figure 5.11 SEM images of GaN bottom surface after ICP etching.

Inserted subfigures on Fig 5.11 showed magnified detail of the etching induced damage [10]. The SEM image of GaN side-wall after ICP etching. Inset figure shows the mesa structure of the etched area [10]. In the process of fabricating a transistor, etching of the semiconductor is an important step. Dry etching and wet etching are the most applicable etching methods. Currently, dry plasma etching is one of the most widely used etching processes for a semiconductor substrate. Usually the semiconductor is partially covered with photoresist. Typically, fabricators use dry etching of GaN with Cl_2/Ar[8],

BCl_3/Cl_2[10] . The ICP etching of GaN has a lot of advantages including wide etching rate range from 370 nm/min to 900 nm/min and anisotropy. However, the etching induced damage could be an issue resulting in side-wall leakage and reduced PL density has been observed. The side-wall etching damage is shown in Fig. 5.10.

5.3.1 Surface roughness after dry plasma etching

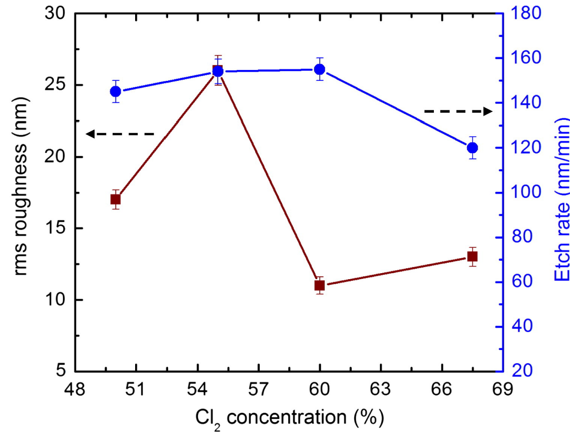

Figure 5.12 Influence of Cl_2 concentration on the surface RMS with 500W ICP power, 60W RF power and 0.66 Pa pressure.

5.4 Atomic Layer Etching of GaN

To remove the etching induced damage, atomic layer etching (ALE) of GaN has been proposed [11]–[13]. For the ALE process, the process starts with an RIE etched surface, an oxygen plasma or H_2O_2 plasma oxidizes the GaN surface, and about 1 ML of Ga_2O_3 is formed. Next, HCl or alternative HF reacts with Ga_2O_3 and leaves $GaCl_3$ or GaF_3 respectively. $GaCl_3$ is volatile at 300 ℃ [14] and GaF_3 can react with $Al(CH_3)_3$ as follows:

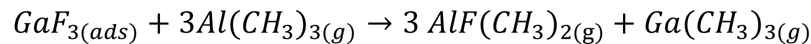

$$GaF_{3(ads)} + 3Al(CH_3)_{3(g)} \rightarrow 3\ AlF(CH_3)_{2(g)} + Ga(CH_3)_{3(g)}$$

The product $AlF(CH_3)_2$ is also volatile at 300 °C. TMA does not react with GaN, which promises a self-limiting reaction for each cycle. Finally, remote inductively coupled $H_2/NH_3/Ar$ plasma cleanup step is applied to the surface. The plasma is H, H_2*, N-H_2, N-H_3* radical enhanced with little ion density to restore stoichiometry [15].

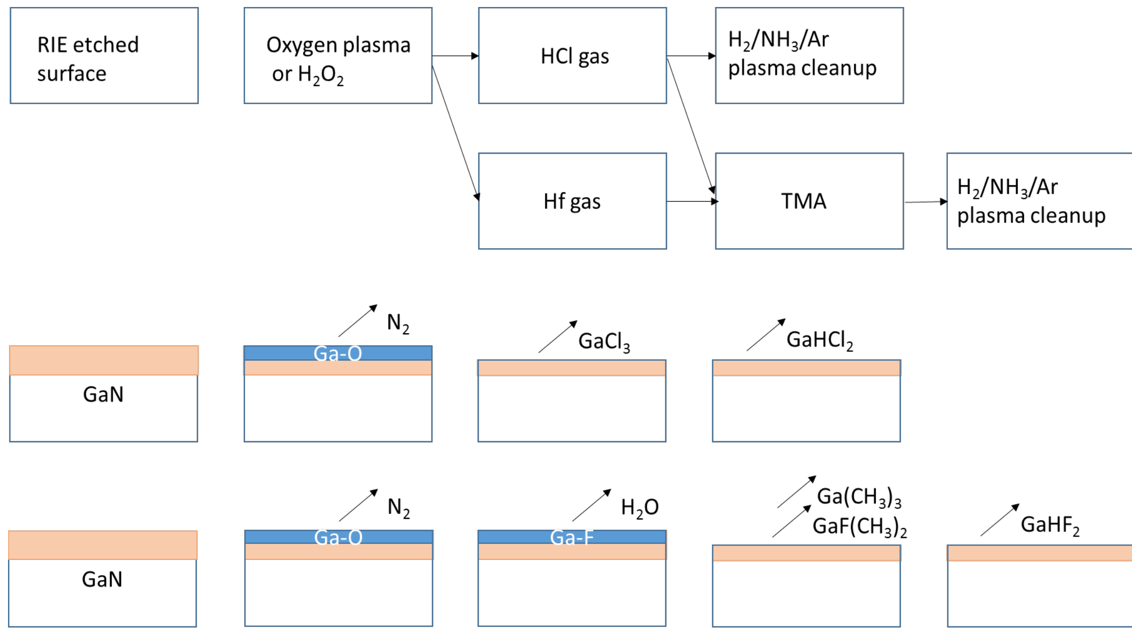

Figure 5.13. Schematic of proposed atomic layer etching (ALE) processes for etch damage removal.

Fig. 5.13 shows the of proposed atomic layer etching (ALE) processes for etch damage removal. The upper figure shows two process sequences and the lower figure show a cross section of the near surface area and the molecular species from the surface. The 2-8 nm etch damaged surface layer is shown in orange, and oxidized surface is shown in blue. The oxide may be removed directly with HCL at 300°C or converted to a fluoride surface. The gallium fluoride (or gallium oxide) layer would be removed with exposure to TMA. A hydrogen/argon remote plasma cleaning is used to remove any residual species. The process is repeated as necessary to remove the etch damaged layer.

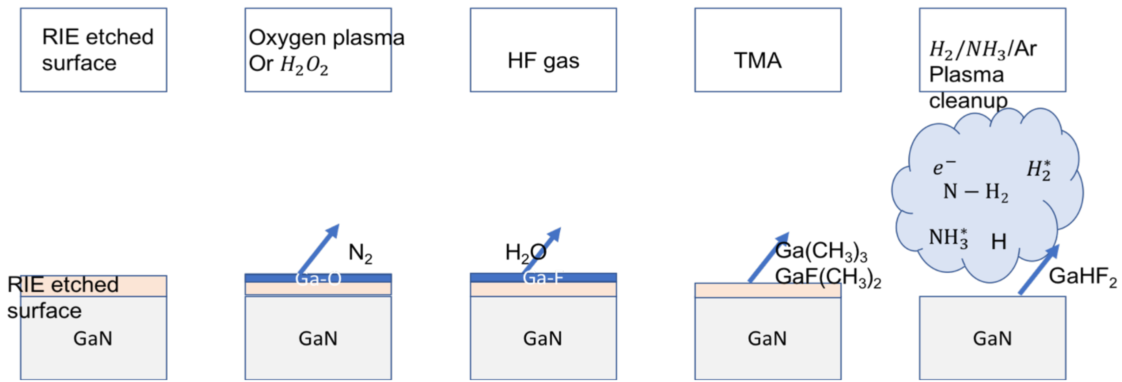

Figure 5.14 GaN ALE process with oxygen plasma or H_2O_2 as oxidizer and HF, TMA as reactants to remove oxides.

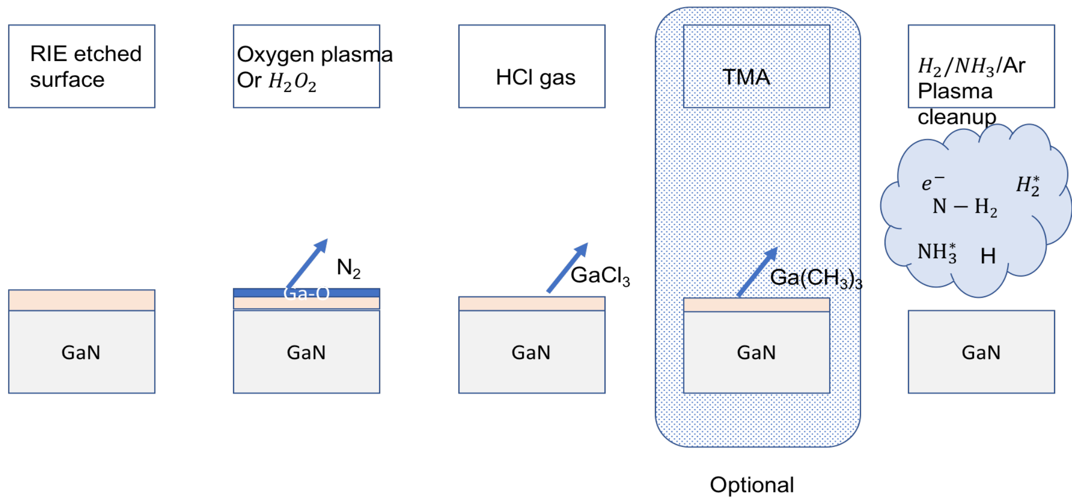

Figure 5.15 GaN ALE process with oxygen plasma or H_2O_2 as oxidizer and HF, TMA as reactants to remove oxides.

Previous to this process, x-ray photoemission spectroscopy is used to calibrate PEALD thin film, and in this study, XPS will be used to calibrate the atomic layer etched GaN surface.

The future plan is to fabricate GaN MOSFET using 18nm PEALD Al_2O_3 as gate insulator, 2nm PEALD Ga_2O_3 as passivation interfacial layer between GaN and Al_2O_3.

Applicate the ALE in the process to achieve an ideal GaN etched surface. GaN MOSFET with high breakdown, low hysteresis and large yield is expected.

5.4 REFERENCE

[1] J. Yang, B. S. Eller, and R. J. Nemanich, “Surface band bending and band alignment of plasma enhanced atomic layer deposited dielectrics on Ga- and N-face gallium nitride,” *J. Appl. Phys.*, vol. 116, no. 12, p. 123702, Sep. 2014.

[2] A. J. Kerr *et al.*, “Preparation of gallium nitride surfaces for atomic layer deposition of aluminum oxide,” *J. Chem. Phys. GaN AlGaN J. Vac. Sci. Technol. A Vacuum, Surfaces, Film. J. Appl. Phys.*, vol. 141, no. 1, 2014.

[3] “Characterization of interface and border traps in ALD Al2O3/GaN MOS capacitors with two-step surface pretreatments on Ga-polar GaN,” *Appl. Surf. Sci.*, vol. 317, pp. 1022–1027, Oct. 2014.

[4] R. J. Shul *et al.*, “ECR, ICP, AND RIE PLASMA ETCHING OF GaN.”

[5] K. Beckmann, J. Holt, W. Olin-Ammentorp, Z. Alamgir, J. Van Nostrand, and N. C. Cady, “The effect of reactive ion etch (RIE) process conditions on ReRAM device performance,” *Semicond. Sci. Technol.*, vol. 32, no. 9, p. 95013, Sep. 2017.

[6] “Recombination-free reactive ion etch for high efficiency silicon solar cells,” *Sol.*

Energy Mater. Sol. Cells, vol. 172, pp. 55–58, Dec. 2017.

[7] "Optimization of inductively coupled plasma deep etching of GaN and etching damage analysis," *Appl. Surf. Sci.*, vol. 257, no. 7, pp. 2700–2706, Jan. 2011.

[8] J. Ladroue, A. Meritan, M. Boufnichel, P. Lefaucheux, P. Ranson, and R. Dussart, "Deep GaN etching by inductively coupled plasma and induced surface defects," *J. Vac. Sci. Technol. A Vacuum, Surfaces, Film.*, vol. 28, no. 5, pp. 1226–1233, Sep. 2010.

[9] D. S. Rawal *et al.*, "GaN etch rate and surface roughness evolution in Cl2/Ar based inductively coupled plasma etching," *Thin Solid Films*, vol. 520, no. 24, pp. 7212–7218, Oct. 2012.

[10] R. Qiu, H. Lu, D. Chen, R. Zhang, and Y. Zheng, "Optimization of inductively coupled plasma deep etching of GaN and etching damage analysis," *Appl. Surf. Sci.*, vol. 257, pp. 2700–2706, 2010.

[11] T. Ohba, W. Yang, S. Tan, K. J. Kanarik, and K. Nojiri, "Atomic layer etching of GaN and AlGaN using directional plasma-enhanced approach," *Jpn. J. Appl. Phys.*, vol. 56, no. 6S2, p. 06HB06, Jun. 2017.

[12] J. Chang and J. P. Chang, "Atomic layer etching of GaN and AlGaN using directional plasma-enhanced approach," *Jpn. J. Appl. Phys*, vol. 56, pp. 6–6, 2017.

[13] C. Kauppinen *et al.*, “Atomic layer etching of gallium nitride (0001),” *J. Vac. Sci. Technol. A Vacuum, Surfaces, Film.*, vol. 35, no. 6, p. 60603, Nov. 2017.

[14] A. Eich, W. Hoffbauer, G. Schnakenburg, T. Bredow, J. Daniels, and J. Beck, “Double-Cube-Shaped Mixed Chalcogen/Pentele Clusters from $GaCl_3$ Melts,” *Eur. J. Inorg. Chem.*, vol. 2014, no. 19, pp. 3043–3052, Jul. 2014.

[15] K. K. Ko, “Controllable layer-by-layer etching of III–V compound semiconductors with an electron cyclotron resonance source,” *J. Vac. Sci. Technol. B Microelectron. Nanom. Struct.*, vol. 11, no. 6, p. 2275, Nov. 1993.

REFERENCES

L. M. Garten, A. Zakutayev, J. D. Perkins, B. P. Gorman, P. F. Ndione, and D. S. Ginley, "Structure property relationships in gallium oxide thin films grown by pulsed laser deposition."

"Polarized Raman spectra in β-Ga2O3 single crystals," *J. Cryst. Growth*, vol. 401, pp. 330–333, Sep. 2014.

L. Li, W. Wei, and M. Behrens, "Synthesis and Characterization of α-, β-, and γ-Ga 2 O 3 prepared from Aqueous Solutions by Controlled Precipitation."

"β-Ga2O3 versus ε-Ga2O3: Control of the crystal phase composition of gallium oxide thin film prepared by metal-organic chemical vapor deposition," *Appl. Surf. Sci.*, vol. 420, pp. 802–807, Oct. 2017.

"Polarized Raman spectra in β-Ga2O3 single crystals," *J. Cryst. Growth*, vol. 401, pp. 330–333, Sep. 2014.

T. C. Lovejoy *et al.*, "Band bending and surface defects in *β* -Ga $_2$ O $_3$," *Appl. Phys. Lett.*, vol. 100, no. 18, p. 181602, Apr. 2012.

H. Feng *et al.*, "Fabrication and UV-sensing properties of one-dimensional β-Ga $_2$ O $_3$ nanomaterials," *Phys. status solidi*, vol. 210, no. 9, p. n/a-n/a, Jun. 2013.

Y. M. Juan *et al.*, "Effects of humidity and ultraviolet characteristics on β-Ga $_2$ O $_3$ nanowire sensor," *RSC Adv.*, vol. 5, no. 103, pp. 84776–84781, Oct. 2015.

M. Higashiwaki, K. Sasaki, A. Kuramata, T. Masui, and S. Yamakoshi, *Appl. Phys. Lett.*, vol. 100, no. 1, p. 13504, Jan. 2012.

"MBE grown Ga2O3 and its power device applications," *J. Cryst. Growth*, vol. 378, pp. 591–595, Sep. 2013.

T. Oshima, T. Okuno, N. Arai, X. Zi-Li, Z. Rong, and X. Chang-Tai, *Appl. Phys. Express*, vol. 1, 2008.

T. Minami *et al.*, *Appl. Phys. Express*, vol. 6, 2013.

M. Nieminen, L. Niinisto, and E. Rauhalab, "Growth of gallium oxide thin films from gallium acetylacetonate by atomic layer epitaxy."

G. Wagner *et al.*, "Homoepitaxial growth of β-Ga $_2$ O $_3$ layers by metal-organic vapor phase epitaxy," *Phys. Status Solidi*, vol. 211, no. 1, pp. 27–33, 2014.

F.-P. Yu, S.-L. Ou, and D.-S. Wuu, "Pulsed laser deposition of gallium oxide films

for high performance solar-blind photodetectors," *Opt. Mater. Express*, vol. 5, no. 5, p. 1240, May 2015.

T. Minami *et al.*, *Japanese J. Appl. Phys. Tadatsugu Minami al Jpn. J. Appl. Phys. Jpn. J. Appl. Phys*, vol. 39, no. 6A, pp. 524–526, 2000.

"Low temperature Ga2O3 atomic layer deposition using gallium tri-isopropoxide and water," *Thin Solid Films*, vol. 546, pp. 31–34, Nov. 2013.

J. Yang, B. S. Eller, and R. J. Nemanich, "Surface band bending and band alignment of plasma enhanced atomic layer deposited dielectrics on Ga- and N-face gallium nitride," *J. Appl. Phys.*, vol. 116, no. 12, p. 123702, Sep. 2014.

Q. Wang *et al.*, "Direct Band Gap Silicon Allotropes," *J. Am. Chem. Soc.*, vol. 136, no. 28, pp. 9826–9829, Jul. 2014.

W. Dai, H. Wang, S. Chen, D. Li, and D. Zhou, "Effect of point defects on band-gap properties in diamond structure photonic crystals," *J. Appl. Phys.*, vol. 111, 2012.

"IEEE Xplore Full-Text PDF:" [Online]. Available: http://ieeexplore.ieee.org/stamp/stamp.jsp?arnumber=43098. [Accessed: 26-Oct-2017].

M. Higashiwaki *et al.*, *Cit. Appl. Phys. Lett. Appl. Phys. Lett. Appl. Phys. Lett. J. Appl. Phys.*, vol. 1031, no. 10, 2013.

M. A. Khan *et al.*, *Cit. Appl. Phys. Lett. J. Appl. Phys. J. Appl. Phys. J. Appl. Phys. Appl. Phys. Lett.*, vol. 77, no. 10, 2000.

R. Vetury, N. Q. Zhang, S. Keller, and U. K. Misha, "The impact of surface states on the DC and RF characteristics of AlGaN/GaN HFETs," *IEEE Trans. Electron Devices*, vol. 48, no. 3, pp. 560–566, 2001.

E. D. Readinger, B. P. Luther, S. E. Mohney, and E. L. Piner, "Environmental aging of Schottky contacts to n-AlGaN," *J. Appl. Phys. Appl. Phys. Lett. J. Vac. Sci. Technol. A Vacuum, Surfaces, Film. Microstruct. Ti/Al ohmic contacts Appl. Phys. Lett. GaN Appl. Phys. Lett.*, vol. 89, no. 75, pp. 1004–2582, 2001.

S. Ganguly, A. Konar, Z. Hu, H. Xing, and D. Jena, "Polarization effects on gate leakage in InAlN/AlN/GaN high-electron-mobility transistors," *Cit. Appl. Phys. Lett*, vol. 101, 2012.

U. Karrer, O. Ambacher, and M. Stutzmann, "Influence of crystal polarity on the properties of Pt/GaN Schottky diodes Influence of crystal polarity on the

properties of PtÕGaN Schottky diodes,” *Cit. Appl. Phys. Lett. Appl. Phys. Lett. J. Appl. Phys. J. Appl. Phys. J. Appl. Phys. Appl. Phys. Lett. Appl. Phys. Lett.*, vol. 771, no. 63, pp. 1267–1685, 2012.

R. Therrien, G. Lucovsky, and R. Davis, “Charge redistribution at GaN–Ga2O3 interfaces: a microscopic mechanism for low defect density interfaces in remote-plasma-processed MOS devices prepared on polar GaN faces,” *Appl. Surf. Sci.*, vol. 166, no. 1–4, pp. 513–519, Oct. 2000.

F. Ren *et al.*, “Effect of temperature on metal–oxide–semiconductor field-effect transistors Effect of temperature on Ga 2 O 3 " Gd 2 O 3 …/GaN metal–oxide–semiconductor field-effect transistors,” *Cit. Appl. Phys. Lett. Appl. Phys. Lett. GaN Appl. Phys. Lett. J. Chem. Phys.*, vol. 73, no. 10, 1998.

C.-T. Lee, H.-W. Chen, and H.-Y. Lee, “Metal–oxide–semiconductor devices using dielectrics on -type GaN Metal–oxide–semiconductor devices using Ga 2 O 3 dielectrics on n-type GaN,” *Cit. Appl. Phys. Lett. Appl. Phys. Lett. J. Chem. Phys. Appl. Phys. Lett. J. Appl. Phys.*, vol. 821, no. 10, 2003.

U. K. Mishra, P. Parikh, and Yi-Feng Wu, “AlGaN/GaN HEMTs-an overview of device operation and applications,” *Proc. IEEE*, vol. 90, no. 6, pp. 1022–1031, Jun. 2002.

“Characterization of interface and border traps in ALD Al2O3/GaN MOS capacitors with two-step surface pretreatments on Ga-polar GaN,” *Appl. Surf. Sci.*, vol. 317, pp. 1022–1027, Oct. 2014.

H.-Y. Shih, F.-C. Chu, A. Das, C.-Y. Lee, M.-J. Chen, and R.-M. Lin, “Atomic Layer Deposition of Gallium Oxide Films as Gate Dielectrics in AlGaN/GaN Metal–Oxide–Semiconductor High-Electron- Mobility Transistors.”

P. K. Rao, “Analysis of leakage current mechanisms in Pt/Au Schottky contact on Ga-polarity GaN by Frenkel-Poole emission and deep level studies,” *J. Appl. Phys. J. Appl. PhysicsAu Schottky contacts Heterostruct. Appl. Phys. Lett.*, vol. 110, no. 94, pp. 13716–23703, 2011.

P. D. Ye *et al.*, “GaN metal-oxide-semiconductor high-electron-mobility-transistor with atomic layer deposited Al2O3 as gate dielectric,” *Appl. Phys. Lett.*, vol. 86, no. 6, p. 63501, Feb. 2005.

D. S. Rawal *et al.*, “GaN etch rate and surface roughness evolution in Cl2/Ar based inductively coupled plasma etching,” *Thin Solid Films*, vol. 520, no. 24, pp. 7212–7218, Oct. 2012.

M. Long, “Power efficiency oriented optimal design of high density CCP and ICP

sources for semiconductor RF plasma processing equipment," *IEEE Trans. Plasma Sci.*, vol. 34, no. 2, pp. 443–454, Apr. 2006.

R. J. Shul *et al.*, "ECR, ICP, AND RIE PLASMA ETCHING OF GaN."

S. Kasthurirangan, A. N. Agnihotri, C. A. Desai, and L. C. Tribedi, "Temperature diagnostics of ECR plasma by measurement of electron bremsstrahlung," *Rev. Sci. Instrum.*, vol. 83, no. 7, p. 73111, Jul. 2012.

A. A. Sahai, T. C. Katsouleas, S. Gessner, M. Hogan, C. Joshi, and W. B. Mori, "Excitation of wakefields in a relativistically hot plasma created by dying non-linear plasma wakefields," 2013, pp. 618–622.

M. Sharif and A. Rafique, "Hot plasma waves in Schwarzschild magnetosphere," *Astrophys. Space Sci.*, vol. 325, no. 2, pp. 227–240, Feb. 2010.

"Cold plasma: A new technology to modify wheat flour functionality," *Food Chem.*, vol. 202, pp. 247–253, Jul. 2016.

G. Foroutan and A. Akhoundi, "Numerical study of an electrostatic plasma sheath containing two species of charged dust particles," *J. Appl. Phys.*, vol. 112, no. 7, p. 73301, Oct. 2012.

"Correlation of the Debye sheath thickness and (Cr,Al)N coating properties for HPPMS, dcMS, CAE and PCAE processes," *Surf. Coatings Technol.*, Sep. 2017.

H. B. Profijt, S. E. Potts, M. C. M. van de Sanden, and W. M. M. Kessels, "Plasma-Assisted Atomic Layer Deposition: Basics, Opportunities, and Challenges," *J. Vac. Sci. Technol. A Vacuum, Surfaces, Film.*, vol. 29, no. 5, p. 50801, Sep. 2011.

H. B. Profijt, P. Kudlacek, M. C. M. van de Sanden, and W. M. M. Kessels, "Ion and Photon Surface Interaction during Remote Plasma ALD of Metal Oxides," *J. Electrochem. Soc.*, vol. 158, no. 4, p. G88, Apr. 2011.

R. K. Ramachandran *et al.*, "Plasma enhanced atomic layer deposition of Ga_2O_3 thin films," *J. Mater. Chem. A*, vol. 2, no. 45, pp. 19232–19238, Oct. 2014.

V. R. Rai, V. Vandalon, and S. Agarwal, "Surface Reaction Mechanisms during Ozone and Oxygen Plasma Assisted Atomic Layer Deposition of Aluminum Oxide," *Langmuir*, vol. 26, no. 17, pp. 13732–13735, Sep. 2010.

H.-Y. Shih, F.-C. Chu, A. Das, C.-Y. Lee, M.-J. Chen, and R.-M. Lin, "Atomic Layer Deposition of Gallium Oxide Films as Gate Dielectrics in AlGaN/GaN Metal–Oxide–Semiconductor High-Electron- Mobility Transistors."

I. Donmez, C. Ozgit-Akgun, and N. Biyikli, “Low temperature deposition of Ga_2O_3 thin films using trimethylgallium and oxygen plasma,” *J. Vac. Sci. Technol. A Vacuum, Surfaces, Film.*, vol. 31, no. 1, p. 01A110, Jan. 2013.

V. R. Rai, V. Vandalon, and S. Agarwal, “Surface Reaction Mechanisms during Ozone and Oxygen Plasma Assisted Atomic Layer Deposition of Aluminum Oxide,” *Langmuir*, vol. 26, no. 17, pp. 13732–13735, Sep. 2010.

K. Knapas and M. Ritala, “In situ studies on reaction mechanisms in atomic layer deposition,” *Crit. Rev. Solid State Mater. Sci.*, vol. 38, no. 3, pp. 167–202, 2013.

K. Knapas and M. Ritala, “In situ Reaction Mechanism Studies on Atomic Layer Deposition of Ir and IrO_2 from $Ir(acac)_3$,” *Chem. Mater.*, vol. 23, no. 11, pp. 2766–2771, Jun. 2011.

R. L. Puurunen, “Growth Per Cycle in Atomic Layer Deposition: Real Application Examplesof a Theoretical Model,” *Chem. Vap. Depos.*, vol. 9, no. 6, pp. 327–332, Dec. 2003.

“Chromium(III) supported on aluminum-nitride-surfaced alumina: characteristics and dehydrogenation activity,” *J. Catal.*, vol. 213, no. 2, pp. 281–290, Jan. 2003.

R. L. Puurunen *et al.*, “Direct wafer bonding of atomic layer deposited TiO2 and Al2O3 thin films,” in *2011 16th International Solid-State Sensors, Actuators and Microsystems Conference*, 2011, pp. 978–981.

T. Kamimura *et al.*, “Band alignment and electrical properties of Al_2O_3/β-Ga_2O_3 heterojunctions,” *Appl. Phys. Lett.*, vol. 104, no. 19, p. 192104, May 2014.

Electronic States of High-k Oxides in Gate Stack Structures.

Y. Ji, Y. Du, and M. Wang, “Electron affinity of GaN(0001) surface doped with Al, Mg,” *Opt. - Int. J. Light Electron Opt.*, vol. 127, no. 7, pp. 3624–3628, Apr. 2016.

J. Robertson and B. Falabretti, “Band offsets of high K gate oxides on III-V semiconductors,” *J. Appl. Phys.*, vol. 100, no. 1, 2006.

“Barrier formation at metal–organic interfaces: dipole formation and the charge neutrality level,” *Appl. Surf. Sci.*, vol. 234, no. 1–4, pp. 107–112, Jul. 2004.

M. Mohamed, K. Irmscher, C. Janowitz, Z. Galazka, R. Manzke, and R. Fornari, “Schottky barrier height of Au on the transparent semiconducting oxide β-Ga_2O_3,” *Appl. Phys. Lett.*, vol. 101, no. 13, p. 132106, Sep. 2012.

"Experimental estimation of charge neutrality level of SiO2," *Appl. Surf. Sci.*, vol. 422, pp. 690–695, Nov. 2017.

T. Onuma *et al.*, *Cit. Appl. Phys. Lett. Appl. Phys. Lett. Appl. Phys. Lett. J. Appl. Phys. Appl. Phys. Lett. J. Chem. Phys.*, vol. 103, no. 10, pp. 41910–13504, 2013.

R. Roy, V. G. Hill, and E. F. Osborn, "Polymorphism of Ga_2O_3 and the System Ga_2O_3—H_2O," *J. Am. Chem. Soc.*, vol. 74, no. 3, pp. 719–722, Feb. 1952.

X. Feng, Z. Li, W. Mi, Y. Luo, and J. Ma, "Mg-doped β-Ga 2 O 3 films with tunable optical band gap prepared on MgO (110) substrates by metal-organic chemical vapor deposition," 2015.

F. Zhu, Z. Yang, W. Zhou, and Y. Zhang, "Synthesis of β-Ga2O3 nanowires through microwave plasma chemical vapor deposition," *Appl. Surf. Sci.*, vol. 252, no. 22, pp. 7930–7933, Sep. 2006.

M. Higashiwaki, K. Sasaki, A. Kuramata, T. Masui, and S. Yamakoshi, "Development of gallium oxide power devices," *Phys. Status Solidi Appl. Mater. Sci.*, vol. 211, no. 1, pp. 21–26, 2014.

F. Litimein, D. Rached, R. Khenata, and H. Baltache, "FPLAPW study of the structural, electronic, and optical properties of Ga 2 O 3 : Monoclinic and hexagonal phases," *J. Alloys Compd.*, vol. 488, pp. 148–156, 2009.

K. D. Chabak *et al.*, *Cit. Appl. Phys. Lett. Appl. Phys. Lett. Appl. Phys. Lett. Appl. Phys. Lett.*, vol. 1091, no. 10, pp. 213501–133503, 2016.

M. D. Heinemann, J. Berry, G. Teeter, T. Unold, and D. Ginley, "Oxygen deficiency and Sn doping of amorphous Ga 2 O 3," *Cit. Appl. Phys. Lett. Appl. Phys. Lett. Appl. Phys. Lett. Appl. Phys. Lett. Appl. Phys. Lett. J. Chem. Phys.*, vol. 108, no. 10, pp. 22107–13504, 2016.

A. A. Dakhel, "W doping effect on the dielectric properties of amorphous Ga 2 O 3 films grown on Si substrate for low-k applications," 2012.

S. Cui, Z. Mei, Y. Zhang, H. Liang, and X. Du, "Room-Temperature Fabricated Amorphous Ga_2O_3 High-Response-Speed Solar-Blind Photodetector on Rigid and Flexible Substrates," *Adv. Opt. Mater.*, vol. 5, no. 19, p. 1700454, Oct. 2017.

H. Lee *et al.*, "ALD and MOCVD of Ga2O3 Thin Films Using the New Ga Precursor Dimethylgallium Isopropoxide, Me2GaOiPr," *Chem. Vap. Depos.*, vol. 17, no. 7–9, pp. 191–197, Sep. 2011.

D. J. Comstock and J. W. Elam, "Atomic Layer Deposition of Ga 2 O 3 Films

Using Trimethylgallium and Ozone."

T. G. Allen and A. Cuevas, "Plasma enhanced atomic layer deposition of gallium oxide on crystalline silicon: demonstration of surface passivation and negative interfacial charge," *Phys. status solidi - Rapid Res. Lett.*, vol. 9, no. 4, pp. 220–224, Apr. 2015.

M. R. Laskar *et al.*, "Atomic Layer Deposition of Al_2O_3–Ga_2O_3 Alloy Coatings for Li[$Ni_{0.5}Mn_{0.3}Co_{0.2}$]O_2 Cathode to Improve Rate Performance in Li-Ion Battery," *ACS Appl. Mater. Interfaces*, vol. 8, no. 16, pp. 10572–10580, Apr. 2016.

C. L. Dezelah, J. Niinistö, K. Arstila, L. Niinistö, and C. H. Winter, "Atomic Layer Deposition of Ga 2 O 3 Films from a Dialkylamido-Based Precursor."

C. L. Dezelah Iv, P. Myllymäki, J. Päiväsaari, K. Arstila, L. Niinistö, and C. H. Winter, "The growth of Er x Ga 22x O 3 films by atomic layer deposition from two different precursor systems," 2007.

D. Pugh, L. G. Bloor, I. P. Parkin, and C. J. Carmalt, "Gallium Hydride Complexes Stabilised by Multidentate Alkoxide Ligands: Precursors to Thin Films of Ga2O3 at Low Temperatures," *Chem. - A Eur. J.*, vol. 18, no. 19, pp. 6079–6087, May 2012.

M. Leskela and M. Ritalä, "Atomic layer deposition (ALD): from precursors to thin film structures," *Thin Solid Films*, vol. 409, pp. 138–146, 2002.

F. K. Shan, G. X. Liu, W. J. Lee, G. H. Lee, I. S. Kim, and B. C. Shin, "Structural, electrical, and optical properties of transparent gallium oxide thin films grown by plasma-enhanced atomic layer deposition," *J. Appl. Phys.*, vol. 98, no. 2, p. 23504, Jul. 2005.

I. Donmez, C. Ozgit-Akgun, and N. Biyikli, "Low temperature deposition of Ga2O3 thin films using trimethylgallium and oxygen plasma," *J. Vac. Sci. Technol. A Vacuum, Surfaces, Film.*, vol. 31, no. 1, p. 01A110, 2013.

K.-W. Chang and J.-J. Wu, "Temperature-controlled catalytic growth of one-dimensional gallium nitride nanostructures using a gallium organometallic precursor," *Appl. Phys. A Mater. Sci. Process.*, vol. 77, no. 6, pp. 769–774, Nov. 2003.

C. A. Kraus and F. E. Toonder ', "TRIMETHYL GALLIUM, TRIMETHYL GALLIUM ETHERATE AND TRIMETHYL GALLIUM AMMINE."

M. Nieminen, L. Niinisto, and E. Rauhalab, "Growth of gallium oxide thin films

from gallium acetylacetonate by atomic layer epitaxy."

M. Passlack, M. Hong, J. P. Mannaerts, R. L. Opila, and F. Ren, "Thermodynamic and photochemical stability of low interface state density Ga2O3–GaAs structures fabricated by in situ molecular beam epitaxy," *Appl. Phys. Lett.*, vol. 69, no. 3, p. 302, Jun. 1998.

A. J. Kerr *et al.*, "Preparation of gallium nitride surfaces for atomic layer deposition of aluminum oxide," *J. Chem. Phys. GaN AlGaN J. Vac. Sci. Technol. A Vacuum, Surfaces, Film. J. Appl. Phys.*, vol. 141, no. 1, 2014.

B. S. Eller, J. Yang, and R. J. Nemanich, *J. Vac. Sci. Technol. A Vacuum, Surfaces, Film. J. Appl. Phys. J. Appl. Phys. J. Vac. Sci. Technol. B Microelectron. Nanom. Struct. Process. Meas. Phenom.*, vol. 31, no. 21, pp. 244503–1828, 2013.

R. D. Long and P. C. McIntyre, "Surface Preparation and Deposited Gate Oxides for Gallium Nitride Based Metal Oxide Semiconductor Devices," *Materials (Basel).*, vol. 5, no. 12, pp. 1297–1335, Jul. 2012.

M. Tutor, E. Preble, M. Williams, X. Xu, D. Tsvetkov, and L. Liu, "Surface preparation of substrates from bulk GaN crystals," *J. Cryst. Growth*, vol. 305, no. 2, pp. 372–376, Jul. 2007.

D. F. Storm *et al.*, "Surface preparation of freestanding GaN substrates for homoepitaxial GaN growth by rf-plasma MBE," *J. Vac. Sci. Technol. B, Nanotechnol. Microelectron. Mater. Process. Meas. Phenom.*, vol. 35, no. 2, p. 02B109, Mar. 2017.

J. Yang, B. S. Eller, and R. J. Nemanich, "Surface band bending and band alignment of plasma enhanced atomic layer deposited dielectrics on Ga- and N-face gallium nitride," *J. Appl. Phys.*, vol. 116, no. 12, p. 123702, Sep. 2014.

Y. C. Chang *et al.*, "MBE grown high k dielectrics Ga 2 O 3 (Gd 2 O 3) on GaN," *J. Cryst. Growth*, vol. 301302, pp. 390–393, 2007.

J. R. Waldrop and R. W. Grant, "Measurement of AlN/GaN (0001) heterojunction band offsets by x-ray photoemission spectroscopy," *Appl. Phys. Lett.*, vol. 68, no. 20, p. 2879, Jun. 1998.

J. R. Waldrop, E. A. Kraut, S. P. Kowalczyk, and R. W. Grant, "Valence-band discontinuities for abrupt (110), (100), and (111) oriented Ge-GaAs heterojunctions," *Surf. Sci.*, 1983.

R. W. Grant, J. R. Waldrop, and E. A. Kraut, "Observation of the Orientation Dependence of Interface Dipole Energies in Ge-GaAs," *Phys. Rev. Lett.*, vol. 40,

no. 10, pp. 656–659, Mar. 1978.

O. Ambacher *et al.*, “Two-dimensional electron gases induced by spontaneous and piezoelectric polarization charges in N-and Ga-face AlGaN/GaN heterostructures,” *J. Appl. Phys.*, vol. 85, no. 3222, 1999.

P. Oelhafen, “Practical surface analysis by auger and X-ray photoelectron spectroscopy : Edited by D. Briggs and M.P. Seah, John Wiley and Sons, 1983, 533pp., ISBN 0471 26279 X,” *J. Electron Spectros. Relat. Phenomena*, vol. 34, no. 2, p. 203, Jan. 1984.